Electron Microscopy a key alliance in Material Science

Eirini Sarigiannidou

MÉMOIRE

En vue d'obtenir l'HDR :

HABILITATION À DIRIGER DES RECHERCHES

École Doctorale I-MEP2 - Ingénierie - Matériaux, Mécanique, Environnement, Energétique, Procédés, Production

Arrêté ministériel : 23 novembre 1988

Présenté par :

Eirini SARIGIANNIDOU

Laboratoire des matériaux et du génie physique (LMGP),

Grenoble INP -UGA, PHELMA

La microscopie électronique, une alliance clé dans la science des matériaux

Electron Microscopy a key alliance in Material Science

Travaux soutenus publiquement le 21 juin 2023,
devant le jury composé de :

Rapporteurs :

Marian CHATENET,
PROFESSEUR DES UNIVERSITES Grenoble INP – UGA
Ngoc Duy NGUYEN,
PROFESSEUR DES UNIVERSITES, Université De Liège
Mona TREGUER-DELAPIERRE,
PROFESSEUR DES UNIVERSITES, Université De Bordeaux

Examinateurs :

Daniel BELLET,
PROFESSEUR DES UNIVERSITES Grenoble INP – UGA
Martien DEN HERTOG
CHARGE DE RECHERCHE, CNRS, Institut Néel, Grenoble
Konstantinos TERMENTZIDIS
DIRECTEUR DE RECHERCHE, CNRS, INSA Lyon

Contents

Curriculum vitae

Eirini Sarigiannidou

Maitresse de conférences, 28ème section, ORCID : 0000-0003-3779-445X
Institut polytechnique de Grenoble / PHELMA
Lab. Matériaux et Génie Physique (LMGP) - Minatec ,3 Parvis Louis Néel, CS 50257 38016 Grenoble France
+33 (4) 56 52 93 33 / eirini.sarigiannidou@grenoble-inp.fr

Formation

En 2004 **Doctorat en Physique**
Electron Microscopy and III-Nitride Nanostructures
CEA-Grenoble/ INAC /SP2M / Laboratoire d'Etude des Matériaux par Microscopie Avancée
Université Joseph Fourier – Grenoble 1 Directeur de thèse : Jean-Luc Rouvière

En 2000 **Master en Physique de Matériaux**
Aristotle University of Thessaloniki /Physics Department, Grèce

En 1998 **Bachelor en Physique**
Aristotle University of Thessaloniki / Physics Department, Grèce

Synthèse de la carrière

Depuis Sep.21 **Vice-Présidente Relations Internationales de Grenoble INP-UGA**

Depuis Sep.06 **Maitresse de conférences**
Institut polytechnique de Grenoble (Grenoble INP-UGA) Ecole PHELMA / Lab. LMGP
Bénéficiaire PEDR : campagne 2012 (PES), campagne 2017 et campagne 2021

Sep.11 - Sep 21 **Coordinatrice du Master Functional Advanced Materials and Engineering (FAME)**
Erasmus Mundus Joint Master degree (EMJMD) label en 2007, en 2012, en 2017 et en 2022

Sep.16- Sep. 21 **Coordinatrice du Master Advanced Materials for Innovation & Sustainability (AMIS)**
Label EIT Raw Materials en 2016 et en 2021

Sep.05-Aout.06 **Post-doctorat:** CEA-Grenoble/INAC/Lab. de Nanophysique et Semiconducteurs
Molecular Beam Epitaxy of (Ga,Mn)N: doping effect and growth of nanostrcutures

Sep.04-Aout.05 **ATER (50%)**, Université Joseph Fourier–Grenoble 1/ Lab. de Spectrométrie Physique,
Molecular Beam Epitaxy of (Ga,Mn)N: a Wide Band Gap semiconductor for Spintronics

Sep.00-Jul.01 **Research Fellow:** Aristotle University of Thessaloniki /Physics Department, Greece
Study by TEM of the interaction between stacking faults & other planar defect in GaN think films

Enseignement

Domaines : Physique et Physique de Matériaux
Niveaux : Licence, Master et Formation Continue / **Volume :** En moyenne ~280h éq.TD / an - décharge incluse.

Recherche

Domaine de compétences : Microscopie électronique en transmission, Semi-conducteurs à grand gap, nanostructures, Caractérisation structurale, Traitement thermiques, Spectroscopie en absorption de Rayons X, Croissance : cristalline, par jets moléculaires et par bain chimique.
Publications : 52 articles RICL, 37 articles ACL, 1 brevet (h-index 23, WOS 2023)
Encadrement : 2 post-docs, 4 thèses, 3 stages Master 2, 4 stages Master 1, 3 stages DUT
Contrats recherche : participation à : 3 contrats EU, 1 FUI, 4 contrats ANR, 6 contrats Carnot ou région

Research activities synthesis

Mots Clés: *Transmission Electron Microscopy techniques, Wide band gap Semiconductors, Nitrides, ZnO Nanostructures, Silicon Carbide, Aluminium Silicon Carbides, Superconductors, Molecular Beam Epitaxy, Crystal growth, Dip Coating, Chemical bath deposition, Thermal treatments, X-ray absorption.*

My research activities are mainly structured around the **characterisation of materials by different modes of transmission electron microscopy** (TEM). Nevertheless, the experience I acquired after the completion of my thesis (ATER and Post-doc) on the elaboration by Molecular Beam Epitaxy of nitride semiconductors allowed me to get involved in research topics related to the **growth of materials** that I will detail later.

Period 1 : sept.2006 – 2011, Equipe Materials for Energy, Axe superconductor, LMGP

For this first reference period, my research activities are focused on two themes.

The first theme concerns **nitride semiconductors**, on which I have been working since my master's years. The experience I have acquired has aroused particular interest in the CEA-Grenoble, which has entrusted me, through a subcontract, with the structural characterisation by Transmission Electron Microscopy (TEM) of nitride-based structures for the STREP Unitride project (14 articles: RICL :23,25,28,30,31,32,33,36, ACL: 10,13,14,15,16,20, 1, Invited Conf. - EDS 2012).

The second theme concerns the **growth and characterisation of oxide buffer layers** for superconducting cables (Superfacts and NoCoCo-3 projects) and solar cells (EPISOL project - 1 patent). I co-supervised two post-docs on the TEM characterisation of different buffer layers for superconducting cables. We carried out an in-depth study of the influence of thermal treatments on the microstructure of $La_2Zr_2O_7$ layers obtained by dip-coating and their epitaxial relationship with the YBCO superconducting layer (4 articles: RICL: 26,27, ACL: 11,12). This theme allowed me to fully integrate the Materials for Energy team of LMGP. I learned to master the chemical growth techniques such as CVD and dip-coating to elaborate these functional oxide materials.

However, as part of a new strategy, the laboratory agreed to stop the research activity on superconductors. So, I joined the LMGP's Cristallogenèse team at the end of 2011 (after my second maternity leave, first maternity leave being in 2008).

Period 2 : 2011 – 2018, Equipe Cristallogenèse, LMGP

My integration within the crystallogenesis team allowed me to get closer to my field of expertise in terms of materials (wide bandgap semiconductors) but also to learn about the **growth of massive crystals** and to discover the importance of simulation in such a process. This integration, was boosted by the co-supervision of the thesis of Mr Nicolaos Tsavdaris which focused on the crystal growth of SiC and the nucleation and propagation of different polytypes such as 15R-SiC (defence in June 2014). He also studied nitrogen doping in SiC crystals obtained by the physical vapour transport method (Marie-Curie project ITN- NetFiSiC). Dr Tsavdaris defended his thesis in January 2015 and his work has resulted in a total of 9 publications (ICLR: 20, ACL: 2-9).

At the same period, Prof. Thierry Ouisse joined the LMGP and more particularly the crystallogenesis team. His activity is focused on the growth of MAX phase crystals and at the beginning, I could collaborate with him to ensure the structural characterization of his crystals. Our collaboration resulted in two publications (RICL: 19,22) but on the one hand Thierry's increasing demand and my own commitments mean that currently the structural characterisation by TEM of his samples is carried out by his external collaborators.

My will to develop my own thematic within the LMGP is manifested by my initiative to valorise a LMGP patent (R. Madar et al., N. Ref: 03568-01 FR, N° of deposit: 10/57685 (24/09/2010)) which concerns the development of a process compatible with the current silicon CMOS technology for the growth of nanowires at temperatures preserving the integrity of integrated circuits. The process for forming the catalyst from nickel silicide is based on low temperature plasma treatments. In order to carry out this study, I supervised two master students and collaborated with specialists in plasma treatment (LPSC laboratory (Prof. Ana Lacoste, M. J. Pelletier). Unfortunately, we could not obtain a funding (e.g. ANR-Blanc Crocofils deposit as coordinator in 2011 and 2012 and Innovative project (ex-BQR) in 2012) and consequently the activity (quite expensive) was extinguished but not my will to initiate my own thematic within the LMGP.

As a result, and thanks to the help of the crystallogenesis team and Didier Chaussende in particular, I developed a new thematic axis on **ternary semiconductors based on Al-Si-C elements**. In this context, the I-MEP 2 doctoral school awarded me a thesis grant in 2014 (Mr Hoang Long LE TRAN) which I co-supervised with Didier. Hoang Long defended in June 2018 (5 papers: RICL: 13,15,17,9, ACL: 1, 9, Invited Lecture - HTCMC-9 2016). In his thesis, Mr. Le Tran studied the vaporisation and condensation phenomena in the Al_4C_3-SiC system and was able to optimise the experimental conditions for the synthesis of this compound, such as initial composition, annealing temperature and temperature gradient. The structural quality and optical absorption of the resulting Al_4SiC_4 crystalline layers are also studied. In his thesis, new heterostructures of the Al-Si-C system on hexagonal SiC substrates (oriented [0001]) are developed and characterised as Al_4C_3/SiC and Al_4SiC_4/SiC. The growth mechanisms and epitaxial relationships were studied at the nanoscale using high resolution TEM. The departure of D. Chaussende from LMGP in 2017 and the lack of funding for this theme (ANR-Blanc 2015, 2016, 2017, ITN in 2018, Fet-Open, 2017-2018) led to the abandonment of this activity within the laboratory.

Another research topic concerns the **structural characterisation of ZnO-based nanostructures** for photovoltaic and lighting applications (Eco-Sesa and Clape projects). This is an internal collaboration at LMGP with Mr. Vincent Consonni. This topic is very close to my field of expertise: materials (wide bandgap semiconductors) and TEM characterization techniques (4 articles: RICL: 16,18,21,24) where the issues of polarity and structural quality (presence of defects, quality of interfaces at atomic scale) are primordial.

Period 3 : 2018 – now, Equipe Nanomatériaux et Hétérostructures Avancées (NANOMAT), Axe Nanofils & Nanostructures Semiconducteurs (NNS), LMGP

The new restructuring of the laboratory in 2018, with the dissolution of the Cristallogenèse team, led me to a natural choice towards the team of Mr. Consonni with whom I have been

collaborating since 2015.

This integration is consolidated by the recruitment of a PhD student, Mr. José Guillermo VILLAFUERTE DÍAZ, whom I co-supervised with Mr. Vincent Consonni and Mr. Julien Pernot from the Institut Néel. His thesis concerns the study of **crystalline defects in unintentionally doped ZnO nanowires** elaborated by chemical bath deposition in order to be integrated in a flexible sensor adapted to biological media (ANR Roller). These crystal defects play a crucial role on their optical and electrical properties, which govern the performance of many engineered devices at the nanoscale scale. Thus, different engineering strategies were adopted (by thermal annealing, by modulating the PH of the chemical bath, and by doping with antimony) in this thesis work to obtain resistive ZnO nanowires by modulating the hydrogen and nitrogen related defects. Mr. Villafuerte defended his thesis in July 2022 and his work can be found in 4 publications (RICL: 1,2,5,7, 12, Invited Conf. - NN22 2022).

In 2018, we recruited another PhD student Mr Alexandre Dieulesaint whom I co-supervise with Mr Consonni to study the **effects of polarity on the properties of ZnO nanowires in relation to hydrogen-related crystal defects**. Alexandre's thesis is carried out in collaboration with Ms. Ana Lacoste of the LPSC in Grenoble for the plasma treatments of our ZnO nanowires (IRGA project). Mr Dieulesaint's defence is planned for summer 2023 and publications of his work are in progress.

In addition to the supervised PhDs, I ensure part of the team's needs in terms of advanced TEM characterisations of various nanostructures based on ZnO wires and other materials, which justifies the presence of my name on some of the team's articles (articles: 3,6,8,11). In the last two years, I have also **taken charge of the team's characterisation activity based on synchrotron X-ray absorption experiments**. Of the three proposals submitted, two were accepted (21 Sept, 22 Nov) by the ESRF (European Synchrotron Radiation Facility) selection committee. The results of the first set of experiments performed in September 2021 on Ga-doped ZnO nanowires have led to a publication that is under review (Physical Review Materials, first author) and an invited conference in the national nanowire community (Invited Conference - J2N 2022).

More generally, apart from my involvement in my team, I collaborate with researchers from: other teams in my laboratory (e.g. Monica Burriel, RICL article: 4), other laboratories in Grenoble (e.g. SIMAP Frederic Mercier, RICL article: 14) and other European laboratories (e.g. Panagiotis Poulopoulos, RICL articles: 10,12), always ensuring their electron microscopy needs.

At the end of document one can find complete information of my scientific production in terms of: publications, oral and poster presentations at conferences, supervision (post-docs, theses, internships) and participation in thesis juries. It should not be forgotten that I am first and foremost a teacher and that my activities and responsibilities in the field of teaching are therefore indicated last, but not least!

Electron Microscopy a key alliance in Material Science

Introduction

Here came the time to make a pause and look behind. It has been now 18 years that I have defended my PhD and yes time goes fast especially when we love what we do and when we do it with people we care. My thesis was on nitride-based nanostructures studied by transmission electron microscopy. Nitrides is a semiconductor family I discovered during my master studies back in 1998, two years after Nakamura published the first paper…. opening the way to white LEDs….Back to that time, in the Physics department of Aristotle Univ. only few "electives" had the right to handle the only TEM we had and I was so deeply hoping to be one of them one day. My dream become reality and I would even say my daily routine during my PhD until nowadays. After my PhD defence in 2004, personal reasons made impossible the physical mobility, so I have chosen to do a thematic mobility from a "TEM girl" to an "MBE (molecular beam epitaxy) grower". Moving from characterisation to growth was not an easy step to take, plus I had to do some teaching. However, I was trained in MBE by a friend, Eva Monroy, and things seem much easier when you know that people believe in you and are willing to help you. The material was still nitrides but this time doping them with a magnetic element (i.e. Mn in my case) since spintronics were quite quoted at this time. So from 2004-2006, no more TEM, but a whole new challenge in front of me: succeed the doping of GaN with Mn without the presence of any secondary phases inside the structure and prove if this pure Gan:Mn is a ferromagnetic semiconducting material. I have learned a lot during these two years, for sure how to use the MBE machine but also many magnetic characterization techniques and most importantly I have done my first experiments in the ESRF, another instrument that always arouses my curiosity …

In 2006, I joined the LMGP laboratory as a young lecturer (maître de conférences) at the ENSPG (École Nationale Supérieure de Physique de Grenoble, actual PHELMA) school of the INPG (at that time, now Grenoble INP - UGA). I was happy to see that the lab had a TEM but no more MBE for me since CVD and chemistry-based methods were the majority of the growth techniques in the lab. The first five year in the lab, I have discovered a new (from myself) class of materials the "oxides" and their use as buffer layer in superconductor cables. Once more I was lucky to learn from a real expert and a friend, Carmen Jimenez. She trained me in the challenges of superconductors and all the secrets of successful annealing, we built a home-made Dip Coating machine and so many other things that I was observing their influence and impact in the TEM observations I was conducting for the first time on a structure other than wurtzite!

In 2011, the LMGP laboratory reorganised its structure. The "Materials for Energy" group, to which I belonged, no longer exists and neither do the activities on superconductors. Very

naturally, I joined the "Cristallogenèse" (XTO) group since silicon carbide was a semiconductor I had already worked with and the need in TEM characterisations was present. Didier Chaussende initiate me to the issues relative to the crystal growth and carbides in general. Together we have initiated a novel area of interest around a new, very promising semiconductor the Al_4SiC_4 and the Al_4C_3. Unfortunately, after several national and European responses to calls for proposals, this subject did not receive the necessary funds to promote it and the activity stopped after the defence of the PhD student we had in common and Didier's departure to another laboratory. Part of these activities will be described in Chapter 1 where the use of TEM to elucidate the structure and stress state of these materials was necessary.

For the past five years, I have been part of Vincent Consonni's team (the NNS) working on ZnO nanostructures. My integration into this team, with which I have always collaborated, was more than natural since ZnO belongs to the same family of wide band gap semiconductors as nitrides and the TEM needs were obvious. Thanks to the dynamic that Vincent and all the members of the team reflect, I am able to fulfil my potential, to open myself up to new perspectives and to dare to venture into areas that I have long left in the shadows... My contribution to the NNS team and my prospects within it for the coming years are discussed in the last chapter.

TEM is a powerful and very useful technique in materials science and being useful to others is something that also characterises me. This text is organised as follows, after this short introduction there are three chapters, each of which refers to a class of materials, i.e. the carbides, nitrides and oxides on which I have worked. The idea is to present the specific materials science issues behind each of these works and how my work as a microscopist has contributed to this knowledge. The paper concludes with the evolution of my research over the last few years and the perspectives I see for the near future.

I hope you enjoy reading it.

Chapter 1 : Carbides

This chapter will be used as an example to demonstrate how I have used electron microscopy techniques as a way to answer material science questions and as a mean to guide the research conducted by Mr. Hoan Long that I co-directed the PhD together with Dr. D. Chaussande.

Introduction

The current semiconductor industry uses several compounds of chemical elements, some of which are either toxic or are classified as critical raw materials. The development of new technologies based on abundant and environmentally friendly elements is therefore highly desirable, with carbon being one of the best candidates. Recently, a lot of extensive research has been carried out to study the band gap engineering of abundant and inexpensive systems such as carbides and/or nitrides [1].

SiC is the only carbon-based semiconductor to have reached a mature technology level, already offering very good performance, especially for high power and high voltage applications. However, SiC alone cannot cover all the applications currently handled by toxic or less abundant elements and the investigation of heterostructures is still limited since only heterostructures using different SiC polytypes [2] has been explored.

There are only a few carbides that are identified as semiconductors and if adding as criterion a band gap higher than 1.5 eV, apart from SiC only two other compounds are suitable: Al_4C_3 [3], Al_4SiC_4 [4]. These compounds are well known for structural and composite applications as they are light and have high hardness combined with superior thermomechanical and chemical resistance. However, very little was known about their semiconducting properties and considerable efforts have been made in our group to elucidate the issue.

Another advantage of these two carbides is that they crystalize in the hexagonal structure making the heteroepitaxial growth in silicon carbides substrate possible [5]. Bandgap energy as a function of lattice constant (a) for different SiC polytypes (6H, 4H, 3C), nitrides, Al_4C_3 and Al_4SiC_4 is shown in the Figure 1. However, these heterostructures still have some drawbacks, such as the instability of Al_4C_3 in air and the large lattice mismatch ($\Delta a/a$) with 4H-SiC substrate (6.8% and 11% for Al_4SiC_4 and Al_4C_3, respectively).

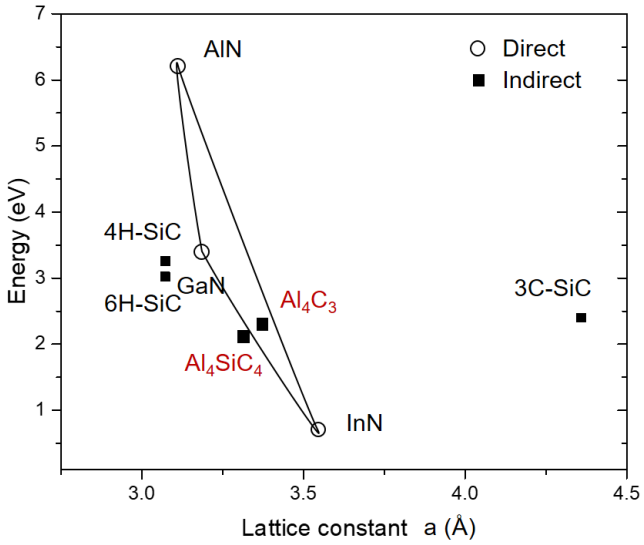

Figure 1. *Bandgap energy versus lattice constant of III-V nitrides and carbides at room temperature.*

In the following the structural, electronic and vibrational properties of the Al_4C_3 crystals will be reported as well as the heteroepitaxy of Al_4C_3/SiC and Al_4SiC_4/SiC heterostructures using HRTEM analysis.

Al_4C_3

Aluminium carbide, Al_4C_3 is an ionocovalent ceramic compound of particular importance as the only intermediate phase in the Al–C binary system. Al_4C_3 could be synthesized by the chemical interaction between aluminium and SiC at temperature near the melting point of Al [6] which is much lower than the growth temperature of SiC and Al_4SiC_4. However, Al_4C_3 easily hydrolyzes at room temperature to form aluminium hydroxide and methane [7]. It is probably the reason why the electrical and optical properties of Al_4C_3 have so far not been experimentally investigated in the literature.

Experimental and theoretical approaches

Al_4C_3 crystals were synthesized by the reaction between SiC and aluminium, as mentioned by Viala et al [6]. Cleaned 4H-SiC wafers (Dow Corning) have been used as the source of carbon and Al pieces (99.5%) have been used as the source of aluminium. Since the formation of Al_4C_3 could prevent the dissolution of SiC in liquid Al [8] the source composition was selected in the aluminium rich area of the ternary phase diagram with the molar fraction $X_{SiC}=n_{SiC}/(n_{SiC} + n_{Al})$ =1%. Details concerning the growth of Al_4C_3 crystals can be found in ref [9].

The Raman spectrum collected from the single crystals of Al_4C_3 is presented in the **Figure 2(a)**. It agrees with the Raman spectrum reported in the literature [10]. Six Raman active modes including 3 modes E_g (252 cm^{-1}, 290 cm^{-1}, 717 cm^{-1}) and 3 modes A_{1g} (341 cm^{-1}, 492 cm^{-1}, 864 cm^{-1}) have been observed. Diffraction analysis of the Al_4C_3 single crystals has been conducted in a θ

- 2θ configuration, which exhibit a diffractogram similar to the poly-crystal as shown in the **Figure 2(b)**. However, the preferred orientation [0001] of Al_4C_3 crystals can still be observed. The lattice constants calculated from the obtained diffraction pattern were: a = 3.002 ± 0.24 Å and c = 24.838 ± 0.042 Å.

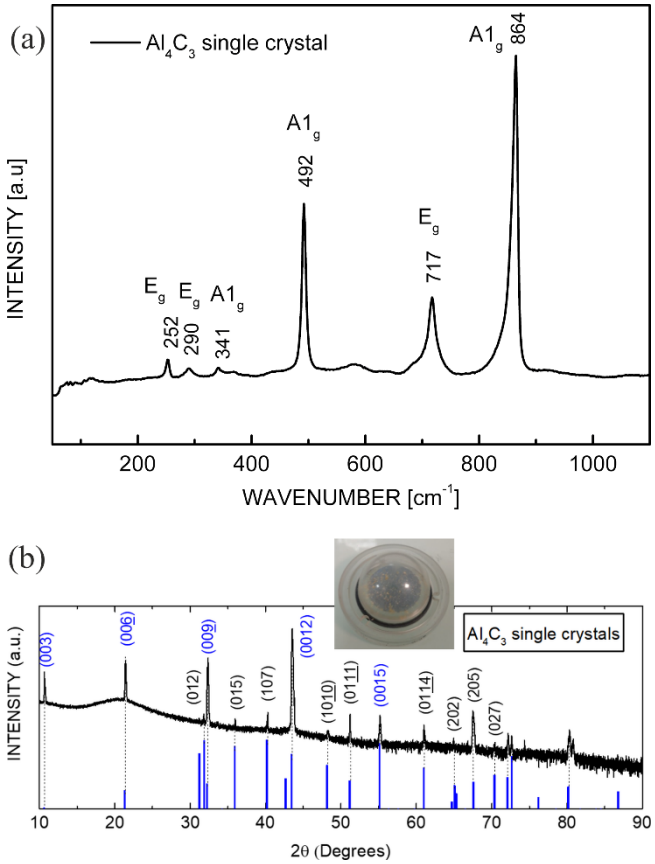

Figure 2. *(a)Raman spectrum collected from the single crystal of Al_4C_3. (b) Diffractogram of the Al_4C_3 single crystals. A sample holder with dome has been used to limit the hydrolysis of the crystals. The preferred orientation has been marked as blue colour [9].*

Figure 3 shows the comparison between the absorption coefficients calculated from the absorption spectra of Al_4SiC_4, Al_4C_3 and 6H-SiC (n-doped) single crystals, which have been collected in the 250-2500 nm wavelength range at room temperature. For Al_4C_3 single crystals, the absorption edge is located around 2.3 eV. This measured optical bandgap was much higher than the calculated so far reported in the literature, hence, we performed advanced Density Functional Theory (DFT) calculations based on the experimental results to clarify the debate.

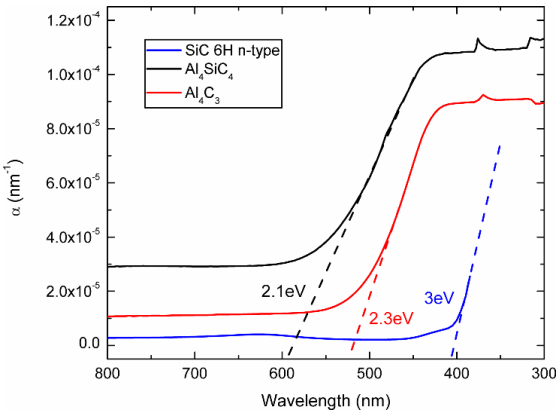

Figure 3. *Absorption coefficients plotted as a function of incident wavelength of Al_4SiC_4, Al_4C_3, and n-type 6H-SiC. The absorption edges are located at 2.1eV, 2.3eV and 3eV for Al_4SiC_4, Al_4C_3, and n-type 6H-SiC, respectively. The measurements have been conducted at room temperature 25°C* [9].

The elastic constants, as presented in **Table 1**, are derived through the calculation of the elastic tensor in VASP by performing six finite distortions of the lattice and deriving the elastic constants from the strain-stress relationship [11]. In **Table 1**, the calculated elastic constants of the Al_4SiC_4 [4] also are given, establishing the similarities of the two materials even on the elastic behaviour.

Table 1. *Elastic constants of Al_4C_3 as calculated with GGA and LDA functionals, compared to calculated results from Ref* [12] *and LDA results of Al_4SiC_4 from Ref. 4*

	Al_4C_3			**Al_4SiC_4**[Error! Bookmark not defined.]
	GGA	LDA	Ref.[**Error! Bookmark not defined.**]	LDA
C_{11}	317.4	407.5	319.1	383.6
C_{12}	114.2	79.1	108.2	121.9
C_{13}	57.4	46.4	52	51.1
C_{33}	357.4	420.1	343.7	411.0
C_{44}=C_{55}	105.5	130.3	105.9	118.4
C_{66}	101.6	164.2	105.4	130.8
B	161.1	175.4	156.2	180.3

The calculated band gaps by the use of the GW approach are 2.06 and 2.12 eV by the use of the GGA and the LDA approximations respectively. The valence band maximum (VBM) is found at the Γ point while the conduction band minimum (CBM) at the L point. Without the GW approach the calculated band gap is 1.25 eV by the use of the LDA approximation. The calculated band

structure by the use of the GW approach and the LDA pseudopotentials is presented in **Figure 4**, having an indirect band gap $\Gamma \to L$ equal to 2.12 eV and $\Gamma \to H$ equal to 3.21 eV while the direct band gap at the Γ point is equal to 6.025 eV. It should be noticed that the M point is almost at the same energy level with the L point in all the cases and should be considered energetically degenerate. In comparison with the Al_4SiC_4 [4] where the calculated indirect $\Gamma \to M$ bandgap was found 2.48 eV, it is clear that Al_4C_3 exhibit similar band structure characteristics (flat conduction band nature *H-K*, *L-M*, indirect band gap), while for Al_4C_3 the lowest and the second lowest bandgaps are narrower than the Al_4SiC_4 [4]. By combining experimental with theoretical DFT based results we achieved to clarify the debate on the electronic properties of Al_4C_3 compound [9].

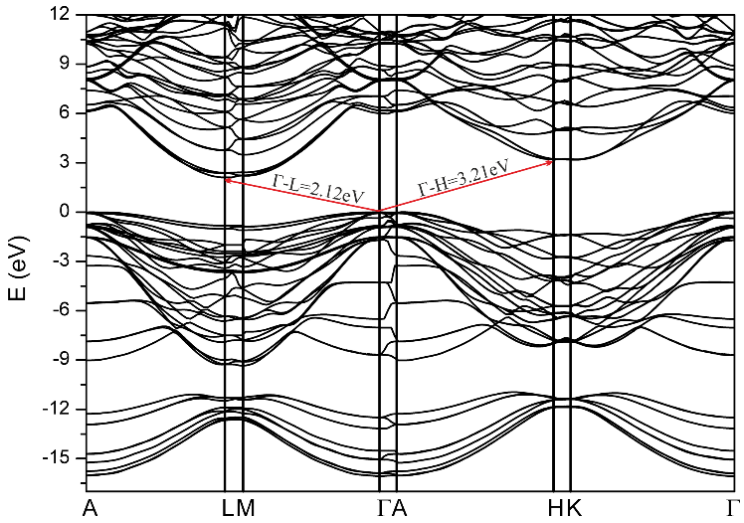

Figure 4. *Electron band structure calculated along the high symmetry points of the hexagonal structure on the framework of scGW approximation[9].*

Al_4C_3/SiC hetero epitaxy

By analogy with the reactive CVD technique for the heteroepitaxial growth of 3C-SiC on Si substrate, we explored the possibility of forming Al_4C_3 epilayers on SiC by direct reaction between Al and SiC. This has also the advantage of protecting the formed Al_4C_3 upon air. Indeed, the Al_4C_3 layer is formed at the interface between the Al layer and SiC substrate. Therefore, the formed Al_4C_3 layer is protected by an Al cover.

The chemical interaction at the Al/α-SiC interface has been investigated by Viala *et al.*[6,8, 13] for the development of the α-SiC-reinforced aluminium composite materials. In this work, a full description of the reaction has been proposed, for a range of temperature varying from the melting point of aluminium (~650°C) to 1347°C. The system is characterized by a metastable equilibrium between α-SiC, Al_4C_3, and aluminium rich ternary liquid phase, which corresponds to the chemical reaction:

$$4Al + 3SiC \rightarrow Al_4C_3 + 3Si \qquad (1)$$

The mechanism and the kinetics of this reaction have been found strongly dependent on the polarity of the substrate. Indeed, the dissolution of SiC in liquid aluminium starts much more rapidly on the Si-face than on the C-face to form an Al_4C_3 layer at the interface [13]. For that reason, [0001] oriented Si-face SiC wafers have been chosen as substrates for the synthesis of the heterostructure with Al_4C_3.

In the following the wetting behaviour between liquid Al and Si-face SiC substrates and the mechanism and kinetics of the formation of Al_4C_3 will be considered by using HRTEM. Further, electron diffraction and strain field analysis will be conducted in order to investigate the epitaxial relationship of the heterostructure, and the strain state of the Al_4C_3 layer.

Al4C3/SiC heterostructure

An experimental process was set up to in order to fabricate the heterostructure Al_4C_3/SiC. In the first step, [0001] Si oriented hexagonal 6H-SiC substrates were covered by a polycrystalline Al layer. This Al layer, with a thickness of 650 nm, was deposited on the Si face of SiC substrate by sputtering using the CIME clean room facilities, and after deoxidization of the SiC substrate surface by wet HF treatment (30 min in HF 50%). The second step of the process is the annealing step. The annealing temperature was varying from 700 to 900°C, and the duration of annealing varied from 5 min to 8 hours. Further experimental details on the annealing process and a study on the wetting behaviour between liquid Al and SiC substrates can be found in ref [14].

In order to investigate the dissolution-precipitation mechanism, the interfacial structure between Al/[0001] Si-face 6H-SiC was be analysed using HRTEM. The analysis has been conducted in the samples annealed at 800° C as it has been proved to be the most interesting and promising results. The interface after annealing for 2 hours has been observed. A low magnification TEM image of the interface of this sample is shown in Figure 5. It is noted that the SiC substrate surface morphology presents a pyramidal shape and is covered by a very thin interfacial Al_4C_3 layer with thickness of 4.6 nm, whereas its sides are exposed to aluminium. This proves that the dissolution-precipitation mechanism of Al/[0001] Si-face 6H-SiC system follows the sayings of Viala *et al.*[13].

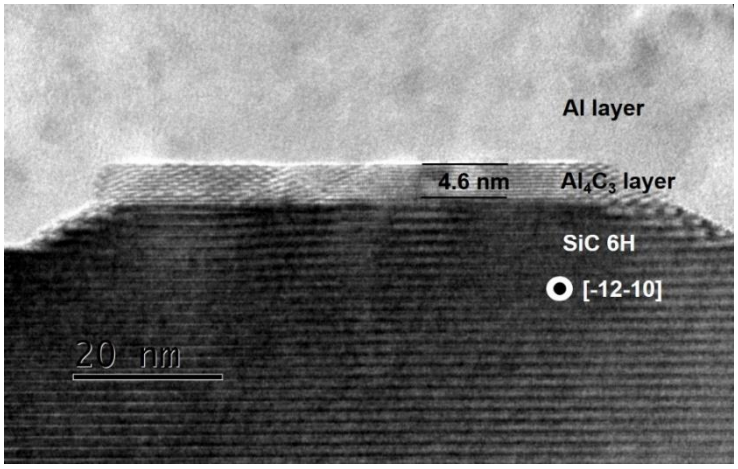

Figure 5. *Low magnification TEM image of the interface between Al and Si-face 6H-SiC substrate after annealing at 800°C for 2 hours.*

In Figure 6, the HRTEM image together with the corresponding fast Fourier transform (FFT) of each layer is given. On the Al are the {111} planes are identified. The {0006} planes of Al_4C_3 are aligned with the {0006} planes of 6H-SiC that proves the epitaxial relationship alors the c direction between the substrate and the formed Al_4C_3 thin layer. Moreover, from the FFT analysis of area 3, the co-existence of Al and Al_4C_3 is clearly identified.

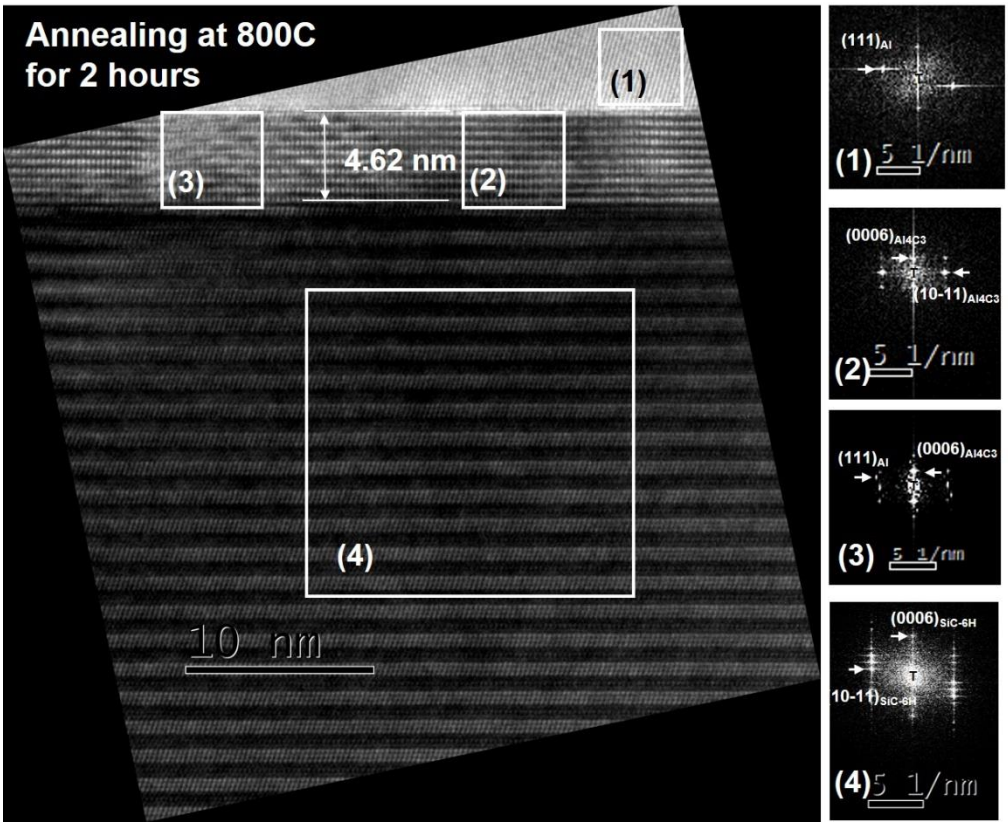

Figure 6. *HRTEM image of the interface after annealing at 800°C for 2 hours and corresponding FFT of different areas such as: (1) Al layer; (2) and (3) intermediate layer; (4) 6H-SiC substrate.*

The strain field analysis on the HRTEM images is performed using the Geometric Phase Analysis (GPA) method [15,16]. In the Figure 7(a), a HRTEM image (part of Figure 6) of Al/Al_4C_3/6H-SiC interface used for the GPA analysis is presented and the corresponding power spectrum is shown in Figure 7(b). The strain analysis is conducted using in-plane and out of plane spatial frequencies by applying a Gaussian mask with size of 0.5g (nm^{-1}). For the GPA strain analysis along the [0001] direction, the GPA mask is placed on the position of the diffraction spot of (0006) planes of Al_4C_3 and (0004) planes of 6H-SiC substrate which has a bulk inter-planar spacing of 4.16 Å, and 3.77 Å, respectively. The power spectrum of the filtered Fourier transform is shown in Figure 7(c). The amplitude image and the phase image of the inverse filtered Fourier transform are given in Figure 7(d) and (e), respectively. The reference region has been chosen inside the 6H-SiC substrate supposing that the strain is zero in the substrate. The strain field image is

presented in Figure 7(f). It should be noted that for the selected diffraction spots, choosing 6H-SiC substrate as the reference, the lattice mismatch (Δd) between bulk Al_4C_3 and bulk 6H-SiC is:

$$\Delta d_{bulk} = \frac{d_{(0006)Al4C3} - d_{(0004)SiC}}{d_{(0004)SiC}} = 10.3\% \quad (2)$$

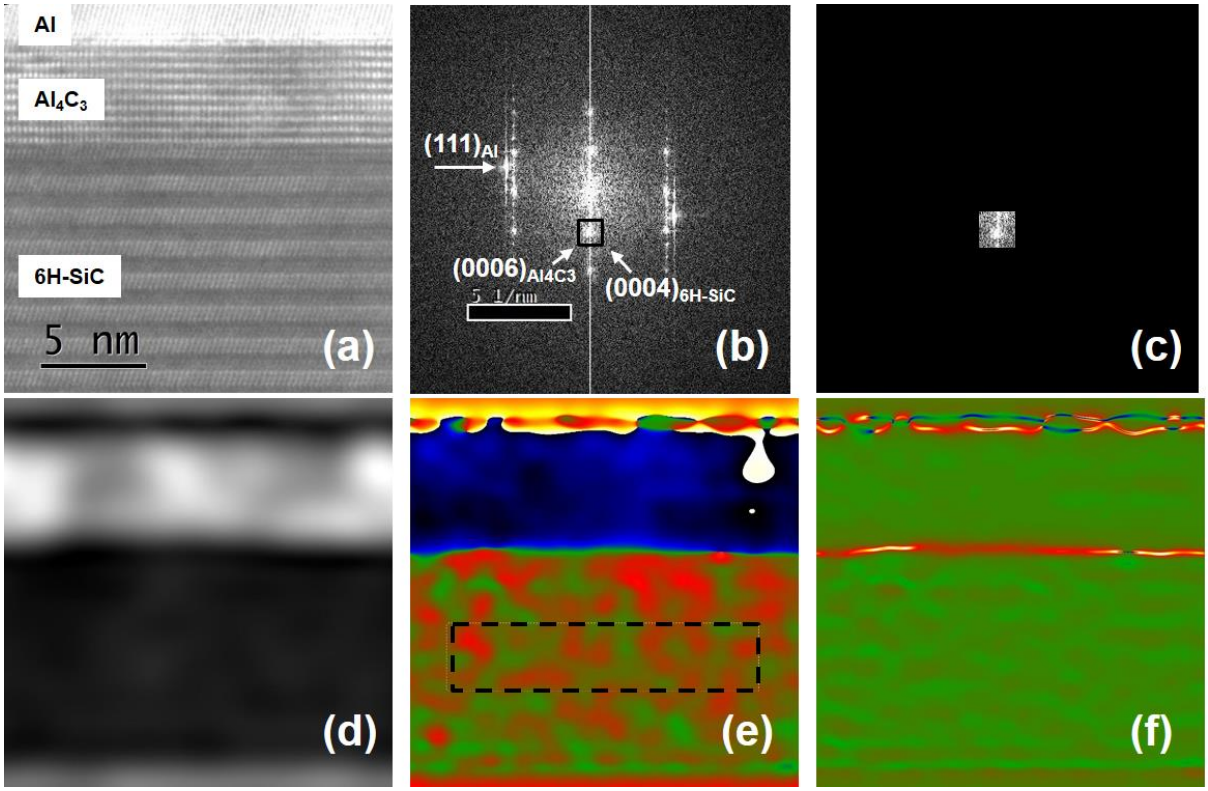

Figure 7. *GPA strain analysis along the [0001] direction. (a) The high resolution TEM image of the interface. (b) Power spectrum of the image (a) allowing to select a frequency* ***g*** *by a Gaussian mask, its position corresponds to the position of the diffraction spots of the plane* $(0006)_{Al4C3}$ *and* $(0004)_{SiC}$*. (c)The power spectrum of the filtered Fourier transform. (d) The amplitude image of the inverse filtered Fourier transform. (e) The phase image with the chosen reference region inside the 6H-SiC substrate. (f) The strain field along the c axis.*

However, the profile of the calculated strain field along the growth direction (Figure 8) reveals that the strain in Al_4C_3 layer and 6H-SiC substrate are almost zero along the ***c*** direction with the presence of a discontinuity along the interface. Hence, the Δd_{bulk} of 10.3% has been absorbed by the lattice structure of Al_4C_3 which is compressed in the ***c*** direction leading to a common diffraction spot of the (0006) plane of Al_4C_3 and the (0004) plane of 6H-SiC substrate.

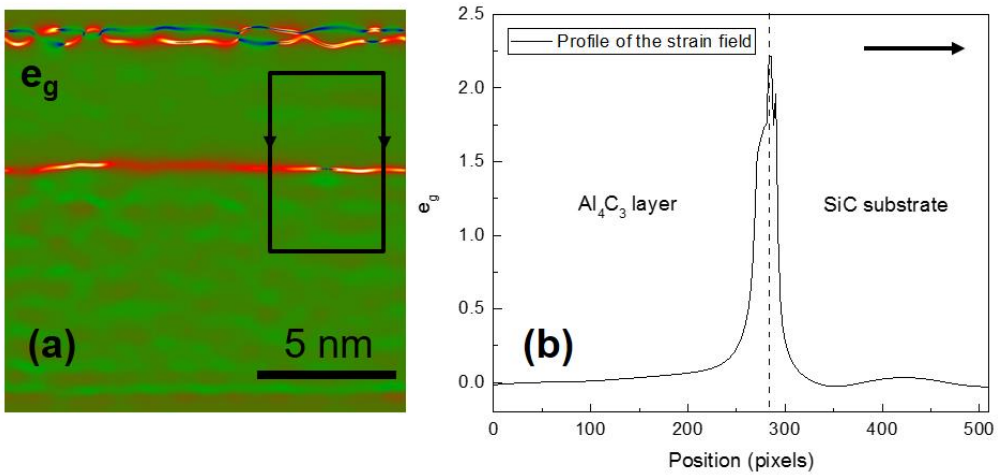

Figure 8. *(a) GPA strain map along the [0001] direction. (b) Strain profile corresponding to the outline presented in (a).*

Regarding the in-plane direction, the {10-17} planes of Al_4C_3 and {10-13} planes of 6H-SiC are considered that have bulk inter-planar spacing of 2.24 Å and 2.35 Å, respectively. For these planes, *Δd* between bulk Al_4C_3 and bulk 6H-SiC is:

$$\Delta d_{bulk} = \frac{d_{(10-17)Al4C3} - d_{(10-13)SiC}}{d_{(10-13)SiC}} = -4.6\% \qquad (3)$$

As revealed previously, that there is no epitaxial relationship along the in-plane direction. Thus, no GPA analysis could be conducted. In order to present how the compressive strain along the *c* axis is relieved in the in-plane direction as tensile strain following the biaxial formulation, the corresponding special frequencies of the FFT of the Figure 9(b) are analysed. A filter mask has been used to select the area which corresponds to the position of the (10-17) plane of Al_4C_3 and the (10-13) plane of SiC, as illustrated in the Figure 9(b).

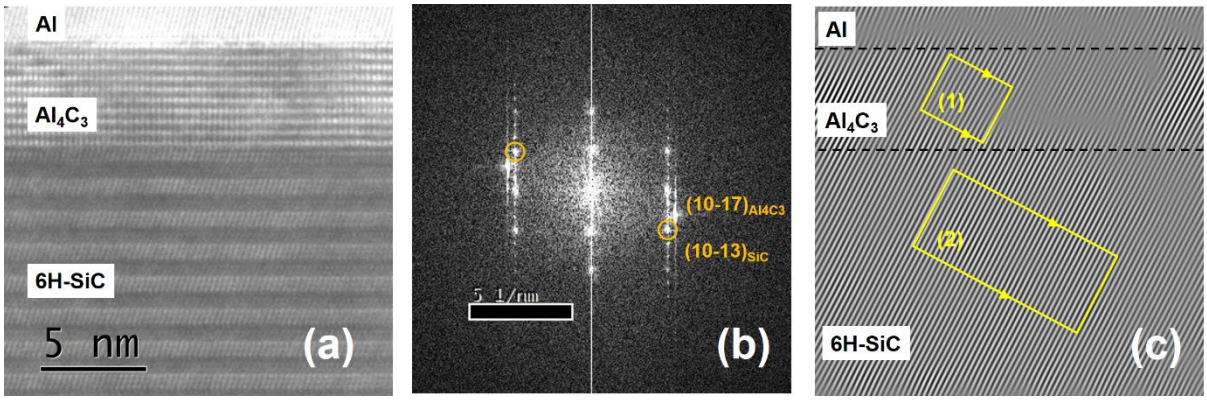

Figure 9. *(a) HRTEM image of the Al/Al_4C_3/6H-SiC interface. (b) Power spectrum of the image (a), the common diffraction spot of the plane (10-17)$_{Al4C3}$ and (10-13)$_{SiC}$ has been selected by a mask. (c) The Bragg image of the masked area.*

From the Bragg image of the masked area presented in Figure 9(c), we compared the interplanar spacing between the Al_4C_3 epilayer and the 6H-SiC substrate. The profiles of the interplanar spacing corresponding to Al_4C_3 and SiC areas are presented in Figure 10. As results, a common interplanar spacing of 2.34 ± 0.01 Å has been found in both areas, which corresponds to the bulk $d_{(10\text{-}13)}$ of the 6H-SiC. It means that the (10-17) plane of Al_4C_3 and the (10-13) plane of SiC have a common diffraction peak which demonstrates the expansion of lattice structure of Al_4C_3 along the ***a*** direction.

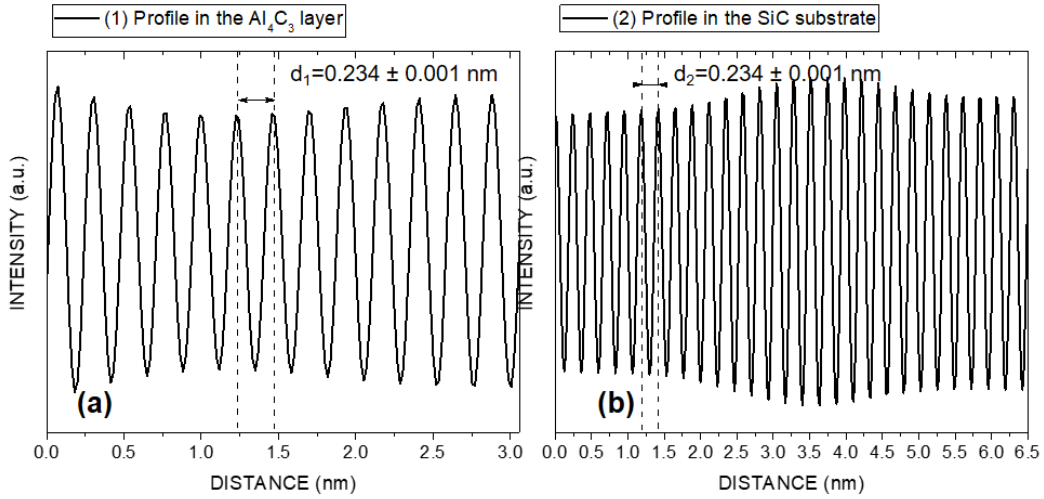

Figure 10. *Intensity profiles corresponding to different outlines presented in the Figure 9(c): (a) the ouline (1) located in the Al_4C_3 layer, (b) the outline (2) located in the 6H-SiC substrate.*

In conclusion, following the [0001] direction, the same interplanar spacing value has been found for both (0006) plane of Al_4C_3 and the (0004) plane of SiC substrate. It demonstrates the compression of the lattice structure of Al_4C_3 in the [0001] direction. The calculated lattice constant *c* of the Al_4C_3 epilayer is found 22.62 ± 0.01 Å which is smaller than the relaxed bulk lattice constant of Al_4C_3 (c_{bulk} = 24.98 Å).

In order to maintain the cell volume, an expansion in the basal plane has been conducted. Indeed, the interplanar spacing of the (10-17) plane of Al_4C_3 epilayer has extended to the one of the (10-13) plane of SiC which has value of 2.34 ± 0.01 Å. In this case, the lattice constant *a* of the Al_4C_3 epilayer could be calculated by the relation between interplanar spacing *d* and *(hkl)* planes in the hexagonal structure [17]:

$$\frac{1}{d^2} = \frac{4}{3}\left(\frac{h^2 + hk + k^2}{a^2}\right) + \frac{l^2}{c^2} \qquad (4)$$

For the (10-17) plane of Al_4C_3 epilayer, we have:

$$\frac{1}{d^2_{(107)}} = \frac{4}{3}\left(\frac{1}{a^2_{epi}}\right) + \frac{7^2}{c^2_{epi}} \qquad (5)$$

Thus, an a_{epi} is 3.92 ±0.03 nm is calculated which is higher than the bulk lattice constant of Al_4C_3 (a_{bulk}=3.329Å). When compared to the lattice constant of SiC (a= 3.0815Å), we found a high lattice mismatch Δa of 27%. With that high mismatch, a possible relaxation mechanism could be through the introduction of basal misfit dislocations at the interface, which are expected to be with $a_{Al4C3} / a_{SiC} = 13/10$ as shown in the simple lattice model given below.

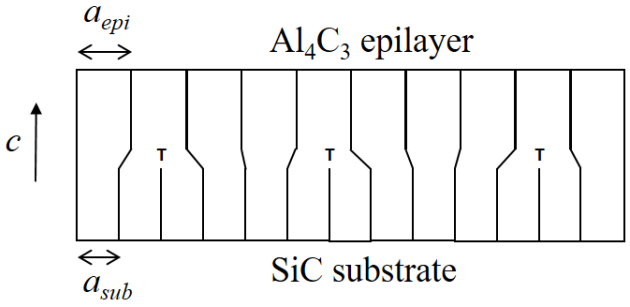

Based on the linear elasticity theory for the case of a hexagonal crystal, the relationship between the elastic constants and the strained lattice constants of the Al_4C_3 epilayer is given by the function:

$$\frac{c_{epi}}{c_{bulk}} = 1 - 2\frac{C_{13}}{C_{33}}\frac{a_{epi} - a_{bulk}}{a_{bulk}} \qquad (6)$$

The calculated value reported in the literature [18] for the C_{13}/C_{33} ratio is:

$$\left(\frac{C_{13}}{C_{33}}\right)_{cal} = \frac{52}{391} = 0.133 \qquad (7)$$

Taking into account the equation (6) and the measured a_{epi} value of Al_4C_3, an c_{epi} value of 23.80 Å is calculated giving a $d_{(0006)}$ of 3.97Å. When comparing with the $d_{(0004)}$ of 6H-SiC (3.773Å), a difference of 5% is calculated. It means that the Al_4C_3 is also strained along ***c*** and that the dominant relaxation mechanism of the Al_4C_3 layer is through a biaxial strain. Although no dislocation has been observed at the interface under the [-12-10] zone axis, there presence should be considered. It should be noticed that the introduction of dislocation is not a consequence of the plastic relaxation mechanism but as a part of the biaxial strain mechanism.

Since the nucleation of Al_4C_3 at the interface experiences a constraint in the growth direction by the liquid Al, an estimation of critical thickness of the Al_4C_3 epilayer could not be done using

the energy balance theory [19]. Further, due to the high lattice mismatch between Al_4C_3 and SiC substrate (f = 8%), this theory is not applicable.

In order to investigate the evolution of the reaction, a sample after 4 h annealing at 800° C was investigated. In figure 11 a low magnification TEM image of the heterostructure of Al/Al_4C_3/SiC is given. The full thickness of the Al_4C_3 layer was found equal to 309±1nm. As expected, the thickness of the Al_4C_3 epilayer is increased with the annealing duration. It should be noted that the thickness of the initial polycrystalline Al layer was 650nm. On the diffraction patterns it is revealed that the only epitaxial relationship is {000l} Al_4C_3||{000l}6H-SiC along the *c* growth axis. The presence of basal stacking faults is identified in the TEM micrograph.

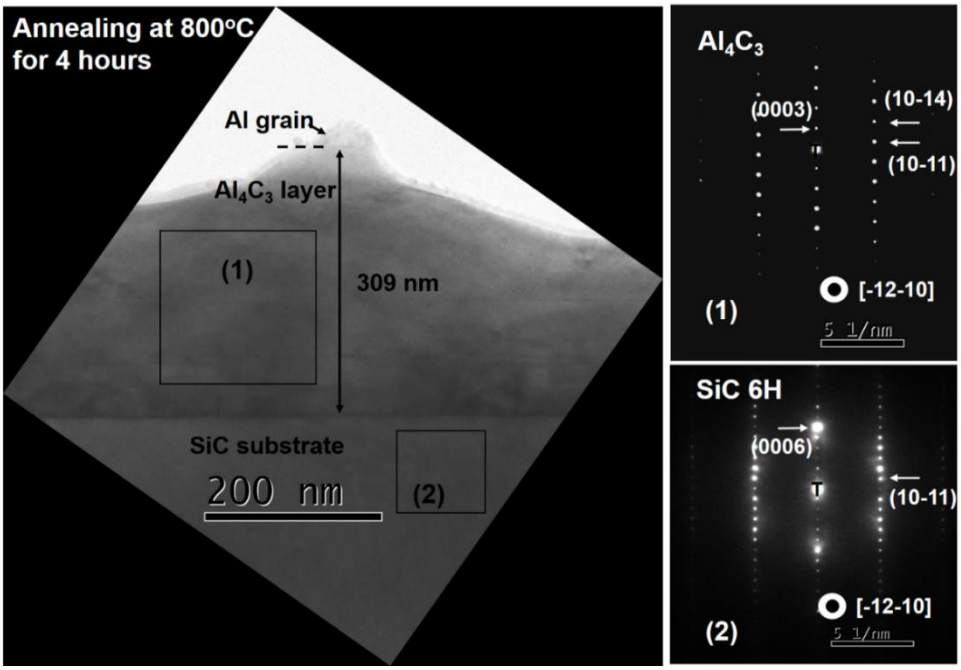

Figure 11. *Low magnification TEM image of heterostructure after annealing at 800°C for 4 hours. The diffraction patterns of the inset pictures are also presented which were identified as (1) Al_4C_3 and (2) 6H-SiC.*

The interface between the Al_4C_3 and Al is shown in the Figure 12 and is found relatively abrupt. The Si as being the product of the reaction, was also observed, as it can be seen in Figure 13, presenting a low magnification TEM image of the heterostructure. The Si grains were found near the surface and they are enclosed by the remaining aluminium.

$$4Al + 3SiC \rightarrow Al_4C_3 + 3Si \quad (8)$$

For the 4h annealed sample, the interface between the Al and Al_4C_3 is analysed with the GPA method and the obtained results are given in Figure 14. A Gaussian mask with size of 0.5g has been used to select the area in the power spectrum, which corresponds to the position of the diffraction spots of the $(-111)_{Al}$ and $(10\text{-}14)_{Al4C3}$ planes. The bulk interplanar spacing of $\{111\}_{Al}$ and

{10-14}$_{Al4C3}$ plane are 2.338 and 2.617 Å, respectively. The amplitude and phase image of the inverse filtered Fourier transform with the reference region selected in aluminium are shown in Figure 14(d) and (e) respectively.

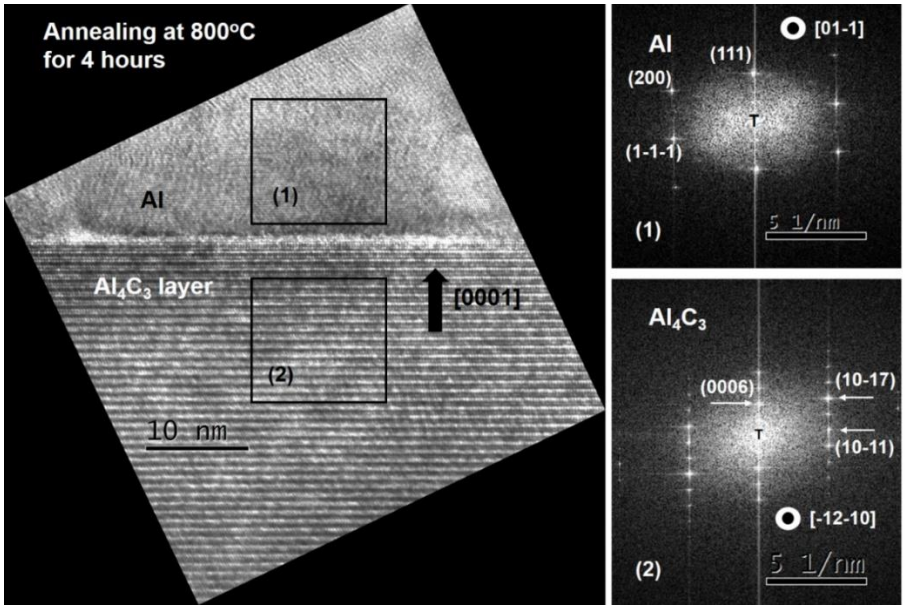

Figure 12. *HRTEM image of the interface between Al and Al_4C_3 layer with corresponding FFT of different areas: (1) Al and (2) Al_4C_3. The sample was annealed at 800°C for 4 hours.*

The calculated strain field image is presented in the Figure 14(f) and the strain profile at the interface is given in the Figure 15. Since Al is chosen as the reference area, the strain in Al is zero, whereas the calculated strain in the Al_4C_3 film has an average value of 13.4 ± 0.35% based on the equation:

$$e_{GPA} = \frac{d_{(10-14)\,Al4C3} - d_{(-111)Al}}{d_{(-111)Al}} = 13.4\% \qquad (9)$$

Considering the bulk theoretical inter-planar spacing $d_{(10\text{-}14)}$ (2.61754 Å) of the Al_4C_3 and the theoretical inter-planar spacing $d_{(\text{-}111)}$ of Al (2.338 Å) the GPA strain is calculated 12%.

$$e_{GPA}^{Theo} = \frac{d_{(10-14)\,Al4C3} - d_{(-111)Al}}{d_{(-111)Al}} = 12.0\% \qquad (10)$$

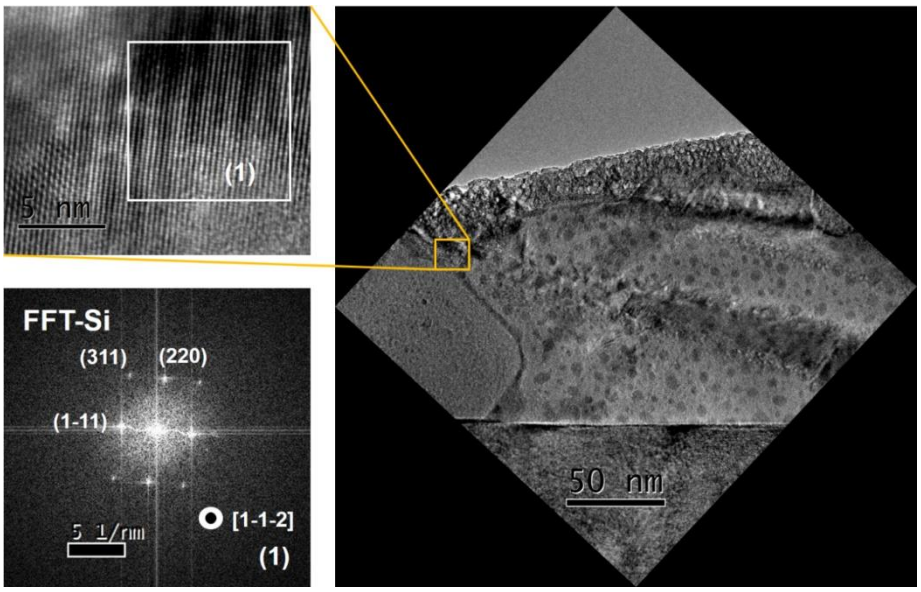

Figure 13. *Low magnification TEM image of the heterostructure Al_4C_3/Si-face 6H-SiC. HRTEM image of the Si grain is given in the inset with the corresponding FFT. The sample was annealed at 800°C for 4 hours.*

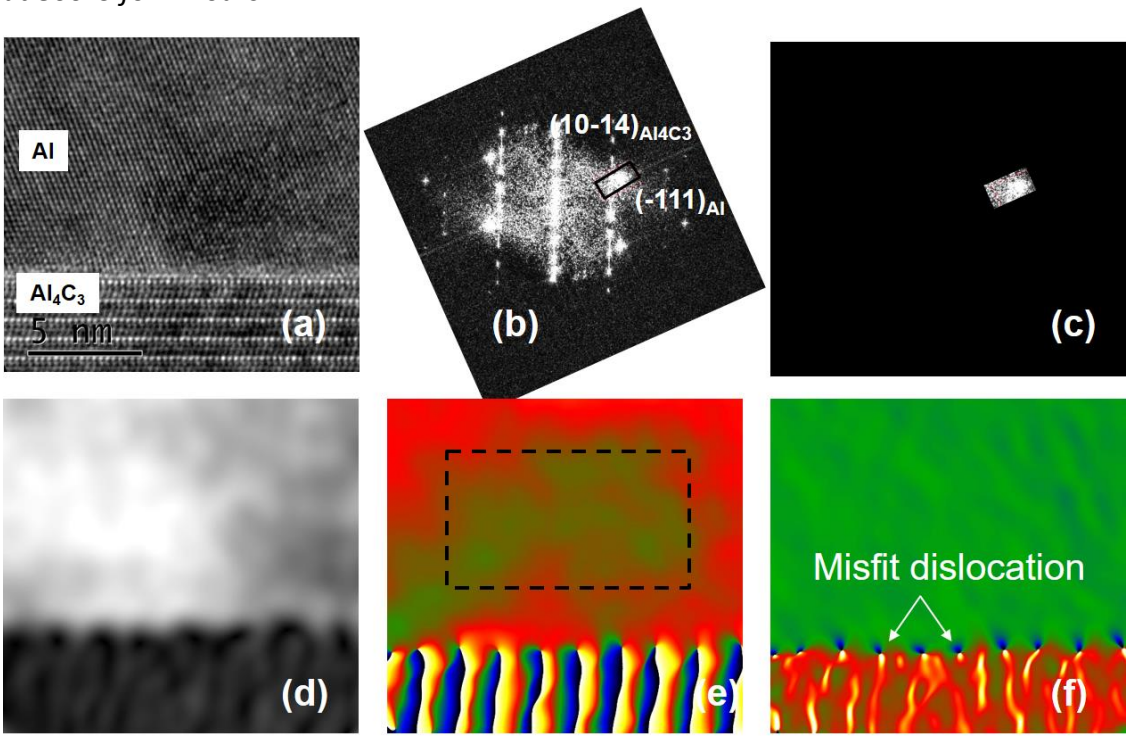

Figure 14. *GPA analysis at Al_4C_3/Al interface. (a) The high resolution TEM image of the interface. (b) Power spectrum of the image (a) allowing to select a frequency **g** indicated by a Gaussian mask, which corresponds to the position of the diffraction spots of the plane $(\text{-}111)_{Al}$ and $(10\text{-}14)_{Al4C3}$. (c)The power spectrum of the filtered Fourier transform. (d) The amplitude image of the inverse filtered Fourier transform. (e) The phase image with the chosen reference region inside the aluminum. (f) The calculated strain field.*

By using the equation (9), the calculated inter-planar spacing $d_{(10\text{-}14)}$ of the Al_4C_3 epilayer is 2.65 ± 0.01 Å, which lead to the conclusion that the Al_4C_3 layer is slightly tensile. This is in agreement with the previous observation with the 2h annealed sample. Moreover, an array of misfit dislocations is observed at the interface introducing a discontinuity in the strain profile.

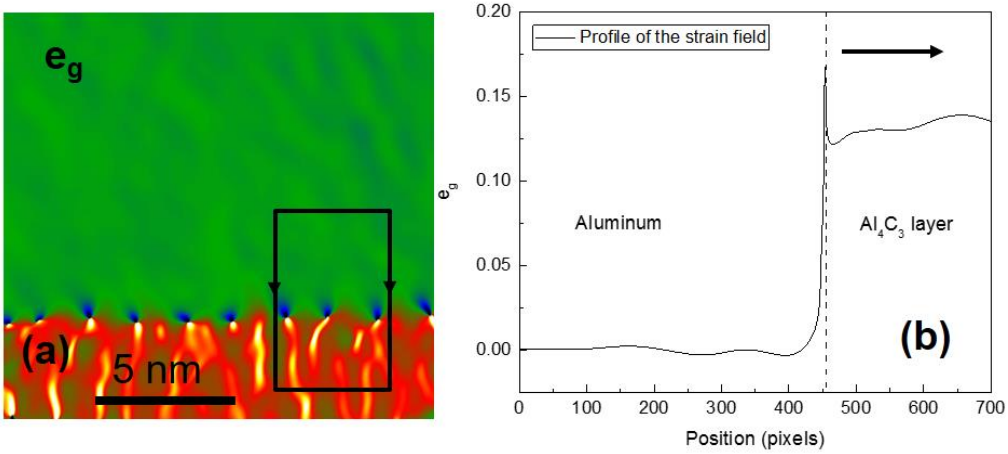

Figure 15. *(a) Result GPA strain map. (b) Strain profile corresponding to the outline area in (a).*

Along the c axis the analysis is conducted by the use of FFT as it is presented in the Figure 16(b). A mask has been used to select the area which corresponds to the position of the diffraction spot of $(00012)_{Al4C3}$ planes. The Bragg image of the masked area is presented in the Figure 16(c) which exhibits well-periodic fringes in the Al_4C_3 area. The intensity profile corresponding to the outline marked in the Al_4C_3 epilayer is given in Figure 17. Based on that, the interplanar spacing $d_{(00012)}$ of the Al_4C_3 epilayer is measured which has value of 2.10±0.01 Å.

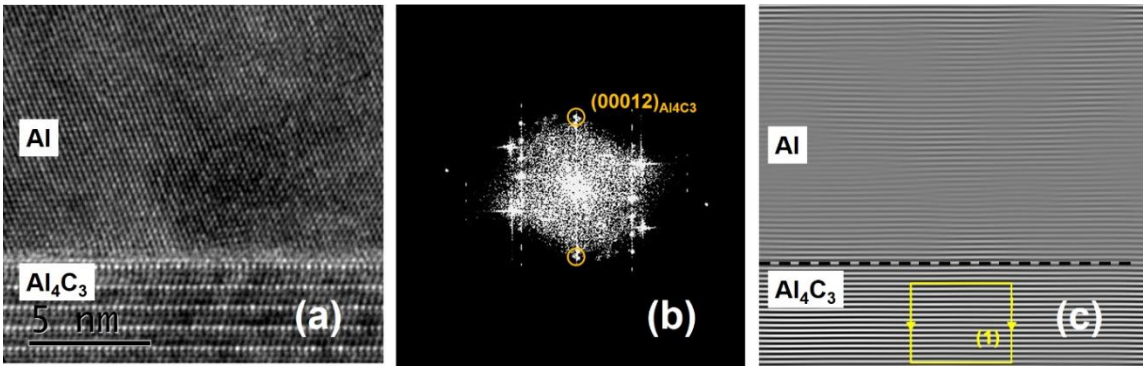

Figure 16. *(a) HRTEM image of the interface Al/Al_4C_3. (b)The fast Fourier transform of (a), a mask has been used to select the area corresponding to the diffraction spot of the $(00012)_{Al4C3}$ plane. (c) The Bragg image of the masked area, an outline of profile is taken in the Al_4C_3 epilayer.*

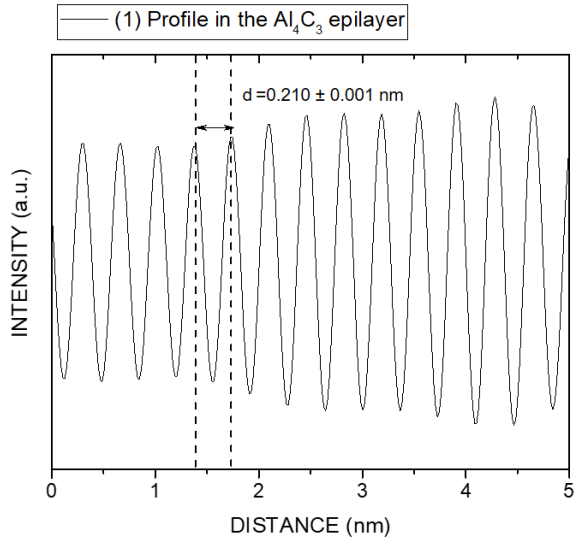

Figure 17. *Intensity profiles corresponding to the outline presented in the Figure 16(c).*

After 4 hours of annealing, the lattice constant c_{epi} and a_{epi} are also calculated from the measured interplanar spacing of (00012) planes and (10-14) planes by using the relation (4).

$$\begin{cases} \dfrac{1}{d_{(0012)}^2} = \dfrac{12^2}{c_{epi}^2} \\ \dfrac{1}{d_{(104)}^2} = \dfrac{4}{3}\left(\dfrac{1}{a_{epi}^2}\right) + \dfrac{4^2}{c_{epi}^2} \end{cases} \tag{11}$$

$$\Rightarrow \begin{cases} c_{epi} = 12.d_{(0012)} \\ a_{epi} = \sqrt{\dfrac{4}{3\left(\dfrac{1}{d_{(104)}^2} - \dfrac{4^2}{c_{epi}^2}\right)}} \end{cases} \tag{12}$$

$$\Rightarrow \begin{cases} c_{epi} = 25.2 \pm 0.12 Å \\ a_{epi} = 3.37 \pm 0.01 Å \end{cases} \tag{13}$$

$$\frac{\Delta a}{a} = \frac{a_{Al4C3-epi} - a_{Al4C3-bulk}}{a_{Al4C3-bulk}} \tag{14}$$

$$\frac{\Delta c}{c} = \frac{c_{Al4C3-epi} - c_{Al4C3-bulk}}{c_{Al4C3-bulk}} \tag{15}$$

Table 2 gathers the lattice constants of the produced Al_4C_3 epilayer for different experimental conditions. In order to evaluate the strain state of the epilayer lattice structure, we define the strain of the epilayer as compared to the bulk: $\Delta a/a$ and $\Delta c/c$ by the following equations:

Table 2. *Lattice constant of Al_4C_3 epilayer for different experimental conditions compared with Al_4C_3 bulk (diffraction pattern: 03-065-9731, Annex 2).*

Samples	Lattice constant (Å)		Strain of lattice constants in epilayer as compared to bulk (%)	
	a	c	*Δa/a*	*Δc/c*
Al_4C_3 bulk	3.329	24.98		
Al_4C_3 epilayer-800°C-2 hours	3.92 ±0.03	22.6 ±0.01	17.7	-9,5
Al_4C_3 epilayer-800°C-4 hours	3.37 ±0.01	25.2 ±0.12	1.3	0.8

As results, from 2 hours to 4 hours of annealing, with the increase of thickness, the in-plane component strain reduces from 17.7% to 1.3% whereas the out-of-plane component reduce from -9.5% to 0.8%. According to these small residual strains after 4 hours of annealing, the Al_4C_3 epilayer is nearly relaxed. The biaxial strain observed after 2 hours of annealing was probably elastically relaxed.

Although, through a dissolution-precipitation mechanism, it is unlikely that complete coverage of the SiC substrate by an Al4C3 layer can be achieved due to the scarcity of the C source provided by SiC dissolution, the procedure is straightforward and produces heterostructures of good structural quality. Thanks to the analysis based on HRTEM images, we managed to confirm the Vialla *et al.* [6,8,13] model concerning the dissolution-precipitation mechanism for Si-face SiC. The case of heterostructures between Al_4C_3 and C-face SiC has not been considered since based on their work, the dissolution-precipitation mechanism on the C-face of SiC is rather different since the C-face is quite stable against the dissolution into the liquid aluminium. As a consequence, they note that dissolution steps were only observed at the surface after a very long reaction time i.e. 1500 hours.

Al_4SiC_4/SiC heterostructure

In the PhD work of Hoang-Long Le-Tran [14] the vaporization and condensation phenomena starting from Al_4C_3 and SiC mixtures have been investigated in view of the Al_4SiC_4 single crystal growth process from the vapor phase. These findings will not be discussed in this work, however further details can be found at ref [20]. Here we will focus on the investigation of the epitaxial relationship and strain field of Al_4SiC_4/6H-or 4H-SiC heterostructure based on HRTEM observations.

The epilayer of Al_4SiC_4 with thickness of 50 µm are grown by sublimation growth process on different [0001] oriented C-face hexagonal SiC substrates: on-axis 6H and 4° off axis [0001] oriented 4H-SiC substrates. Source materials were composed of a mixture of high purity powders of Al_4C_3 (Alfa Aesar, 99+% purity) and SiC (Sika tech E301) with a molar ratio X_{Al4C3}=0.2. The growth

temperature was 1800°C and the pressure was 300 mbar. The deposition duration was 2 hours with a temperature difference of 29°C between source and seed in order to avoid the condensation of parasitic phases.

In Figure 18 the HRTEM image of the deposited Al_4SiC_4 layer is given. The crystalline layer of the Al_4SiC_4 has been identified free of defects. The lattice constants measured from the TEM observations are found equal to $a_{epi} = 3.27 \pm 0.02 Å$. They are in good agreement with the bulk lattice parameters of Al_4SiC_4 (diffraction pattern: 04-009-0133, Annex 2).

Figure 19 presents the diffraction pattern of the interface of the heterostructure. It is clearly seen that the {11-20}Al_4SiC_4||{11-20} SiC as well as {000l}Al_4SiC_4||{000l} SiC, revealing a fully epitaxial relationship between the two materials.

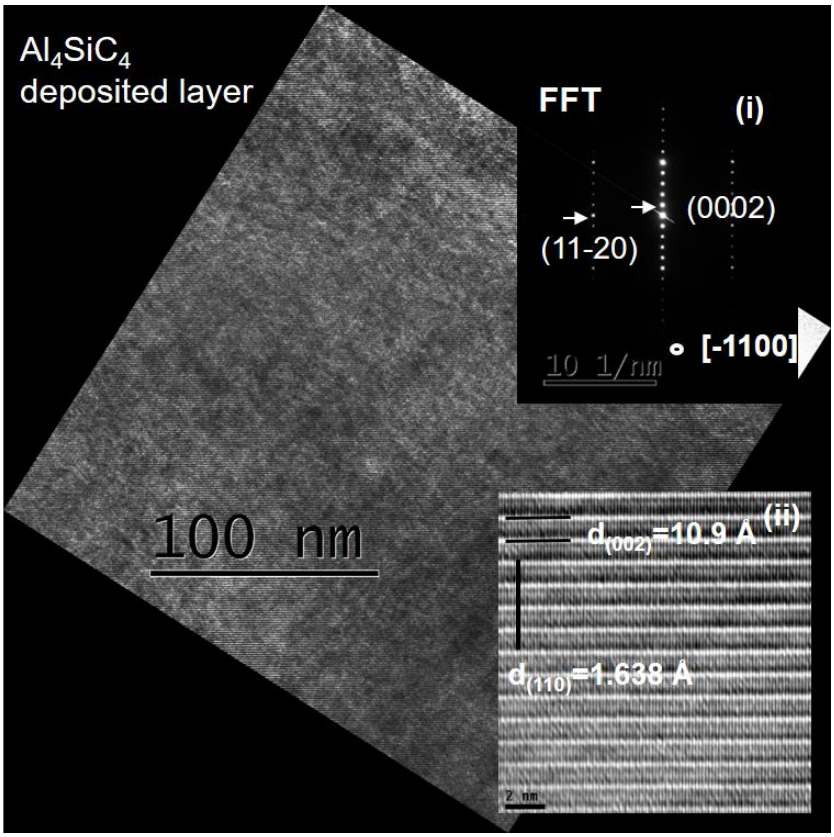

Figure 18. *TEM picture of the Al_4SiC_4 deposited layer observed along the [-1100] zone axis; (i) diffraction pattern of the Al_4SiC_4 crystal; (ii) high resolution image of the Al_4SiC_4 crystal structure.*

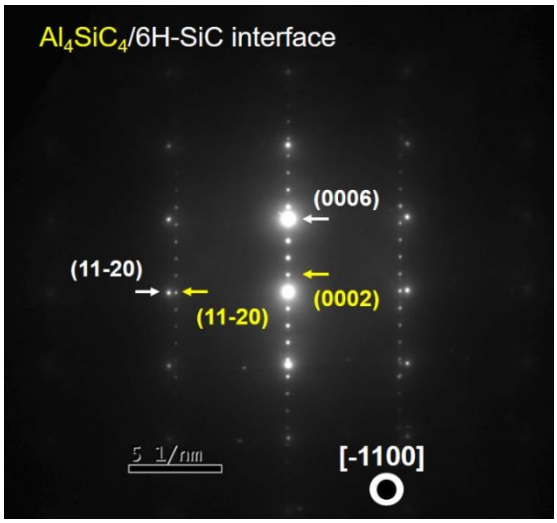

Figure 19. *Diffraction pattern of the interface between Al_4SiC_4 and 6H-SiC.*

From low magnification TEM images, like the one presented in Figure 20, a rough interface was observed putting in evidence the dissolution of 6H-SiC at the early stage of the condensation phenomena while contacting with the vapor dominated by Al-containing species. Further, from HRTEM images, like the one in Figure 20(b), an interfacial superstructure layer with the thickness of 37.4 nm has been found. It could present an intermediate phase between 6H-SiC and Al_4SiC_4 which was formed from the Al rich vapor at the early stage of the growth process. The lattice mismatch of about 6.5% between Al_4SiC_4 and 6H-SiC is accommodated by this interfacial superstructure, since no defects are observed at the Al_4SiC_4 epilayer.

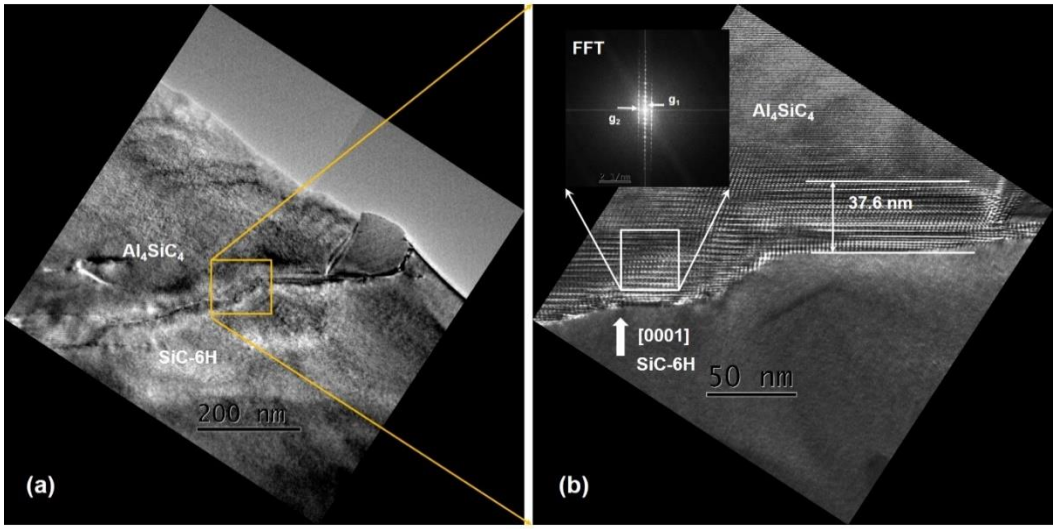

Figure 20. *(a) Low magnification TEM image of the interface Al_4SiC_4/6H-SiC, (b) HRTEM image of the interface Al_4SiC_4/6H-SiC. A superstructure layer has been found along the observed interface. The FFT of the interfacial layer is shown in the inset.*

A HRTEM image at the interfacial area of the heterostructure between Al_4SiC_4 and 4° off axis [0001] oriented 4H-SiC substrate is depicted in Figure 21 with the corresponding FFT image. In contrast with the 6H-SiC case, no interfacial superstructure layer was found in the observed interface. The epitaxial relationship between the two materials is{10-10}Al_4SiC_4||{10-10} SiC and {000l}Al_4SiC_4||{000l} SiC.

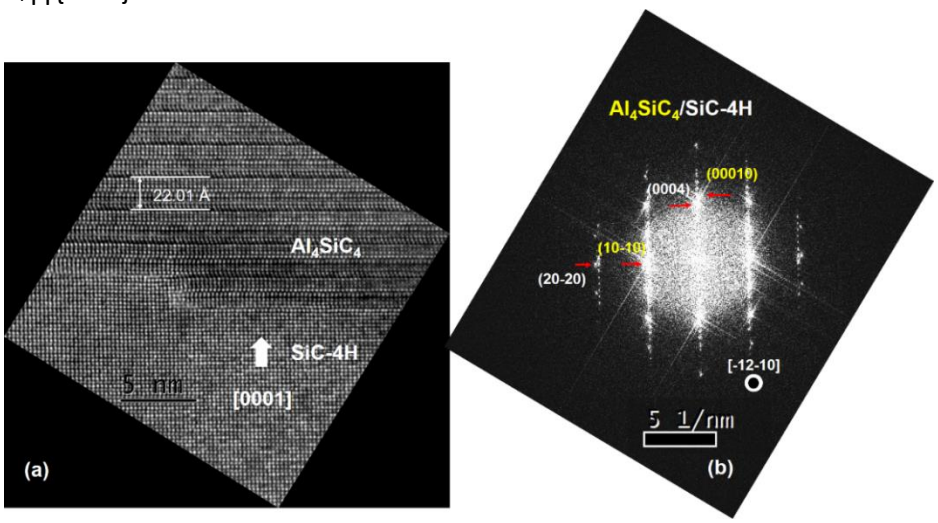

Figure 21. *(a) HRTEM image of the interface between Al_4SiC_4 and [0001] oriented SiC-4H. (b) Indexed FFT of (a).*

The GPA strain analysis is conducted by the use of the 10-10 spatial frequencies is given in Figure 22 using a Gaussian mask of 0.5g (nm^{-1}). Considering that the strain is zero in the SiC substrate as being our reference, the strain in Al_4SiC_4 layer is measured equal to 3 ± 0.6 %. The calculated GPA strain using the bulk interplanar distances is equal to 6.3%. This means that the Al_4SiC_4 is compressed along the *a* direction. From the GPA analysis the *a* lattice constant of the Al_4SiC_4 epilayer is measured equal to a_{epi}=3.175 ± 0.017 Å smaller than the bulk value of 3.28 Å.

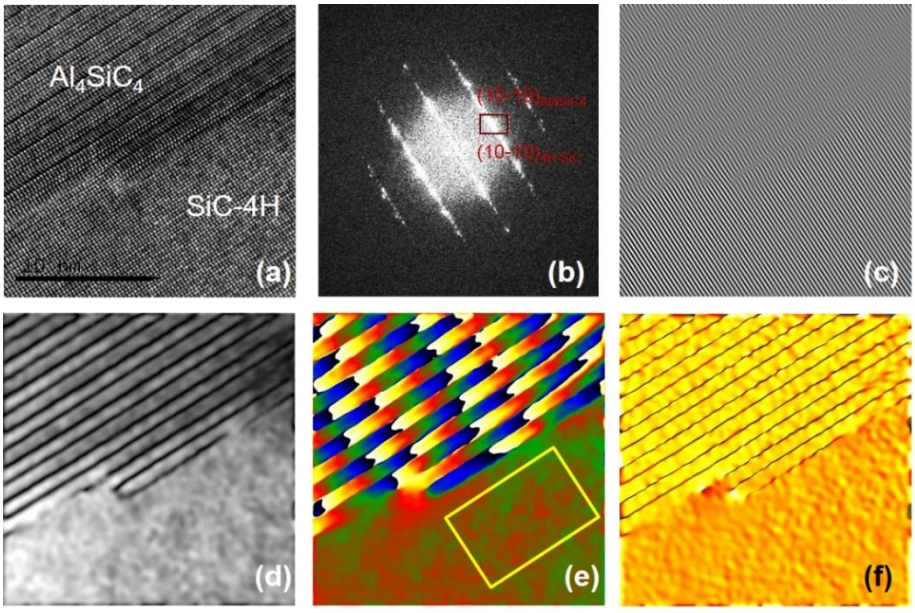

Figure 22. *GPA strain analysis along the [10-10] direction. (a) HRTEM image of the interface. (b) Power spectrum of the image (a) allowing to select a frequency* ***g*** *by a Gaussian mask, which corresponds to the position of the diffraction spots of the plane* $(10\text{-}10)_{Al_4SiC_4}$ *and* $(10\text{-}10)_{SiC}$*. (c)The Bragg image of the filtered Fourier transform. (d) The amplitude image of the inverse filtered Fourier transform. (e) The phase image with the chosen reference region inside the SiC substrate. (f) The strain field along the [10-10] direction.*

The GPA strain analysis conducted using the 000l spatial frequencies is given in Figure 23. A Gaussian mask of 0.5g (nm^{-1}) was applied. The calculated GPA strain using the bulk interplanar distances is equal to 7.9%. On average, the measured GPA strain is higher than the calculated one marked by the blue line in Figure 23(f). Thus, the lattice constant *c* of the Al_4SiC_4 epilayer is higher than the *c* of the relaxed structure. This means that the Al_4SiC_4 is tensiled along the *c* direction.

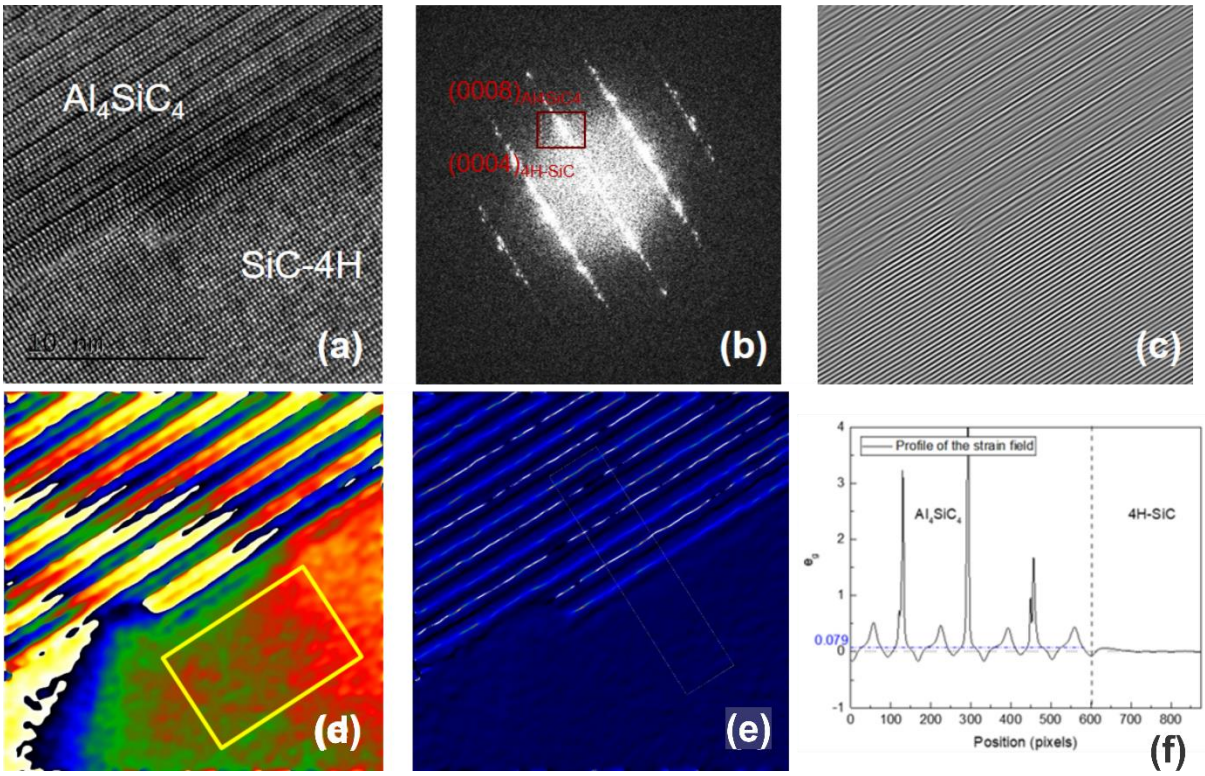

Figure 23. *GPA strain analysis along the [0001] direction. (a) HRTEM image of the interface. (b) Power spectrum of the image (a) allowing to select a frequency* ***g*** *by a Gaussian mask, which corresponds to the position of the diffraction spots of the plane* $(0008)_{Al_4SiC_4}$ *and* $(0004)_{SiC}$*. (c)The Bragg image of the filtered Fourier transform. (d) The phase image with the chosen reference region inside the SiC substrate. (e) The strain field along the [0001] direction (f) Strain profile corresponding to the outline presented in (e). The relaxed strain of* Al_4SiC_4 *is given by the blue dot line.*

The biaxial strain found at the interface of Al_4SiC_4 epilayer and 4° off axis 4H-SiC substrate is probably related with the misorientation of the substrate and the absence of an interfacial superstructure layer. In case of vicinal substrates, since the growth is governed by the step flow growth mechanism, strains and defects (i.e. dislocations) are introduced at the interfacial steps to accommodate the change in stacking sequence and the lattice mismatch in the growth direction [21].

An atomic model has been built to simulate the interface structure of Al_4SiC_4/4H-SiC shown in the HRTEM image (Figure 24). The Al_4SiC_4 epilayer has been grown on the 2c step of 4H-SiC substrate and the interface has been indicated by the black lines. The atomic model is just an arrangement of the relaxed lattice structures, thus it is rather different to the structure observed in the HRTEM images, where the Al_4SiC_4 epilayer is not relaxed. However, some similarities could be observed. Indeed, the shift of the atomic plane indicated by the red line, are observed in both images, which are caused by the different stacking sequence and lattice mismatch between $2\boldsymbol{c}$ of 4H-SiC and $\boldsymbol{c}$ of Al_4SiC_4 ($\Delta\boldsymbol{c}$ = 1.6 Å). Beside of that, an interfacial dislocation is also observed (**T**) in order to accommodate the in-plane lattice mismatch Δa between Al_4SiC_4 and 4H-SiC.

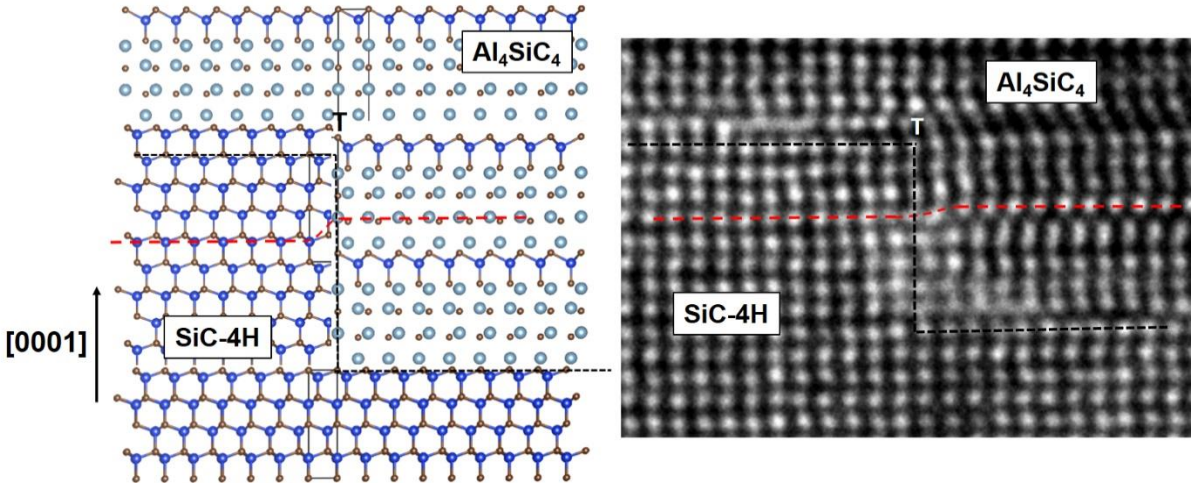

Figure 24. *High resolution TEM image of the interface of Al_4SiC_4/4H-SiC and corresponding atomic model. The zone axis of the TEM image is [-12-10]. The Al_4SiC_4 has been grown on 2c step of 4H-SiC substrate and the interface has been indicated by the black lines.*

CONCLUSION OF THE CHAPTER

Knowing that SiC alone cannot cover all the applications currently handled by toxic or less abundant elements and that SiC-based heterostructures are still limited since only heterostructures using different SiC polytypes have been explored, two different materials and heteroepitaxial structures of the Al-Si-C system have been investigated: Al_4C_3/SiC and Al_4SiC_4/SiC. The properties of these heterostructures in terms of crystallographic orientations, growth mechanism and epitaxial relationship, strain state, have been mainly analysed at a nanoscopic scale by using different TEM methods.

The optical absorption of Al_4C_3 crystals are studied and the bandgap is measured at 2.3 eV, which is much higher than the calculated one reported in the literature and validated by our DFT based investigation on the structural, electronic and vibrational properties of the Al_4C_3 [9].

An indirect process based on the chemical interaction between Al deposit and the Si face of [0001] oriented 6H-SiC substrate has been proposed to fabricate the Al_4C_3/SiC heterostructure. As product of the reaction, Al_4C_3 layer is formed at the interface of Al and SiC. By using different characterization methods, the wetting behaviour of the system, as well as the dissolution-precipitation of Al_4C_3 layer at the interface has been verified. Using electron diffraction analysis, the only epitaxial relationship between Al_4C_3 layer and [0001] oriented Si-face 6H-SiC substrate was along the *c* growth axis. On the basal plane, no epitaxial relationship was found, since the {10-11} planes of Al_4C_3 and the {10-11} planes of 6H-SiC form an angle of 3.5°. A strain analysis at interface of the heterostructure has been conducted using the GPA method on HRTEM images as function of annealing duration. At early stage of the reaction (i.e. after 2 hours), a biaxial strain was found. Indeed, the lattice structure of Al_4C_3 is compressed along the growth direction and extended along the basal direction leading to a strained crystalline structure. As the reaction proceeds further (i.e. after 4 hours annealing), with the increasing of the thickness, the lattice structure of Al_4C_3 epilayer is nearly relaxed when reaching the interface with the top Al layer. The biaxial strain observed at early stage is almost elastically relaxed.

For Al_4SiC_4/SiC heterostructure, the sublimation growth process has been used. The Al_4SiC_4/SiC heterostructures have been fabricated using two different types of substrates: [0001] on-axis C-face 6H-SiC and [0001] 4° off-axis C-face 4H-SiC. From the electron diffraction analysis a fully epitaxial relationship between the two materials was found with the {11-20}Al_4SiC_4||{11-20} 6H-SiC as well as {000l}Al_4SiC_4||{000l} 6H-SiC. For the Al_4SiC_4/4° off-axis 4H-SiC heterostructure a fully epitaxial relationship between the two materials is also found as following: {10-10}Al_4SiC_4||{10-10} 4H-SiC and {000l}Al_4SiC_4||{000l} 4H-SiC. According to the GPA strain field analysis, a different elastic behaviour has been observed for different type of substrates. In the case of the growth on on-axis C-face 6H-SiC substrates, the relaxation of the Al_4SiC_4 epilayer has been demonstrated through the negligible difference between the lattice constant of the epilayer and the bulk material. The lattice mismatch of about 6.5% is accommodated by the presence of an interfacial layer. However, for the growth on off-axis C-face 4H-SiC substrates, no interfacial layer was observed, leading to a significant biaxial strain and the presence of misfit dislocations the interface, introduced to accommodate the lattice mismatches both in the basal plane and along the growth direction.

Chapter 2 : Nitrides

Nitrides occupied me for a long period of my scientific life! It started in my master's thesis in 1999 where I worked on extended defects and more specifically stacking faults in GaN. Then my PhD was on the structural characterization of nitride nanostructures (i.e. AlN and/or GaN quantum wells and quantum dots) using various TEM-based methods. The research that I carried out during the two years following my thesis also focused on nitrides and in particular on Mn-doped GaN but this time assuming their growth by molecular beam epitaxy and their magnetic characterization. When I jointed the LMGP, although I didn't initiate any research subject on nitrides, I had to ensure the TEM characterization of samples from a European project (minimum 10 samples per year) via a subcontract. In this chapter, I give the main conclusions of my ATER and post-doctoral research on GaM:Mn because they have a link with my future perspectives. Another nitride that I had the opportunity to characterize structurally thanks to a collaboration with researchers from the SIMAP laboratory in Grenoble, is NbN and (Nb,Ti)N. This work will not be presented in this manuscipt but all the obtained results can be found in ref [22] which includes the main results on (Nb,Ti)N and Manoel Jacquemin's thesis on NbN [23].

(Ga,Mn)N semiconductor: a diluted magnetic wide band-gap semiconductor

My Goal: *Achieve the growth of high structural quality (Ga,Mn)N films by molecular beam epitaxy and characterize their magnetic properties.*

Collaborations: *E. Monroy, H. Mariette from CEA Grenoble // F. Wilhelm, A. Rogalev from ESRF, Grenoble // R.M. Galera, J. Cibert from Institute Neel, Grenoble*

In early 2000, Dietl's paper in Science [24] stimulated worldwide research on wide band gap dilute magnetic semiconductors (DMS) due to the prediction of above room temperature ferromagnetism for materials such as (Ga,Mn)N, (Zn,Mn)O and Mn-doped diamond. In the case of (Ga,Mn)N, the debate was quite challenging because, while theoretical calculations predicted a low Tc [25-26], we could find in the literature experimental works predicting for their (Ga,Mn)N films a ferromagnetic state with a T_C that varies from liquid helium [27] up to 940 K [28]. In this context, I started my one-year ATER contract in the CEA-CNRS-UJF "Nanophysics and Semiconductors" mixed group (together with the CEA Grenoble) in October 2004 and stayed until September 2006 as a post-doctoral fellow at CEA Grenoble to finish the work! Before reaching the stage where we could magnetically characterise our (Ga,Mn)N film, I did a enormous work optimising the growth of the layers as they suffered from parasitic phases which happen to be ferromagnetic! I cannot thank my mentor Eva Monroy enough for teaching me how to use the molecular beam epitaxy chamber and all the secrets of growing high-quality nitrides. She was there to encourage me not to give up, because for the first six months, as soon as I opened the Mn source, the RHEED patterns turned into a "sky full of stars"! The fact that I had a new approach and a new perspective in growth as I had never done this before helped me to keep the faith and try new approaches as I had no habits as a novice. It is funny to say that my first pure (Ga,Mn)N film was grown on my 30th birthday (I remember cancelling the big party at the last minute as for the first time I had a nice RHEED pattern in the screen and I couldn't just stop growing and go party!

In Figure 1 we can see RHEED patterns from my (Ga,Mn)N films [29]. In (a) we can see a characteristic RHEED pattern of a low structural quality (Ga,Mn)N films since we see additional spots from the secondary phases in the pattern. A typical RHEED pattern for the optimal conditions is shown in Figure 1 (b) and the absence of secondary phases is further confirmed by XRD pattern. In figure 1 (c) we see the case of heavily N-rich conditions (Ga/N < 0.90), where Mn is substitutionally incorporated into the wurtzite lattice, but the surface morphology becomes rough. Thanks to these conditions N-rich conditions we managed to grow (Ga,Mn)N inside an AlN matrix.

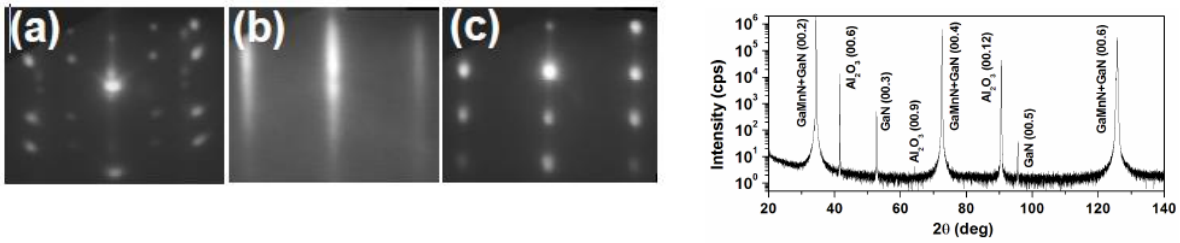

Figure 1 : *RHEED patterns in the < 1120 > azimuth for (a) Mn accumulation on the surface, (b) optimal growth conditions, (c) extremely N-rich conditions, all with the same Mn and (left side)* X-ray diffraction 2θ - θ scan of a (Ga,Mn)N epilayer with 6.3% Mn.

Once the growth was optimised, I discovered a host of new possibilities for the magnetic characterisation of films. Many new collaborations were initiated and, for the first time, I had the opportunity to make measurements with the synchrotron and analyse the data. Figure 3 [29] gathers the obtained experimental and theoretical results we obtained from XANES (X-ray Absorption Near Edge Structure) and XLD (X-ray Linear Dichroism) experiments recorded at the Ga and Mn K-edges in beamline ID12 of ESRF. We notice that ,the XLD spectrum recorded at the Mn K-edge exhibits very similar spectral shape as the spectrum at the Ga K-edge, but with a 1.8 times smaller amplitude. In contrast, the XANES spectra at the Mn K-edge are quite different from those recorded at the Ga K-edge. From simulations done using the FDMNES code [30], we have calculate the edge part of the Ga and Mn K-edge XANES and XLD spectra for a GaMnN supercell corresponding to the Mn content (using the lattice parameter of bulk GaN). For all possible Mn sites occupation (i.e. Mn in Ga site, Mn in N site or Mn in interstitial site), we observed a very good agreement in spectral shape and amplitude between calculated and experimental XANES and XLD spectra for both Mn and Ga atoms only for the case where Mn atoms substitute Ga atoms. The Mn K-edge XLD signal was the same in shape and in amplitude (within 3%) for all measured (Ga,Mn)N samples with a Mn concentration ranging from 6.3% down to 0.04% defined previously by SIMS. At that low concentrations, the presence of secondary phases is unlikely. Moreover, if metallic Mn cluster or $GaMn_3N$ or Mn_4N phases were present in our samples, that would be manifested in both the XANES and the XLD spectra which was not the case. As a conclution, the XLD experiments allowed us to say that the Mn atoms are Ga substituted and do not reveal the presence of any secondary phases or metallic clusters.

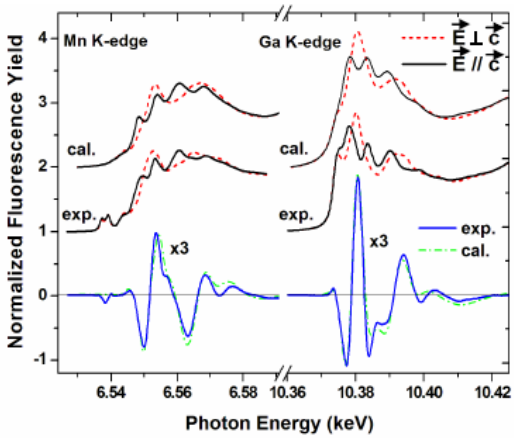

Figure 2: *Normalized experimental XANES spectra (shifted by 1) for linearly-polarized x-ray light oriented perpendicular and parallel to the c-axis and XLD (no shift, blue (dark grey) line) signal recorded at the Mn and Ga K-edge for a (Ga,Mn)N epilayer with 6.3% Mn. The calculated normalized convoluted XANES spectra (shifted by 2) are given together with the corresponding calculated XLD spectra (no shift, green (light grey) line).*

Magnetization measurements performed in a 5 T SQUID magnetometer, revealed the ferromagnetic order at 2K in our samples. In order to further demonstrate the intrinsic magnetic properties of (Ga,Mn)N, we have performed element selective magnetic studies using XMCD (X-ray Magnetic Circular Dichroism) measurements performed at the Mn K-edge [29]. The obtained results are given in Figure 3 where a very intense XMCD signal (1.6% with respect to the edge jump) is observed mainly at the first peak of the XANES spectrum. Knowing that the XMCD signal at the K-edge is proportional to the orbital polarization of the absorbing atom [31], our result clearly demonstrated that the Mn atoms in (Ga,Mn)N carry an orbital magnetic moment.

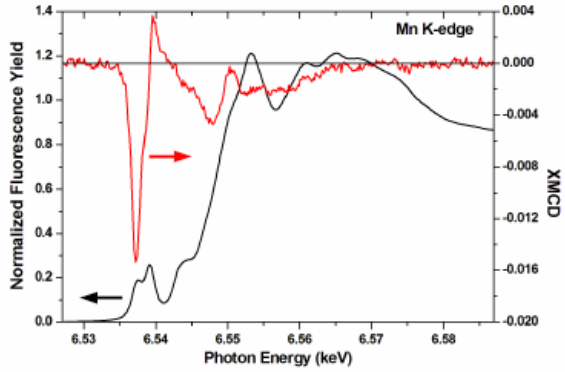

Figure 3: *Isotropic XANES spectra (left scale) and its corresponding XMCD signal (right scale) recorded at the Mn K-edge measured under 60 kOe in-plane field and at 7 K for a sample with 6.3% Mn.*

In conclusion, we achieved to demonstrate that wurtzite (Ga,Mn)N of high structural quality can be grown by plasma assisted MBE. Based on detailed structural analysis with x-ray diffraction and x-ray linear dichroism we show that Mn atoms occupy Ga sites with predominately valence 3+ state. Further, by combining macroscopic and element-selective magnetic measurements, we determined a spontaneous magnetic moment of 2.4 μB per Mn at 2 K and a T_C of only 8 K. Our results changed completely the state of research on GaN-based DMS since although the presence of intrinsic ferromagnetism in (Ga,Mn)N was confirmed the T_C was found very low (few Kelvin) excluding the use of (Ga,Mn)N in devices working in room temperature. In a personal level, these findings resulted in several invited talks in international conferences and in high sited publications.

Chapter 3 : Oxides

Since I joined the LMGP laboratory, I have discovered the world of oxides. I started with oxides such as $La_2Zr_2O_7$ used as buffer layers in $YBa_2Cu_3O_7$ based superconducting cables. Later I focused on ZnO, a wide band gap semiconductor that is very close in structure and in applications to the III-nitride semiconductors I worked on during my PhD and post-doc. In the last two years I have also had the opportunity to work on perovskites for nanoionic devices. In this chapter, I present some of the results obtained with emphasis on my personal contribution to these scientific activities.

$La_2Zr_2O_7$ an efficient buffer layer for YBCO based superconductors

My Goal: Characterize the $La_2Zr_2O_7$ (LZO) thin films in order to check their microstructure after the various annealing steps and their compatibility with the deposition of the $YBa_2Cu_3O_7$ superconductor on metal tapes of Ni based alloys.

Collaborations: *L. Porcar, J.-L. Soubeyroux, P. Odier-Institut Neel, C. E. Bruzek-Nexans, Thierry Waeckerle Aperam*

In the field of applied superconductivity, wires and tapes based on coated conductors are of great interest. Achieving the epitaxial growth of $YBa_2Cu_3O_7$ (YBCO) on metal tapes of Ni based alloys using buffer layers in between to act as diffusion barrier against nickel and oxygen while transferring the epitaxial growth was a nice challenge. In this perspective, the use of La2Zr2O7 (LZO) in a pyrochlore structure has proven to be an effective buffer layer [32,33]. However, when grown by Metal Organic Decomposition (MOD) process, chosen as a low-cost technique compatible with the willing of scaling up the new generation of coated conductors to an industrial environment, it suffers from presence of voids that are detrimental to the role of LZO as oxygen diffusion barrier. The formation of voids is attributed to the MOD process [34], since the microstructure of LZO prepared by other chemical routes such as MOCVD shows a dense layer [35]. Hence, those voids should be inherent to the growth mechanism occurring during chemical solution deposition. In particular, they can be attributed to the pyrolysis process since evacuation of the pyrolysis products proceeds via diffusion in the viscous matrix for a given temperature range. The shape and size of those voids were found to vary with the annealing treatment [34], for instance their size increased with decreasing heating ramp. When I joined the project, we hired a post-doc (Virginie Roche) that I co-supervise together with Carme Jimenez. The goal was to optimise the annealing process in purpose to obtain LZO buffer layers with a microstructure compatible to act as diffusion barrier against nickel and oxygen while transferring the epitaxial growth to the superconducting YBCO layer. The obtained results can be found in reference [36]

We achieved the optimisation by introducing an out-gassing /pyrolysis plateau under vacuum at low temperatures and before the crystallization step at 980°C. To reach this optimised "recipe" the following parameters were varied and controlled: plateau temperature, pyrolysis

atmosphere, dwell duration, heating ramp and decrease of the LZO layer thickness but coating multiple time to ensure a good diffusion barrier during YBCO deposition. The deposited films and their microstructure were characterised by XRD, EBSD (Electron BackScattered Diffraction), FTIR (Fourier Transform InFrared) and of course several means of TEM. The optimum pyrolysis temperature was defined to be 350°C under vacuum rather than a continuous $Ar+H_2$ flow of 30 slh. Under these conditions and a duration between 30-60min, smaller pores, with a lower variance in size distribution were reached as it can be seen in Figure 1.

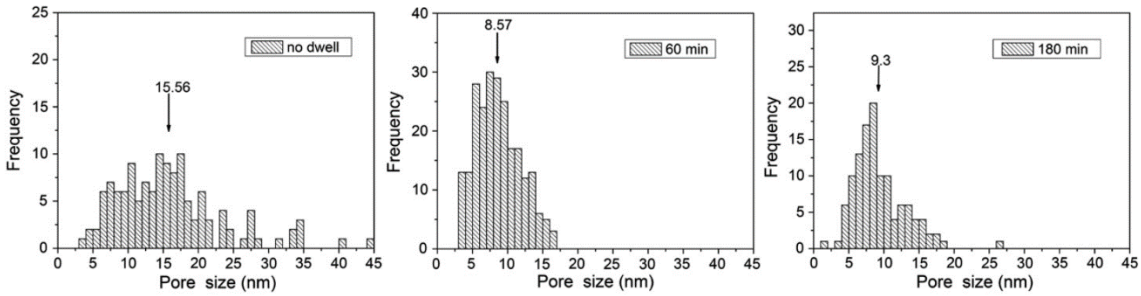

Figure 1: *Histograms of the pore size for samples pyrolysed at 350°C for different times and crystallized at 980°C. The heating ramp used for these samples was of 500°C per hour. Pore size was obtained from measurements made on different areas of various TEM images of LZO layers grown on $LaAlO_3$ substrates. The average value is shown on each graph.*

In order to evaluate the impact of carbon in our double dip LZO layers we realised Energy-Filtered Transmission Electron Microscopy (EFTEM) measurements. EFTEM mapping at the C K-edge has revealed the carbon influence on homogeneous nucleation which provokes the loss of epitaxy during the crystallization step. The presence of carbon at the double dip interface resulted in the stopping of the progression of the texture transmission between the two layers. The effect of carbon seems also important when pyrolysis is performed at temperatures lower than 350 °C, since we obtained layers which are not completely textured through the whole film thickness as it can be seen in Figure 2.

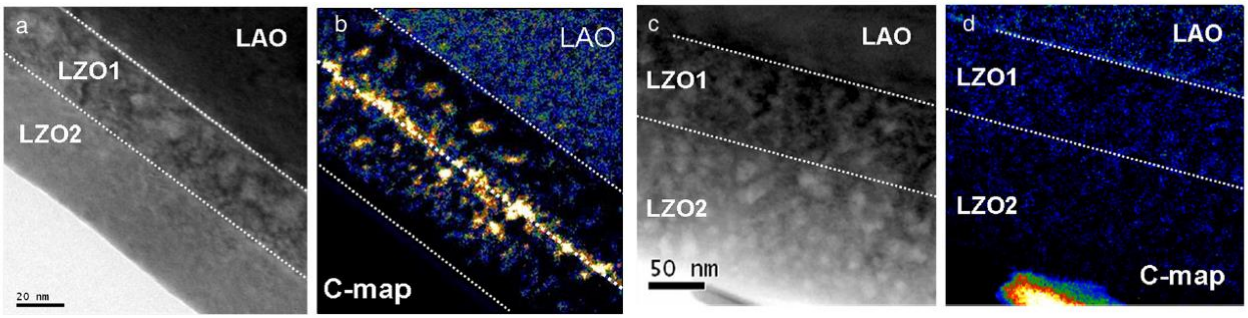

Figure 2: *EFTEM images obtained from two different tries of double dip LZO layers on $LaAlO_3$: (a, c) elastic electron images and (b, d) carbon mapping. White lines indicate the interface areas.*

After optimising the growth and annealing of the LZO buffer layer on both LAO and Ni-5 at.%W RABiTS®tapes of 80µm thickness, the next step was to grow and characterise the

superconducting YBCO layer in terms of microstructure, texture and magnetic measurements. Preparing TEM lamella of LZO/YBCO samples on Ni-5 at.%W RABiTS® tapes of 80µm thickness was more than challenging and demanded to invent a special set-up in order to succeed the "sandwich" and its mechanical polishing without affecting the structure of all the epilayers. Focus Ion Beam lamellas were also prepared for comparison. The results obtained from YBCO wires are described in reference [37]. Figure 3 gathers TEM images we obtained to characterize structurally the various layers. We can see from the dark field image in Figure 3(b) that the YBCO grains with lateral size in the range of 200nm are extended over the whole thickness. To estimate the disorientation angle between grains a parameter that is crucial to insure the superconducting properties of YBCO, we have proceeded as following: (i) we have oriented one of them along the [1,0,0] zone axis and registered the diffraction patterns of the neighbouring grains and (ii) we have compared the experimental diffraction images to disoriented calculated ones using the JEMS program [38]. From such comparison we have estimated that the disorientation angle between two grains is around 2.6° ±0.2° a result that was compatible with the EBSD measurements. The grains themselves present a very high structural quality with no defects as we can see from the high-resolution image of Figure 3 (a). The desired pyrochlore phase of the LZO buffer layer was confirmed by electron diffraction measurements (figure 3 (c).

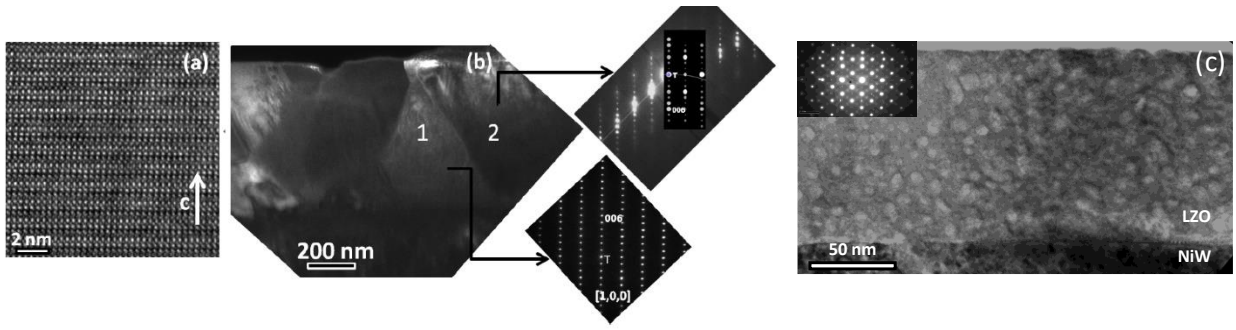

Figure 3: *TEM pictures obtained on a transversal cross section of an YBCO-covered wire. (a) High-resolution TEM image of grain 1. (b) Dark-field TEM image and corresponding diffraction patterns of grains 1 and 2. Grain 1 is oriented along the [1, 0, 0] zone axis. A calculated diffraction pattern corresponding to a disorientation angle of 2.6_ is superimposed to the experimental one from grain 2. (c) TEM image of an LZO buffer layer deposited on Ni-5 at.%W RABiTS®tape presenting the pyrochlore structure phase.*

A sharp Tc transition (1.4 K) above 90 K was measured for a sample presenting at 77 K a Jc medium value of 0.13 MA/cm^2, as measured by transport, and a locally Jc value of 0.3 MA/ cm^2. The weak point of this study remained the diffusion barrier of LZO. The entirety of the buffer layer is a key factor to avoid diffusion of NiW species in the YBCO layer during deposition, since the chemical contamination appears to be responsible for the low Jc values measured. A single LZO layer seems inadequate to overcome the mechanical strain valorising the previous mentioned results. That was the reason why we have tried double diped LZO layers mentioned previously. The oxidation of the Ni-5 at.%W RABiTS®tape substrates during the YBCO growth

forming an NiO layer varying from 150-1200nm at the LZO interface was revealed in one of the FIB lamella we observed. Figure 4 shows the obtained results. A bird eye view of our FIB prepared lamella is since in figure 4(a) from the assemble of several low magnification TEM images. The epitaxial relationship between the LZO buffer layer and the YBCO superconductor is seen in Figure 4 (b) from the electron diffraction. Generally speaking the YBCO layer present a high structural quality although some stacking faults have been identified. The porous nature of LZO is also put in evidence. The oxidation of the Ni-5 at.%W RABiTS®tape substrate is also seen since we distinguish two consecutive layers on the top of the substrate: a NiWO4 one and a NiO layer forming an interface with the buffer layer of LZO. Both electron diffraction and EDS experiments confirmed the above saying.

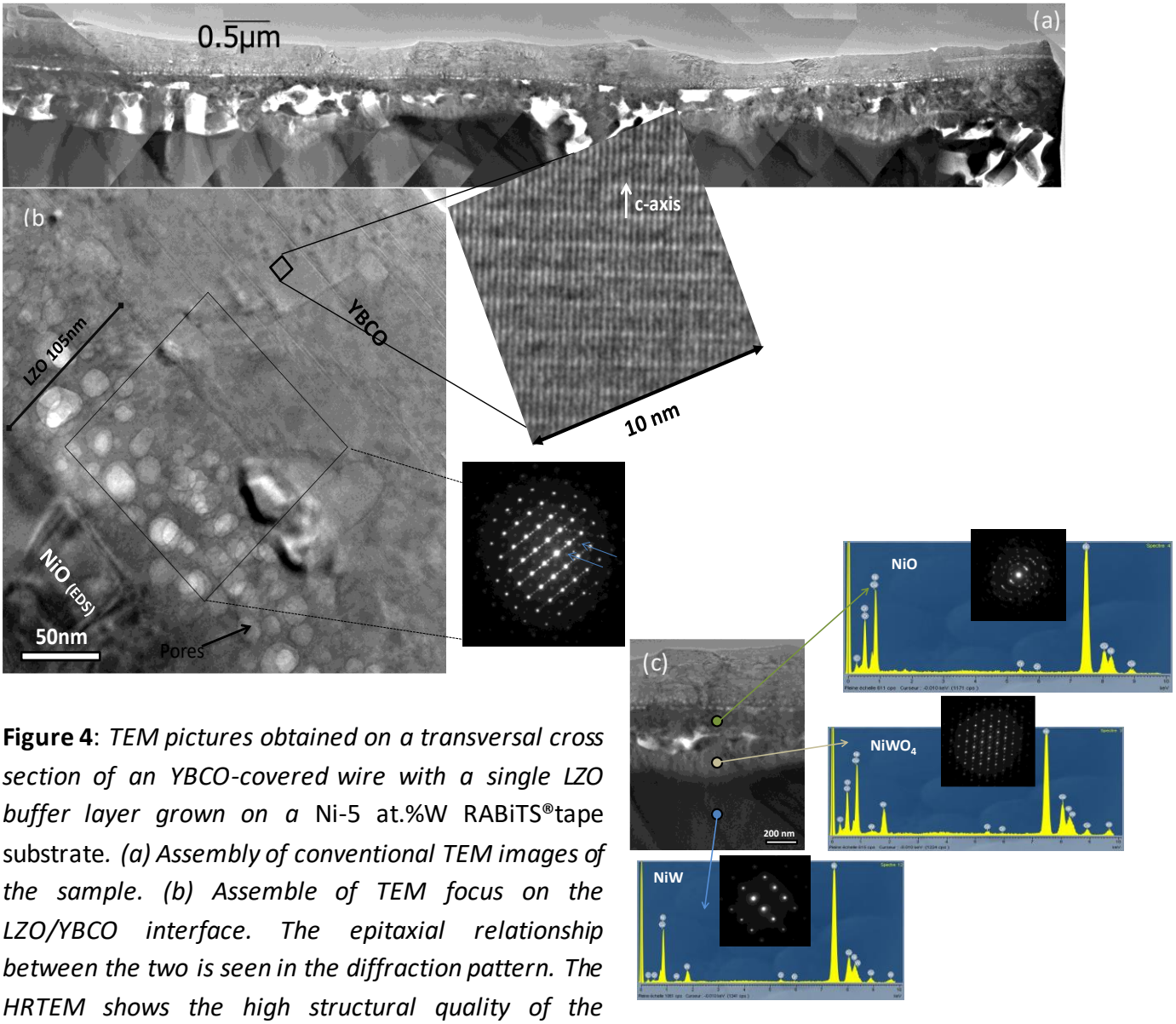

Figure 4: *TEM pictures obtained on a transversal cross section of an YBCO-covered wire with a single LZO buffer layer grown on a* Ni-5 at.%W RABiTS®tape substrate. *(a) Assembly of conventional TEM images of the sample. (b) Assemble of TEM focus on the LZO/YBCO interface. The epitaxial relationship between the two is seen in the diffraction pattern. The HRTEM shows the high structural quality of the deposited YBCO layer. (c) EDS profiles taken at 3 different areas in the lamella.*

The ZnO !

In this section, I will present four examples that I have selected to demonstrate that the use of various TEM techniques is crucial in advancing scientific research topics related to ZnO nanowires (NWs) and nanostructures.

Selective Area Growth of Well-Ordered ZnO Nanowire Arrays with Controllable Polarity

My Goal: Check the polarity (by CBED) and the structural quality (by HRTEM) of selective area grown ZnO nanowires

Collaborations: *A. Bocheux, I.-C. Robin from CEA-LETI, Grenoble /J. Kioseoglou from Aristote Univ. Of Thessaloniki, Greece and F. Robaut from CMTC, Grenoble*

The aim of these collaborative work was to achieve the formation of highly dense epitaxial ZnO NW arrays with high structural uniformity and controllable polarity by combining selective area growth (SAG), over large surface areas using patterned c-plane ZnO single crystals by electron-beam lithography and reactive ion etching with Chemical Bath Deposition (CBD) growth. All obtained results can be found in reference [39]. My contribution to this work was to investigate the structural morphology and growth mechanisms of ZnO NWs grown on patterned ZnO substrates by SAG as well as to determine their polarity, using Convergent Beam Electron Diffraction (CBED) measurements.

By convention in the wurtzite crystalline structure, that the O-polarity corresponds to the growth along the $[000\bar{1}]$ direction where the $[000\bar{1}]$ axis is considered as parallel to the O-Zn bonding, as depicted in Figure 1(b). In contrast, the [0001] axis is considered as parallel to the Zn-O bonding, hence the growth along the [0001] axis is defined as the Zn-polarity, as presented in Figure 2(b). The CBED technique is based on constructive and destructive interferences involving more than two diffracted electron beams. A contrast difference in the intensity distribution basically occurs within the (0002) and $(000\bar{2})$ diffracted discs of the CBED patterns, hence distinguishing between the O- and Zn-polarity of ZnO. The contrast difference depends both on the zone axis and crystal thickness as well as on the materials involved. It is well-established that the polarity of semiconductors with the wurtzite crystalline structure can reliably be characterized with the CBED patterns when collected along the $<10\bar{1}0>$ zone axis for a crystal thickness larger than 50 nm. The O- and Zn-polarity of bulk c-plane ZnO single crystals is revealed in Figure 1(c) and 2(c). Multiple experimental and simulated CBED patterns with EMS software using Block's wave method [38] were collected on different crystal thickness (i.e., smaller and larger than 100 nm) in order to unambiguously determine the polarity of ZnO NWs. The contrast difference of the (0002) and $(000\bar{2})$ diffraction disc is clearly revealed along the $<10\bar{1}0>$ zone axis in Figure 1(d) and 2(d) as well as the agreement between the experimental and simulated CBED patterns. Importantly, ZnO NWs are found O-polar when grown on O-polar c-plane ZnO single

crystals while they are Zn-polar when grown on Zn-polar c-plane ZnO single crystals. Consequently, ZnO NWs retain the O- or Zn-polarity of c-plane ZnO single crystals.

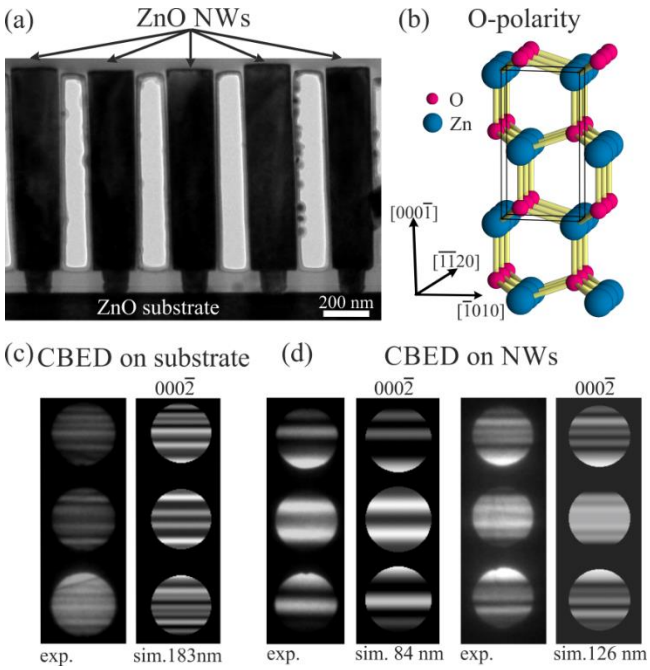

Figure 1. *(a) Low-magnification cross-section conventional TEM image taken along the <10$\bar{1}$0> zone axis of ZnO NWs grown by CBD on patterned O-polar c-plane ZnO single crystals. (b) Atomistic view along the <11$\bar{2}$0> direction of wurtzite O-polar c-plane ZnO. (c) Experimental and simulated CBED patterns taken along the <10$\bar{1}$0> zone axis for thickness of 183 nm, revealing that c-plane ZnO single crystals are O-polar. (d) Experimental and simulated CBED patterns taken along the <10$\bar{1}$0> zone axis for both thickness of 84 and 126 nm, showing that ZnO NWs are O-polar. The central disk is the transmitted electron beam.*

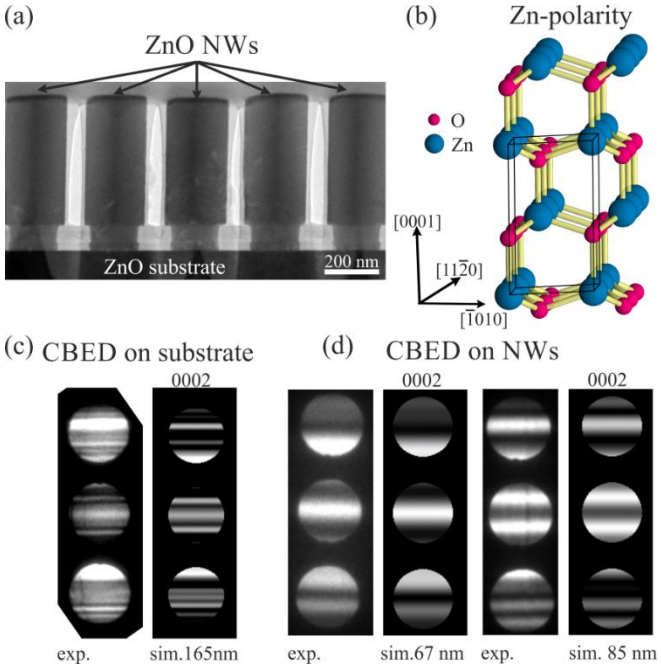

Figure 2. *(a) Low-magnification cross-section conventional TEM image taken along the <10$\bar{1}$0> zone axis of ZnO NWs grown by CBD on patterned Zn-polar c-plane ZnO single crystals. (b) Atomistic view along the <11$\bar{2}$0> direction of wurtzite Zn-polar c-plane ZnO. (c) Experimental and simulated CBED patterns taken along the <10$\bar{1}$0> zone axis for thickness of 165 nm, revealing that c-plane ZnO single crystals are Zn-polar. (d) Experimental and simulated CBED patterns taken along the <10$\bar{1}$0> zone axis for both thickness of 67 and 85 nm, showing that ZnO NWs are Zn-polar. The central disk is the transmitted electron beam.*

Further to the CBED measurements and simulations, extensive HRTEM images were recorded along the <11$\bar{2}$0> zone axis, especially on the interface area in between ZnO single crystals and NWs as well as along the growth of ZnO NWs in and outside the mask region. In

Figure 3, characteristic HRTEM images for both polarities are presented where the wurtzite crystalline structure is clearly undisturbed. If a basal inversion domain boundary had grown at the interface area or along the growth of ZnO NWs, a characteristic defect would have been identified in the HRTEM images: a basal IDB contains Zn-Zn and/or O-O bonds and hence it should disturb the …ABABAB… stacking sequence of the wurtzite crystalline structure. Our HRTEM images clearly reveal that ZnO NWs are free of any extended defects such as stacking faults, twins, dislocations or IDBs both at the interface area and inside or outside the mask region.

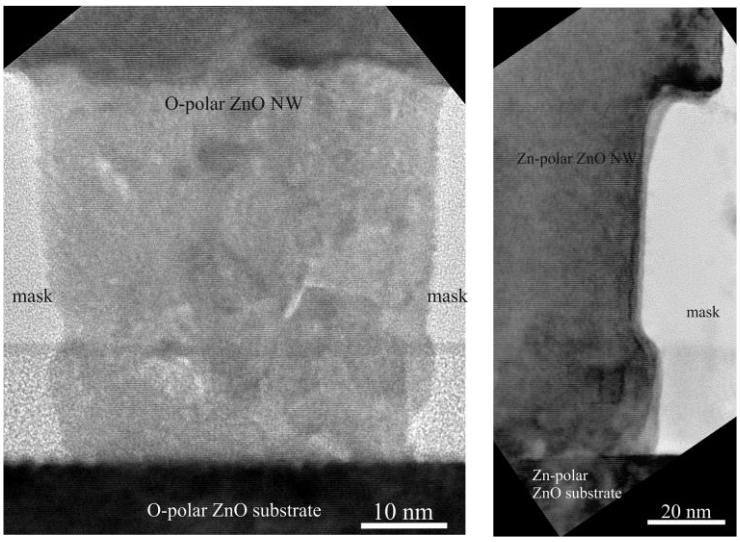

Figure 3: *HRTEM image taken along the <11-20> zone axis revealing the interface between: (left side) the O-polar ZnO NW and O-polar c-plane ZnO single crystal, (right side) the Zn-polar ZnO NW and Zn-polar c-plane ZnO single crystal as well as the region of the ZnO NW grown inside the double mask, and the interface between the ZnO NW grown inside and outside the hole delimited by the mask.*

Our findings were very important in the ZnO community, since we demonstrated the possibility to control the polarity of ZnO NWs grown in solution by SAG in addition to their position and structural uniformity (i.e., length, diameter, period). This is remarkable both fundamentally and technologically and differs from the growth of ZnO NWs by vapor phase deposition techniques, in which Zn-polar ZnO NWs are usually formed instead of O-polar ZnO NWs [40,41,42]. On the technological side, the control of the polarity, position and structural uniformity of ZnO NWs opens the way to their efficient integration in electronic, optoelectronic and photovoltaic devices. The need for assembling bare ZnO NW ensembles with a pure single polarity is essential for piezoelectric nanogenerators, in which the piezoelectric potential field along the polar c-axis is created under elastic deformation [43]. Further, the light management in ZnO NW ensembles for light emitting diodes or solar cells (i.e., dye-sensitized solar cells, [44] extremely thin absorber solar cells, [45] type II heterojunction solar cells, [46]) is strongly affected by the structural dimensions and uniformity of ZnO NWs.

In situ analysis of the nucleation of O- and Zn-polar ZnO nanowires using synchrotron-based X-ray diffraction

My Goal: Identify the structural characteristics of both O- and Zn- polar nucleation layers

Collaborations : *H. Renevier V. Cantelli, LMGP, F.Carlá ESRF, Grenoble // B. Bérini, J.M. Chauveau, Univ. Versailles Saint-Quentin, Versailles // D. Fong Argonne national laboratory, USA*

As we have seen from the previous analysis, the selection of the polarity of ZnO nanowires grown by chemical bath deposition offers a great advantage for their integration into a wide variety of engineering devices. In this study, we wanted to identify the nucleation process of ZnO nanowires and its dependence on their polarity. To investigate this major issue, we combined an *in-situ* analysis of the nucleation process of O- and Zn-polar ZnO nanowires on O- and Zn-polar ZnO single crystals, respectively, using synchrotron radiation-based grazing incidence X-ray diffraction with ex situ transmission and scanning electron microscopy. In this work, I was in charge of the TEM experiments and interpretation. The obtained results can be found in reference [47].

In order to reveal the morphology and crystalline phase and orientation of the ZnO nuclei grown on both O- and Zn-polar ZnO single crystals I performed conventional, high-resolution and Automatic phase and orientation mapping (ASTAR)TEM measurements. The ACOM-TEM [48] (or ASTAR if combined with a precession module) tool is similar to the electron backscattered diffraction (EBSD) technique used in SEM but for TEM. It allows the analysis of the structural state of materials through the indexing of the diffraction patters. In few words, the incident electron beam of a few nanometers in size and is processed to reduce the dynamical effects and to enhance the indexing quality with a precession system. The electron beam is simultaneously scanned over the area of interest to record an electron diffraction pattern at each location. The experimental electron diffraction patterns are compared with the complete set of theoretical diffraction patterns, which are computed for every expected crystalline phase and for a large number of orientations. The best match between the experimental and theoretical electron diffraction patterns allows the identification of both the crystalline phase and orientation with high precision.

As we can see in Figure 4 from the cross-sectional TEM images of ZnO nuclei grown on the O- and Zn-polar ZnO single crystals it exists several striking differences regarding their shape and size. ZnO nuclei grown on the Zn-polar ZnO single crystal exhibit an elongated shape marked by the formation of inclined facets with a mean tilt angle that is often close to 73° (or 107°), corresponding to the (2-1-11) planes, as seen in Figure 4(a). The mean in-plane diameter of ZnO nuclei grown on the Zn-polar ZnO single crystal is 66 ± 27 nm. Their mean out-of-plane length is larger and equal to 72 ± 25 nm. The aspect ratio of ZnO nuclei grown on the Zn-polar ZnO single crystal is therefore higher than 1, exhibiting an elongated shape that is fairly similar to the NW shape. In contrast, ZnO nuclei grown on the O-polar ZnO single crystal exhibit a platelet shape marked by the systematic formation of perpendicular facets corresponding to the low energy

non-polar m-planes, as seen in Figure 4 (e-f). The mean in-plane diameter of ZnO nuclei grown on the O-polar ZnO single crystal lies in the range of several tens of nanometers. However, their mean out-of-plane length is smaller and equal to 17 ± 2 nm. The aspect ratio of ZnO nuclei grown on the O-polar ZnO single crystal is consequently lower than 1, accounting for their platelet shape. The ASTAR maps given in Figure 4 (b-d), confirmed the homoepitaxial relationship of the ZnO nucleus with the ZnO single crystal substrate and revealed that all ZnO nucleus have the same crystal orientation which is along the <0001> growth direction.

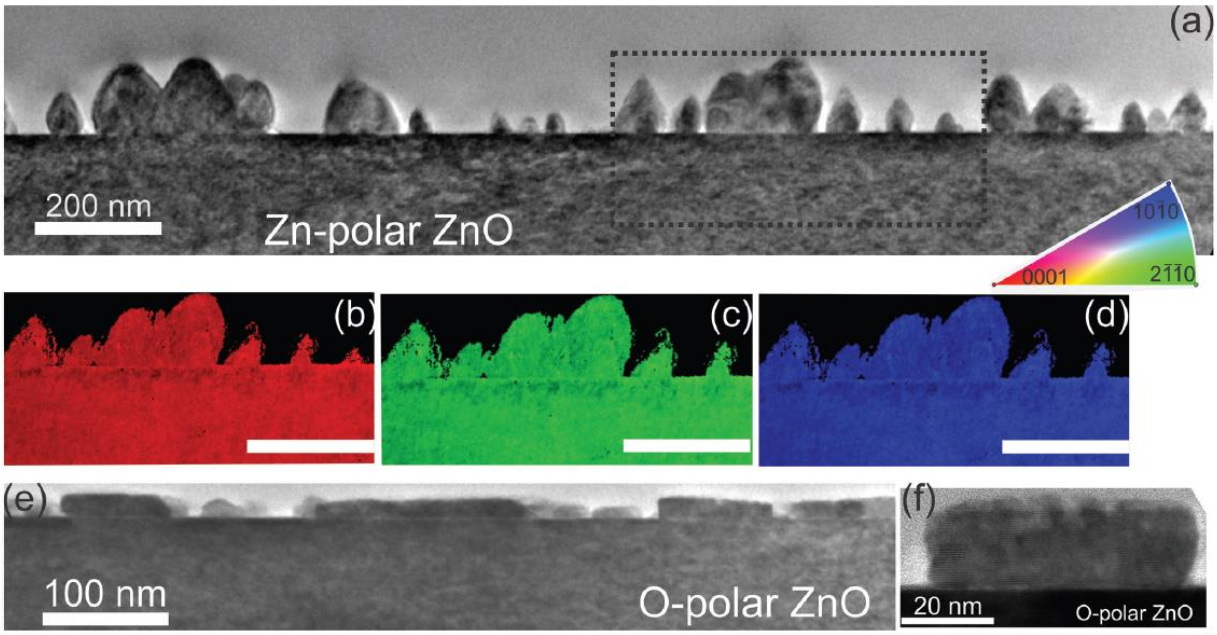

Figure 4: *(a) TEM image of ZnO nuclei grown on the Zn-polar ZnO single crystal along the ⟨01-10⟩ zone axis. ASTAR maps collected in the rectangular area representing the crystal orientation (b) along the ⟨0001⟩ growth direction and (c and d) along the perpendicular ⟨2-1-10⟩ and ⟨10-10⟩ directions, respectively. The color scale is given as an inset. The scale bar denotes 200 nm. (e) TEM image of ZnO nuclei grown on the O-polar ZnO single crystal along the ⟨2-1-10⟩ zone axis. (f) High-resolution TEM image of a ZnO nucleus grown on the O-polar ZnO single crystal.*

Using filtering of HRTEM images we further revealed that the ZnO nuclei preferentially form on defects located at the interface area such as surface steps as it can be seen in Figure 5.

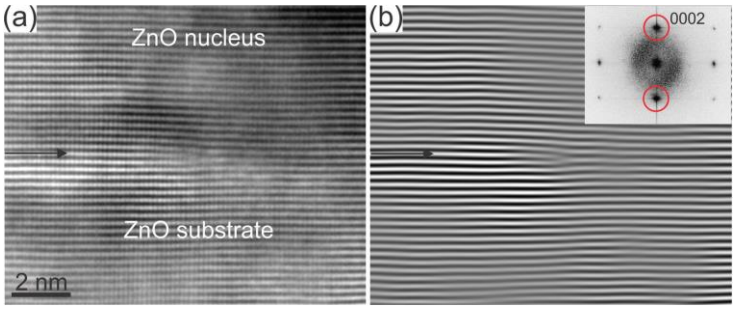

Figure 5: *(a) HRTEM image of the interface region between the ZnO nucleus and the Zn-polar ZnO single crystal. The arrow denotes the interface. (b) Corresponding 0002 Bragg image of the interface area through the use of a mask on the 0002 spatial frequencies to reveal only the (0002) planes. The inset shows the electron diffraction pattern with the 0002 peaks circled.*

In conclusion, in this work based on *in-situ* analysis of the nucleation process of O- and Zn-polar ZnO NWs grown by CBD on O- and Zn-polar ZnO single crystals, respectively, using synchrotron radiation-based GIXRD measurements with *ex-situ* TEM and FESEM imaging in different modes, we show that the formation of ZnO nanowires obeys three successive phases from the induction, through nucleation to growth phases. The characteristics of each phase, including the nucleation temperature, the shape and dimension of nuclei, as well as their radial and axial development are found to depend on the polarity of ZnO nanowires.

Spontaneous shape transition of thin films into ZnO nanowires with high structural and optical quality

My Goal: HAADF-STEM study of ZnO NW nucleus as well as EDS-STEM elemental mapping of the silicon, zinc and oxygen elements. ASTAR maps investigation, representing the crystal orientation.

Collaborations : *F. Donatini, Institut Néel, G. Renou, SIMAP, Grenoble // G. Bremond INSA Lyon*

In this study, we have explored an original way to form ZnO nanowire arrays by the spontaneous transformation of a ZnO thin film deposited by sol–gel process on a silicon substrate following a simple annealing under argon flux at 900°C for varying annealing times in the range of 30 min to 10 h. My contribution was to check the crystal quality of these object and provide information about their morphology, orientation, phase, defect presence and relation with the silicon substrate. The whole results of this work can be found in reference [49].

We have shown in our paper that the development of these ZnO NWs takes place via successive spontaneous shape transitions, involving the intermediate formation of full and truncated pyramid-shaped islands. The formation mechanisms are expected to be governed by thermodynamic considerations, in which the NW shape can minimize the surface energy in the absence of any significant strain and interface energy as well as edge energy. It is further assisted

by the drastic reordering of the matter via the massive transport of zinc and oxygen atoms towards the growth localized areas, which is also combined with concomitant massive recrystallization phenomena.

In order to investigate in more detail, the formation mechanisms of ZnO NW nuclei following the spontaneous shape transition process from a ZnO thin film, several TEM and STEM measurements are made as seen in Figures 6–8. A typical low-magnification TEM image taken along the $<11\bar{2}0>$ zone axis of a ZnO NW nucleus with a diameter of 170 nm at its bottom and a length of 150 nm is presented in Figure 6(a). The ZnO NW nucleus lies on a ZnO thin film with a thickness of about 26 nm, which is composed of very small ZnO grains with a mean diameter smaller than 8 nm, as shown by HRTEM, HAADF-STEM and ASTAR images of Figures 6(c), 7(a) and 8, respectively. An amorphous phase also occurs between these ZnO grains as revealed in Figure 6(c). This may be related to the native amorphous silicon oxide surface on the (100) silicon substrate, on top of which ZnO thin film and nanostructures are nucleated. The ZnO NW nucleus is lightly tapered through the presence of slightly rough side facets with a tilt angle of about 75° with respect to the substrate surface, which is larger than the mean tilt angle of about 60 to 70° for the pyramid shaped islands. Furthermore, it has a wurtzite crystalline phase and is oriented along the polar c-axis, as shown by the SAED pattern in the inset of Figure 6(a). Owing to the hexagonal section of ZnO NW nuclei, their sidewalls are therefore composed of non-polar planes. Interestingly, the ZnO NW nucleus is almost free of any extended defects, apart from the occurrence of few I_2-type stacking faults (SFs) at its very bottom. The I_2-type SF sequence is AaBbCcAaCc. [50] Two of them are shown in Figure 6(d) together with a $10\bar{1}0$ Bragg filtered image in (e), which reveals a shift of the $(10\bar{1}0)$ planes characterizing the basal SFs in the wurtzite crystalline phase. It should be noted that the absence of a c/2 component in the 0002 Bragg filtered images allowed us to distinguish these I_2-type SFs from the I_1-type SFs. The formation of these SFs is probably related to the shape transition process itself that may involve stress effects.

To check the chemical composition of the nuclei, we conducted HAADF-STEM and EDS-STEM experiments. The obtained results are shown in Figure 7. We can clearly see that the zinc and oxygen atoms are homogeneously distributed in the ZnO NW nucleus and thin film. Silicon atoms are mainly located in the substrate, but a small proportion of these atoms is also measured in the centre of the thin film composed of ZnO grains. In contrast, no silicon atoms are revealed in the ZnO nanostructures. It is thus very likely that these silicon atoms are not incorporated in the ZnO grains, but are located in the amorphous phase between the small ZnO grains.

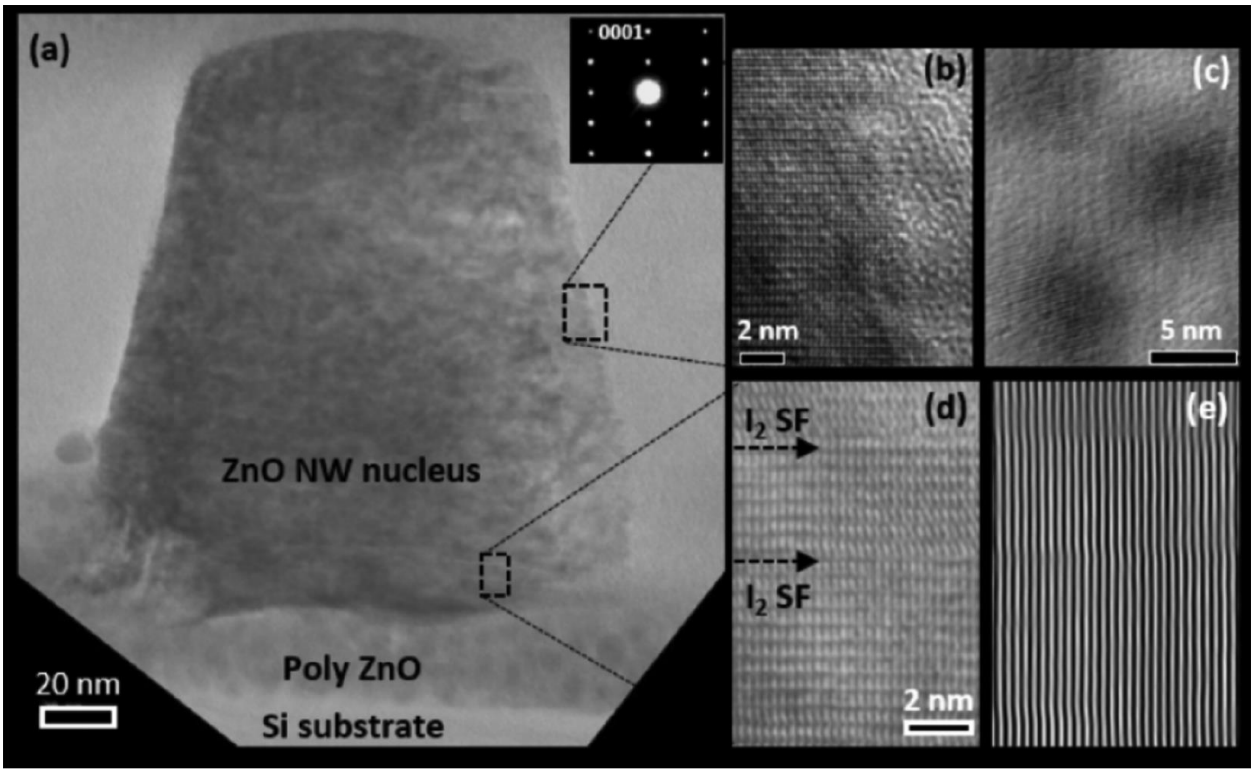

Figure 6. *(a) Low-magnification TEM image of a ZnO NW nucleus spontaneously formed on top of the ZnO thin film during the third step of the process. The inset is a SAED pattern of the ZnO NW nucleus. (b) HRTEM image of the slightly rough side facets of the ZnO NW nucleus (dotted rectangle area in (a)). (c) HRTEM image of the ZnO grains composing the underneath ZnO thin film (dotted rectangle area in (a)). (d) HRTEM image of the ZnO NW nucleus at its bottom, showing the occurrence of I_2-type SFs close to the interface with the ZnO thin film. (e)* $10\bar{1}0$ *Bragg filtered image of (d) revealing the shift along the* $(10\bar{1}0)$ *planes that is characteristic of I_2-type SFs. All TEM images are collected along the* $<11\bar{2}0>$ *zone axis.*

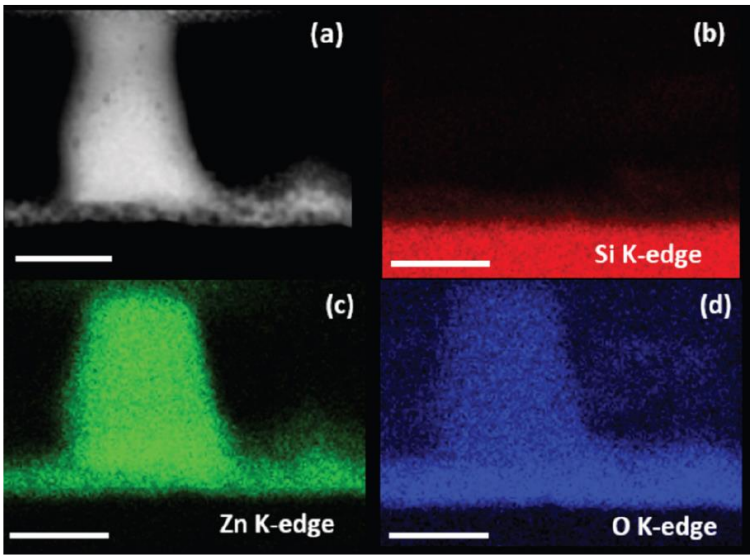

Figure 7: *(a) HAADF-STEM image of a ZnO NW nucleus spontaneously formed on top of the ZnO thin film during the third step of the process. (b–d) Corresponding EDS-STEM elemental mapping of the silicon, zinc and oxygen elements, respectively. The scale bar is 100 nm.*

The local orientation of the ZnO NW nucleus and of each ZnO grain composing the underneath thin film is presented in Figure 8 by ASTAR images. The orientation of the ZnO NW nucleus along the polar c-axis is confirmed in red color in Figure 8 (a), although the majority of ZnO NW nuclei are twisted with each other as seen in Figure 8 (b). More interestingly, the underneath thin film consists of randomly oriented ZnO grains with a very small diameter. This is in contrast to the initial highly textured ZnO thin film, suggesting that massive recrystallization phenomena also take place during annealing. In particular, no specific nucleation sites consisting in c-axis oriented ZnO grains for instance are revealed, in contrast to the typical formation mechanisms of ZnO NWs by CBD. [51] In that sense, the ZnO NW nucleus has no structural relationship with the underneath ZnO thin film.

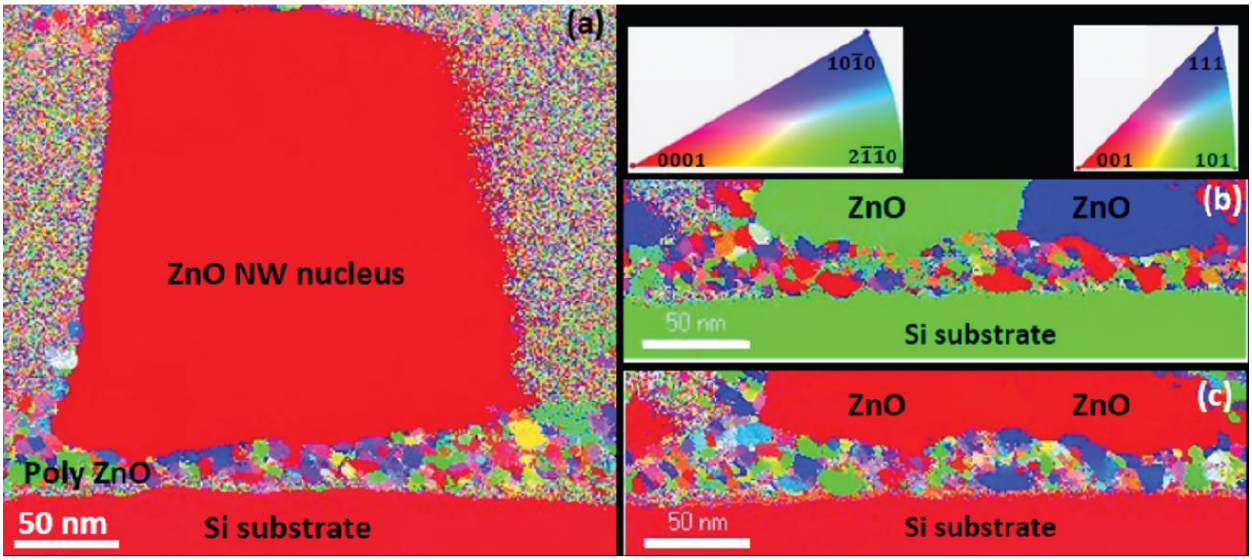

Figure 8: *ASTAR maps representing the crystal orientation (a) along the growth axis of a ZnO NW nucleus spontaneously formed during the third step of the process as well as (b) in the basal plane and (c) along the growth axis of the underneath ZnO thin film. The color scales are given in the insets.*

Taking into account both the high structural and optical quality of the resulting ZnO nanowires, these findings open the way to the technological development of a promising approach with a great potential (i.e. low-cost and easiness of sol–gel process and simple annealing) that is alternative to the more usual bottom-up approach.

Morphology Transition of ZnO from Thin Film to Nanowires on Silicon and its Correlated Enhanced Zinc Polarity Uniformity and Piezoelectric Responses

My Goal: Structural investigation of ZnO NWs and identification of basal stacking faults.

Collaborations: *G. Ardila and X. Mescot from IMEP-LAHC, Y. Guerfi, F. Bassani and B. Salem from LTM, F. Donatini Institut Neel.*

In this work, using Pulsed-Liquid Injection MOCVD (PLI-MOCVD), we have shown the morphology transition of ZnO deposits on silicon from stacked thin films to nanowires through columnar thin films by only varying the growth temperature from 400 to 750 °C while fixing the other growth conditions. Detailed analysis of their formation mechanisms has further been revealed with a complete growth diagram. The morphology transition results in a strong enhancement of the crystallinity of ZnO deposits and of their growth texture along the c-axis, together with massive relaxation of the strain in nanowires. This further leads to a prevailed zinc polarity, for which its uniformity is greatly enhanced in nanowires. The transition is additionally associated with a significant improvement of the piezoelectric amplitude, as determined by piezoresponse force microscopy measurements. My contribution to this work was related to the structural characterisation of the formed ZnO nanowires, with a special attention to the interface with the silicon substrate and the presence of defects such as stacking faults that influence the optical properties of the nanowires as confirmed by cathodoluminescence (CL) measurements. The whole study can be found in the reference [52].

A very important result that came out from the TEM experiments was the fact that the nucleation of ZnO nanowires is directly achieved on a very thin, amorphous, native SiOx layer without the formation of a continuous ZnO wetting layer. This is illustrated in the TEM image of ZnO deposits grown at 700 °C by PLIMOCVD given in Figure 9. The direct nucleation of ZnO nanowires on Si substrates without using any seed/wetting layers is remarkable in the MOCVD process. It is definitely in contrast to the formation of ZnO nanowires by chemical bath deposition, requiring the typical use of a polycrystalline ZnO seed layer. [53] The transition from thin films to nanowires as the growth temperature is increased was reported on the (0001) sapphire substrate in ref [54], for which the nucleation and growth mechanisms were driven by the epitaxy between the ZnO deposits and sapphire. In that sense, the orientation of sapphire substrates has a strong influence on the morphology of ZnO [55]. Instead, no epitaxial relationship occurs in the present case, as shown in Figure 9 (e). At the bottom of the c-axis-oriented nanowires, a polycrystalline thin layer with a thickness of several tens of nanometers is mostly oriented along the polar c- axis, as revealed in the selected area diffraction (SAED) patterns in Figure 9 (c) and by the HRTEM image in Figure 9 (e). It is basically formed prior to the formation of nanowires during growth. Following its thickening during growth, the development of vertical, elongated, c-axis-oriented grains prevail over the grains oriented along other directions during a

competitive process. This leads to the formation of isolated c axis- oriented nanowires with high density, as shown in the SAED pattern in Figure 9 (b) and by the TEM image in Figure 9 (a).

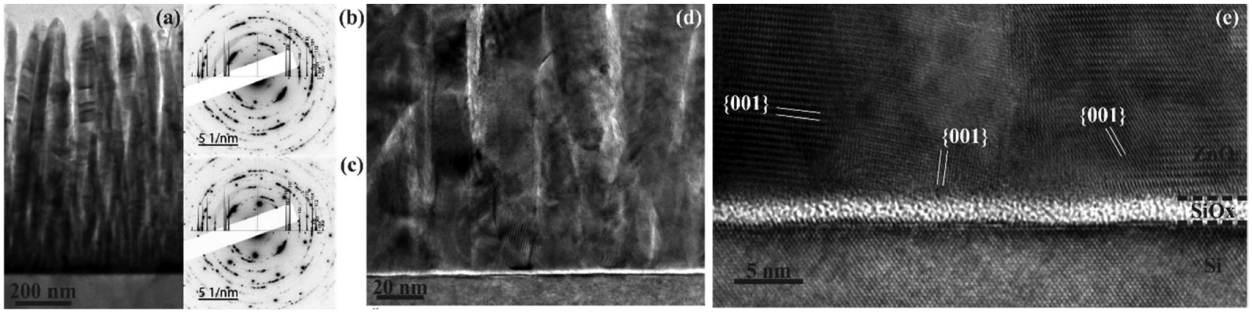

Figure 9: *(a) Low-magnification TEM image of nanowires grown at 700 °C by PLI-MOCVD. (b, c) SAED patterns recorded at the top and at the bottom of nanowires, respectively. (d, e) TEM and HRTEM images at the ZnO/Si interface, respectively.*

The TEM and HRTEM images in Figure 10 clearly reveal the presence of basal-plane stacking faults (BSFs) in the center of nanowires. They are basically identified as being of I_1-type with the plane stacking sequence ...ABABABCACACA.... [56] This type of BSF is typically not related to strain relaxation but nucleates during growth owing to its low formation energy. Importantly, the I_1-type BSFs are expected to form a quantum well-like structure that can confine excitons and induce an emission at about 3.321 eV in ZnO thin films and 3.329 eV in ZnO nanowires, as reported in refs [57, 58] respectively. Based on this observation, both the two-electron satellites (i.e., Al_{Zn} and carbon species) at 3.323 eV and the BSF line (i.e., I_1) at 3.329 eV contribute to the intense line located at the intermediate energy of 3.326 eV we observed in our CL spectra.

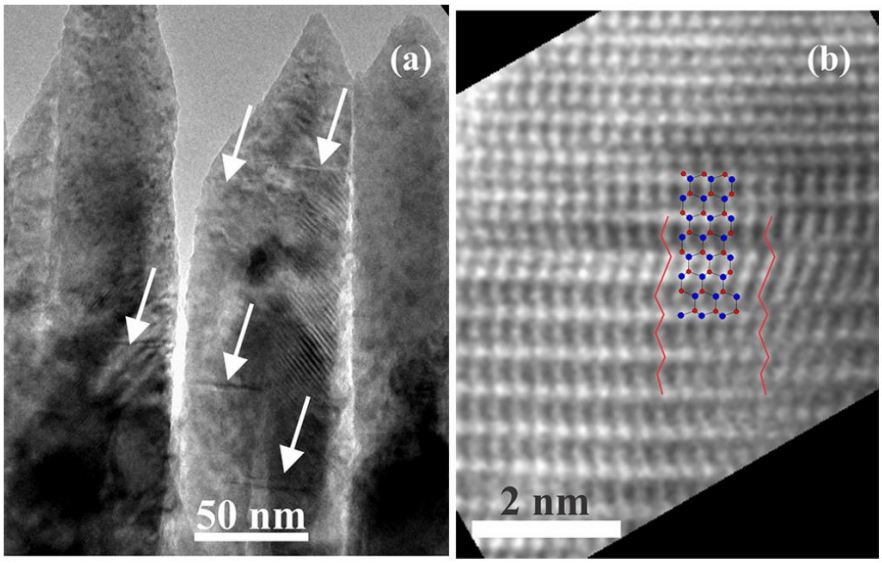

Figure 10: *(a) Low-magnification TEM image of ZnO nanowires grown at 700 °C by PLI-MOCVD. The arrows indicate the presence of BSFs. (b) HRTEM image, where the stacking sequences and atomic model of an I_1-type stacking fault have been superimposed.*

Conclusions and Perspectives

Considering that there is no doubt that Transmission Electron Microscopy (TEM) will bring significant impact in broad areas of research from materials science to physics, chemistry and biology my main research area was, is and will be TEM techniques. With the advances of TEM, it has been possible to achieve 0.7 Å spatial resolution using an aberration corrected TEM and electron energy loss spectroscopy (EELS) enables the study of materials with an energy resolution down 1 or 2 meV. Certain laboratories in Grenoble have state-of-the-art TEM machines and the collaborations already established will allow me to have access to them to carry out my future experiments.

The previous five years I was focusing in ZnO nanowires. The nature of intrinsic/extrinsic point defects governing the electronic structure properties of ZnO in its form of single crystals and epitaxial films has been highly debated over the last two decades [59, 60]. The oxygen vacancy (V_O) with its low formation energy over a broad range of Fermi level has been identified, in the past, as one of the major intrinsic point defects. A consensus has however emerged progressively on the fact that V_O acts as a deep donor and thus it cannot account for the high electron density in unintentionally doped ZnO [61, 62]. The zinc vacancy (V_{Zn}) with its low formation energy when the Fermi level is close to the conduction band minimum (CBM) has been shown to be formed as well, but it acts as a deep acceptor and thus it cannot explain the source of n-type conductivity in unintentionally doped ZnO either [63, 64]. Instead, the predominance of hydrogen-related defects has been more and more emphasized by using density-functional theory (DFT) calculations from the pioneered work of Van de Walle, showing that hydrogen exhibits a unique positive charge state over the expected range of Fermi level in ZnO. Hydrogen can be incorporated in ZnO in the form of interstitial hydrogen (H_i), substitutional hydrogen on the oxygen lattice site (H_O), as well as zinc vacancy – hydrogen (V_{Zn}-nH) defect complexes where n is the number of involved H_i atoms and typically lies in the range of 1-4. The presence of hydrogen in ZnO has been experimentally proved by electron paramagnetic resonance and electron nuclear double resonance spectroscopy, infrared absorption spectroscopy, photoluminescence, and Raman spectroscopy. While H_i in the bond-centered site (*i.e.* H_{BC}) has been identified as the most stable configuration, the vast number of configurations related to (V_{Zn}-nH) defect complexes is a complex issue that still needs to be clarified. In particular, the expected number of involved H_i atoms in that defect complex has not been completely identified yet. Several reports have contradictorily shown from DFT calculations that (V_{Zn}-2H) or (V_{Zn}-3H) could be the most stable defect complexes. More importantly, the electronic structure properties of unintentionally doped ZnO NWs grown by CBD have mostly been related to the formation of single vacancies including V_O and V_{Zn}. However, no direct correlation has thoroughly been achieved with hydrogen although the growth medium is full of hydrogen atoms in the form of water molecules and hydroxide ions. A big part of the PhD work of José Villafuerte that I co-supervised together with Vincent Consonni and Julien Pernot, was dedicated to the in-depth study of the intrinsic and

extrinsic point defects of ZnO nanowires toward their optimization for piezoelectric devices. José has initially focused on a in depth investigation on the nature and identification of the hydrogen- and nitrogen-related defects incorporated within the crystal structure of spontaneously grown ZnO nanowires, originating from residual impurities from the chemical precursors [65]. The thermal stability and combined reaction mechanisms of those defects when thermally annealed under oxygen atmosphere at different temperatures was studied in details his PhD and he achieved correlation of the effect of thermal annealing on the electrical properties of the ZnO NWs [66]. Typical Raman and CL spectra he obtained are given in Figure 1.

Figure 1: *Raman and 5 K CL spectra of unintentionally-doped ZnO NWs grown by CBD and annealed for 1 h under oxygen atmosphere in the temperature range of 200 to 1000 °C.*

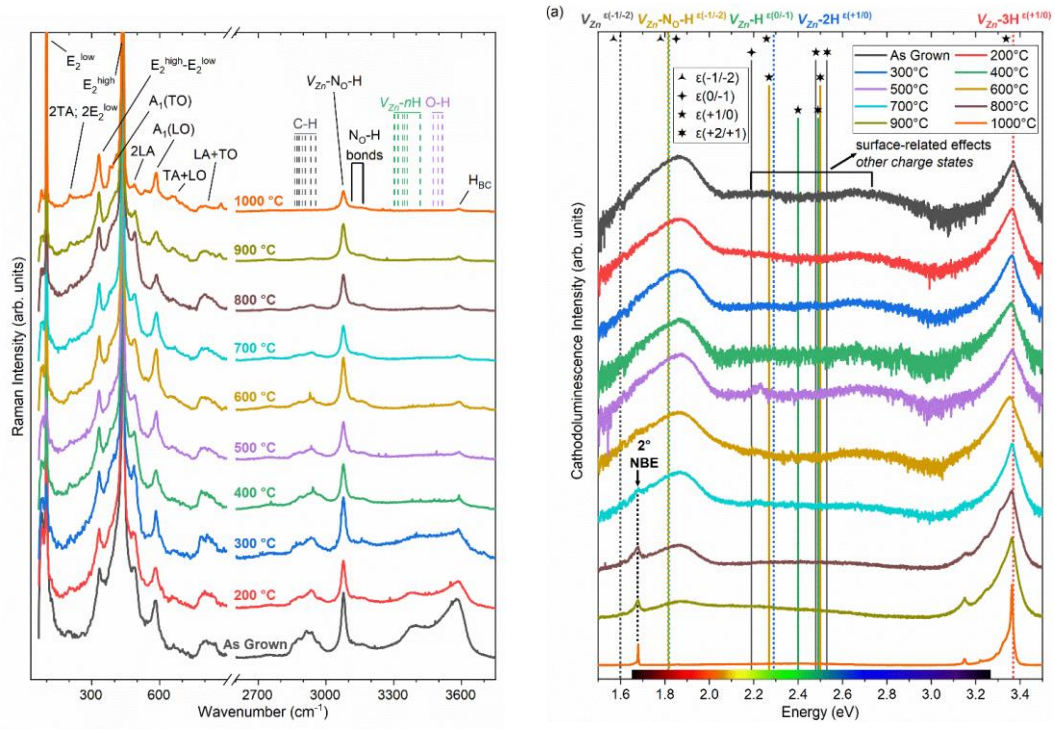

Another part of his PhD work was on the modulated incorporation of hydrogen- and nitrogen-related defects through the modification of the pH in the CBD solution, when growing unintentionally doped ZnO nanowires via CBD [67]. A schematic illustration showing an overall summary of the influence of pH0 on the CBD solution for the growth of ZnO NWs is shown in Figure 2.

After José's PhD defence, we are continuing our work on intrinsic and extrinsic point defects in ZnO nanowires with a new PhD student Alexandre Dieulesaint. Part of Alexandre's work is to examine the impact of plasma and UV-Ozone treatments on our ZnO nanowires. Alexandre is currently writing his PhD in order to defend it in the academic year 2022-2023.

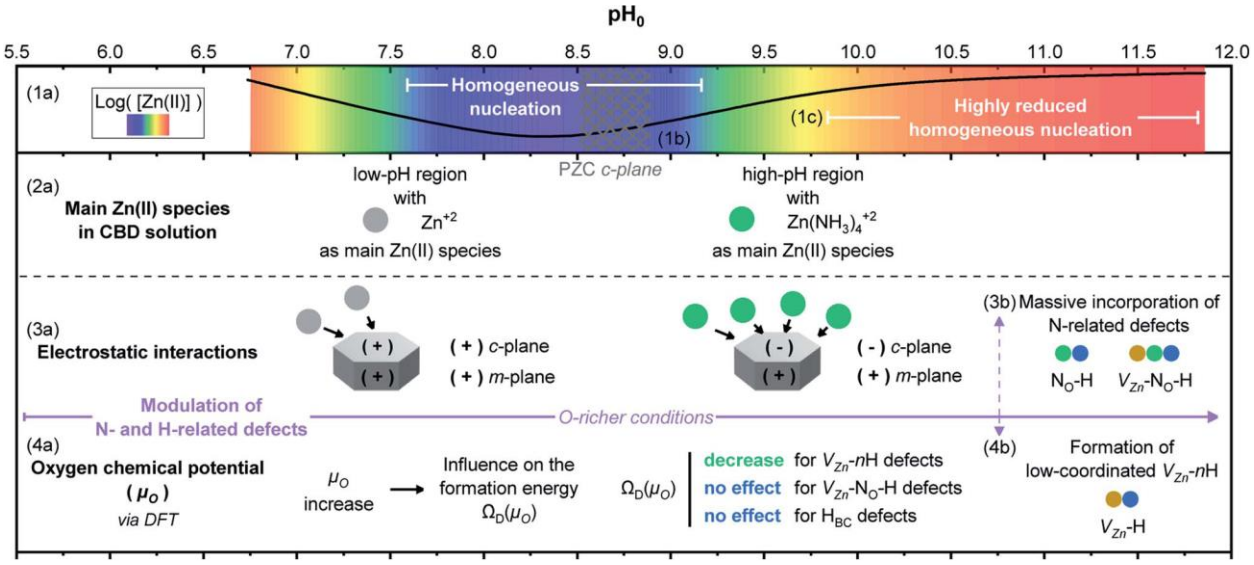

Figure 2: *Schematic illustration showing an overall summary of the influence of pH_0 on the CBD solution for the growth of ZnO NWs. (1a) The color-coded map illustrates the theoretical equilibrium Zn(II) species concentration as calculated using Visual MINTEQ with a black solid line and (1b) the PZC of the polar c-plane is represented by a meshed area. (1c) One region shows where the homogeneous nucleation is highly promoted and another region where it is highly reduced. (2a) The main Zn(II) species in the CBD solution in the low- and high-pH region are depicted. (3a) The electrostatic interactions existing between the ZnO NW surfaces and the charged Zn(II) species in solution illustrate how a massive incorporation of nitrogen-related defects is expected in the high-pH region (3b). (4a) The relation between the pH of the CBD solution, the oxygen chemical potential (mO) and the formation energy of point defects $\Omega_D(\mu_O)$ is shown. (4b) Due to the modulation of mO, a massive formation of low coordinated V_{Zn}-nH defects is revealed. Note: the Zn^{2+} and $Zn(NH_3)_4^{2+}$ ions, as well as the N_O-H, V_{Zn}-N_O-H, and V_{Zn}-H defects are represented via spheres for illustration purposes with no real scale.*

In semiconductors technology the next “big thing” is the Gallium oxide (Ga_2O_3). Gallium oxide as an ultrawide band gap semiconductor with a long-term stability, a high melting point of approximately 1800 °C, a high breakdown electric field of 8 MV/cm, and a high electron mobility of around 300 cm2/V s, has received increasing attention in the fields of solar blind/ ultraviolet photodetection, gas sensing, power electronics, and field-effect transistors [68, 69]. A striking particularity of Ga_2O_3 is related to the existence of five polymorphs, namely, the corundum (α), monoclinic (β), defective spinel (γ), and orthorhombic (ε) phases, with the δ phase being a type of orthorhombic phase. Under ambient pressure and temperature conditions, the monoclinic β phase of Ga_2O_3 represents the most stable crystal structure and has attracted much attention. As high-aspect-ratio structures at respective nano- and microscale dimensions, Ga_2O_3 wires and rods have emerged as building blocks for many of these applications. The growth of Ga_2O_3 wires and rods has typically been achieved in the framework of the vapor−liquid−solid/vapor−solid approaches using metal catalysts [70].

In our team we have studied the development of a double-step process for forming pure β-Ga_2O_3 microrods with different morphologies on silicon. The obtained results can be found in ref [71]. Our process involves the growth of α-GaOOH microrods on silicon by CBD and their further structural conversion to β-Ga_2O_3 microrods by postdeposition thermal treatment. The $Ga(NO_3)_3$ concentration has been found to drastically affect the morphology, dimensions (i.e., diameter and length), and density of α-GaOOH microrods by CBD. This represents an efficient way to tune the resulting morphological properties of β-Ga_2O_3 microrods over a broad range following the postdeposition thermal treatment. In TEM images of Figure 3 we see microrods collected before and after thermal treatment. The microrods have the round-plate rod, morphology obtained when using the CBD process with a $Ga(NO_3)_3$ concentration of 25 mM. Before thermal treatment, the formation of α-GaOOH microrods with the orthorhombic structure occurs on the native SiOx amorphous layer with a thickness of 4.5 ± 0.3 nm, as shown in Figure 3(a). The Fourier-filtered enhancement of the GaOOH area confirms the presence of gallium nitrate hydrate precursor residues ($Ga(NO_3)_3{\cdot}8H_2O$). The microrod further exhibits a high density of small porous domains with a mean size of less than 5 nm. After thermal treatment, the formation of β-Ga_2O_3 microrods with the monoclinic structure is shown in Figure 3(b). The SiO_x amorphous layer has been thickened during thermal treatment to reach a mean value of 22 ± 7 nm. The microrod exhibits a reduced density of porous domains, but their size is 4 times larger on average. Also, a number of extended defects have been formed in the structure, as revealed in Figure 3(c). Interestingly, the 001 reflection of the β-Ga_2O_3 microrod is misaligned by an angle of approximately 17.5° with respect to the {111} planes of silicon. The thickening of the native SiO_x amorphous layer along with the fairly small misalignment of β-Ga_2O_3 microrods indicate that their crystallization during thermal treatment is assisted by diffusion and is strongly affected by the silicon (111) surface underneath.

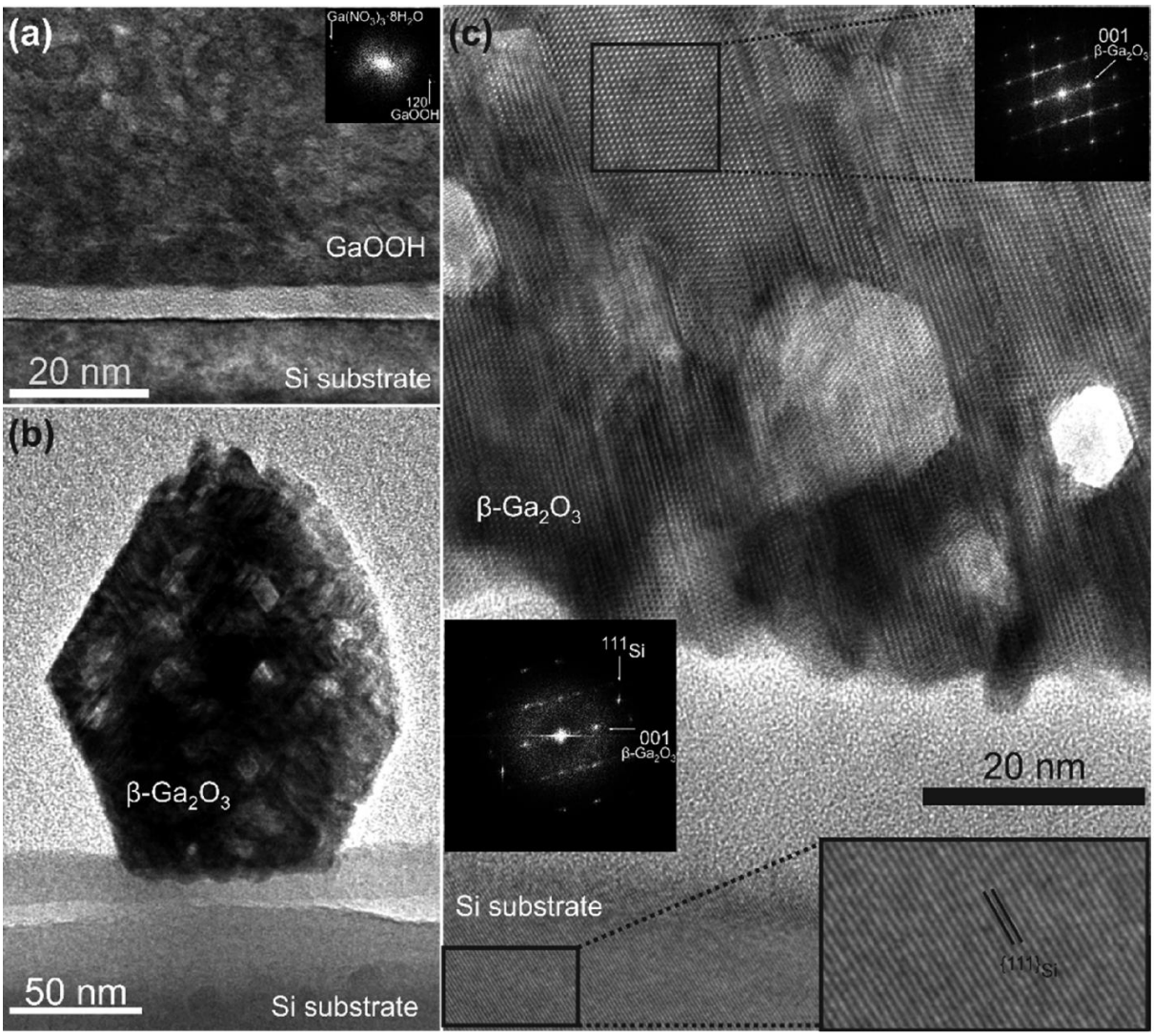

Figure 3: *(a) Low-magnification cross-sectional TEM image of the interfacial region of an as-grown GaOOH microrod on silicon. The FFT of a GaOOH area is given as an inset. (b) Low-magnification cross-sectional TEM image of a porous β-Ga_2O_3 microrod after thermal treatment on silicon. (c) HRTEM image of the interfacial region of a β-Ga_2O_3 microrod after thermal treatment on silicon. The {111} planes of silicon are denoted in a magnified inset. The FFTs of the interfacial area and of the β-Ga_2O_3 area along the [010] zone axis are shown in the respective insets.*

Besides the TEM methods, the new research direction I would like to introduce in my team is the Synchrotron Radiation related techniques. It is well established that the accurate and precise determination of the local atomic structure around an intentional dopant is a prerequisite to control the physical properties of NWs and hence to tune the macroscopic response to different solicitations for engineering devices. X-ray diffraction, X-ray photoelectron spectroscopy, high-resolution transmission electron microscopy, Raman spectroscopy and X-ray absorption spectroscopy (XAS) can provide detailed information on the local electronic and atomic structure. Nevertheless, discriminating the nature of dopant-induced defects that are present in a host lattice still constitutes a challenging task. XAS provides a set of element-specific probes that are suitable for studying thin films and nanomaterials. For example, X-ray absorption near edge structure (XANES) and extended X-ray absorption fine structures (EXAFS) have extensively been used to reveal the presence of cobalt vacancy-related complexes in Co-doped ZnO films [72] or V_{Zn} in Cu-doped ZnO diluted magnetic semiconductor films [73]. However, the sensitivity of those methods relies on the small modifications of the relative intensity of all the spectral features of the XANES measurements or on the complicated data treatment within EXAFS analysis. In contrast, X-ray linear dichroism (XLD) allows to probe the local structural environment and, as a differential spectroscopy method, it is inherently a very sensitive characterization technique. The power of XLD was first demonstrated in our work on Mn-doped GaN films [74] and then on Co-doped ZnO films [75] to quantitatively assess the fraction of the absorbing atomic species incorporated at a specific lattice site in diluted magnetic semiconductors. To investigate the local atomic structure of our metal-doped ZnO NWs (e.g. Ga and Cu doped ZnO NW) we received beamtime in the ID12 beamline of the ESRF thourgh the acceptance of our proposals. The experiments we performed in September 2021 allowed us to investigate the local structural environment around Ga dopants in ZnO nanowires by combining synchrotron radiation-based X-ray linear dichroism with density-functional theory calculations. We have shown that the family of V_{Zn}-Ga_{Zn}-nH defect complexes is predominantly formed and hence that hydrogen acts as an efficient passivating species even for intentional dopants like Ga. The residual and intentional doping processes are found to be highly correlated through significant interplay effects. Our findings revisit the nature of intentional dopant-induced defects and defect complexes in ZnO nanowires. They further reveal that hydrogen should be taken into account in unintentionally doped ZnO nanowires grown by chemical bath deposition as major defects, but also in intentionally doped ZnO nanowires through its efficient passivating effect, opening perspectives to more finely control their optical and electrical properties (Figures 4 and 5). Our results have been submitted to Physical Review Materials journal and are under revision [76]. The experimental results we obtained for the Cu-doped ZnO NW are under investigation.

Those three orientations are going to be my priority the coming years together with the usual teaching and administrative duties.

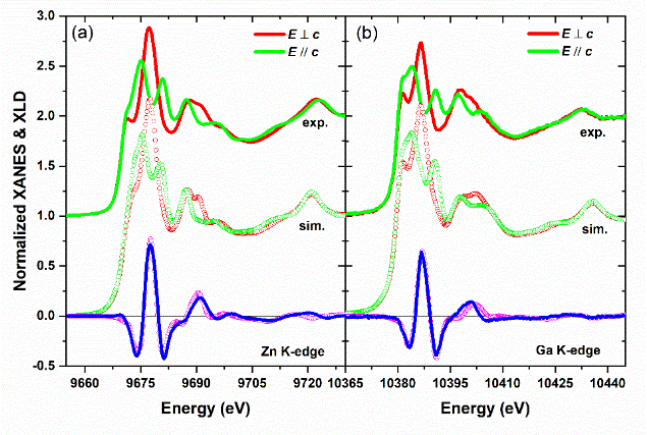

Figure 4: *Experimental (solid lines) and simulated (open symbols) normalized XANES spectra recorded with two orthogonal linear polarizations and the corresponding XLD spectra for Ga-doped ZnO NWs at the (a) Zn K-edge and (b) Ga K-edge.*

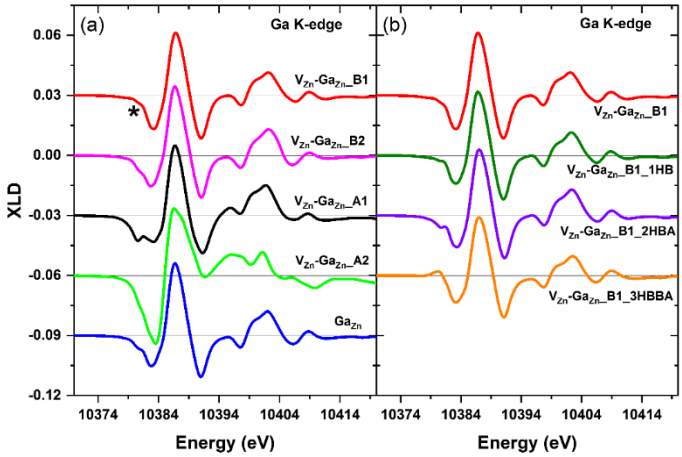

Figure 5: *(a) Simulated XLD spectra for various relaxed structural models combining one V_{Zn} in axial A1/A2 or B1/B2 positions with one Ga_{Zn} as V_{Zn}-Ga_{Zn} defect complexes. (b) Simulated XLD spectra for various relaxed structural models combining one V_{Zn} in basal B1 position with one Ga_{Zn} and the presence of one, two or three hydrogen atoms close to the V_{Zn} in axial A and/or basal B positions as V_{Zn}-Ga_{Zn}-nH defect complexes. The A1 and B1 nomenclature stands for the first coordination shell in the axial and basal positions, respectively, while the A2 and B2 nomenclature stands for the second coordination shell in the axial and basal positions, respectively. All spectra are convoluted with only the Ga core-hole lifetime.*

Scientific Production

ORCID : 0000-0003-3779-445X / Web of Science ResearcherID: B-6811-2019

To date, my total scientific output is 89 publications (RICL and ACL) (h-index: 23, according to WOS). The following figure shows my bibliometric data as recorded in Web of Science in January 2023 and the Table summarises my scientific output in terms of number and type of publications.

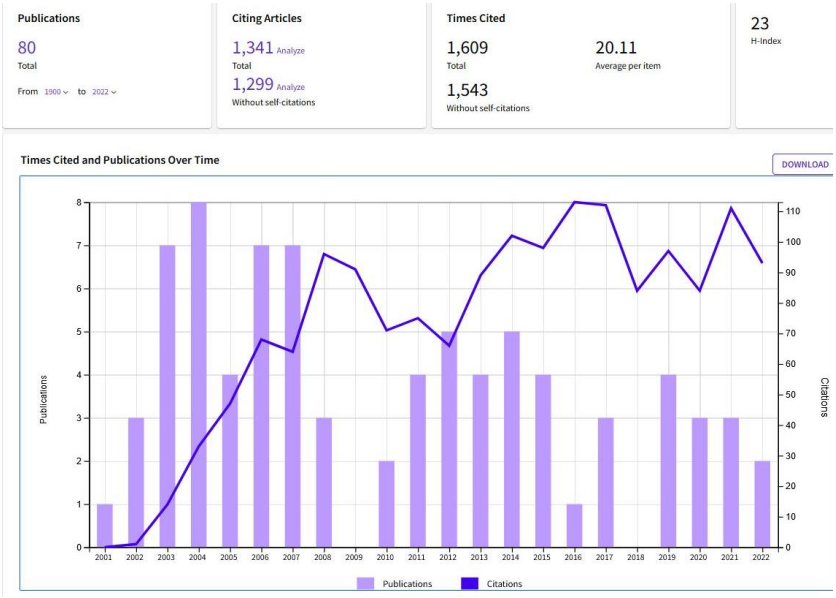

Tableau : *Summary of statistics in terms of scientific production*

Type de publications	Nombre
Publications dans les revues internationales (RICL)	52
Publications dans des actes de conférences à comité de lecture (ACL)	37
Brevet	1
Autres (e.g. ESRF Highlight)	1

Publications dans des revues internationales à comité de lecture (RICL)

1. Optimization Strategies Used for Boosting Piezoelectric Response of Biosensor Based on Flexible Micro-ZnO Composites

X.T. Zhang, J. Villafuerte, V. Consonni, E. Sarigiannidou, J.F. Capsal, A. Bruhat, D. Grinberg, L. Petit, P.J. Cottinet, M.Q. Le Biosensors Basel, **12,** 245 (2022) *Impact factor: 5,743*

2. Modulating the growth of chemically deposited ZnO nanowires and the formation of nitrogen- and hydrogen-related defects using pH adjustment

J. Villafuerte, E. Sarigiannidou, F. Donatini, J. Kioseoglou, O. Chaix-Pluchery, J. Pernot, V. Consonni Nanoscale Advances, **4,** 1793 (2022) *Impact factor : 5,11*

3. In situ analysis of the nucleation of O- and Zn-polar ZnO nanowires using synchrotron-based X-ray diffraction

V. Cantelli, S. Guillemin, E. Sarigiannidou, F. Carla, B. Berini, JM Chauveau, DD Fong, H. Renevier, V. Consonni
Nanoscale, **14,** 680, (2022) *Impact factor: 8,307*

4. Epitaxial LaMnO3 films with remarkably fast oxygen transport properties at low temperature R. Rodriguez-Lamas, C. Pirovano, A. Stangl, D. Pla, R. Jonsson, L. Rapenne, E. Sarigiannidou, N. Nuns, H. Roussel, O. Chaix-Pluchery, M. Boudard, C. Jimenez, RN. Vannier, M. Burriel
J. Materials Chemisty A, **9**, 12721 (2021) *Impact factor: 11,03*

5. Engineering nitrogen- and hydrogen-related defects in ZnO nanowires using thermal annealing J. Villafuerte, O. Chaix-Pluchery, J. Kioseoglou, F. Donatini, E. Sarigiannidou, J. Pernot, V. Consonni,
Physical Review Materials **5**, 056001 (2021) *Impact factor: 4,86*

6. Chemical Synthesis of β-Ga2O3 Microrods on Silicon and Its Dependence on the Gallium Nitrate Concentration

G. Hector, E. Appert, E. Sarigiannidou, E. Matheret, H. Roussel, O. Chaix-Pluchery, V. Consonni
Inorg. Chem. **59** (21) 15696–15706 (2020)

7. Zinc Vacancy-Hydrogen Complexes as Major Defects in ZnO Nanowires Grown by Chemical Bath Deposition

J. Villafuerte, F. Donatini, J. Kioseoglou, E. Sarigiannidou, O. Chaix-Pluchery, J. Pernot, V. Consonni,
Journal of Physical Chemistry CVolume **124**, (30) 16652 (2020) *Impact factor: 4,189*

8. Morphology Transition of ZnO from Thin Film to Nanowires on Silicon and its Correlated Enhanced Zinc Polarity Uniformity and Piezoelectric Responses

Q.C Bui, G. Ardila, E. Sarigiannidou, H. Roussel, C. Jimenez, O. Chaix-Pluchery, Y. Guerfi, F. Bassani, F. Donatini, X. Mescot, B. Salem, V. Consonni
ACS APPLIED MATERIALS & INTERFACES, **12** (26) 29583 (2020) Impact factor: 8,758

9. Structural, Electronic and Vibrational Properties of Al4C3

J. Kioseoglou, Joseph, H.L. Le-Tran, S. Giaremis, I. Gelard, T. Ouisse, D. Chaussende, E. Sarigiannidou
PHYSICA STATUS SOLIDI B-BASIC SOLID STATE PHYSICS **256** 1900037 (2019) Impact factor: 2,291

10. Paramagnetic gold in a highly disordered Au-Ni-O alloy

A. Stamatelatos, P. Poulopoulos, A. Goschew, P. Fumagalli, E. Sarigiannidou, L. Rapenne, C. Opagiste, S. Grammatikopoulos, F. Wilhelm, A. Rogalev
SCIENTIFIC REPORTS **9** 13137 (2019) Impact factor: 3,998

11. Formation mechanisms of ZnO nanowires on polycrystalline Au seed layers for piezoelectric applications

C. Lausecker, B. Salem, X. Baillin, H. Roussel, E. Sarigiannidou, F. Bassani, E. Appert, S. Labau, V. Consonni
NANOTECHNOLOGY **30** (34) 345601 (2019) Impact factor: 3.551

12. Unexpected Development of Perpendicular Magnetic Anisotropy in Ni/NiO Multilayers After Mild Thermal Annealing

D.I. Anyfantis, E. Sarigiannidou, L. Rapenne, A. Stamatelatos, D. Ntemogiannis, V. Kapaklis, P. Poulopoulos
IEEE MAGNETICS LETTERS **10** 6104105 (2019) Impact factor: 0.89

13. Vaporization and condensation in the Al4C3-SiC system

H.L. Le-Tran, E. Sarigiannidou, I. Gelard and D. Chaussende
JOURNAL OF THE EUROPEAN CERAMIC SOCIETY, **37 (15),** 4475 (2017) *Impact factor: 3,536*

14. A Chemical Vapor Deposition Route to Epitaxial Superconducting NbTiN Thin Films

N. Tsavdaris, D. Harza, S. Coindeau, G. Renou, F. Robaut, E. Sarigiannidou, M. Jacquemin, R. Reboud, M. Hofheinz, E. Blanquet et F. Mercier
Chemitry of Materials, **29 (14)** 5825 (2017) *Impact factor: 9,842*

15. Al4SiC4 vibrational properties: density functional theory calculations compared to Raman and infrared spectroscopy measurements

L. Pedesseau, O. Chaix-Pluchery, M. Modreanu, D. Chaussende, E. Sarigiannidou, A. Rolland, J. Even, O. Durant
Journal of Raman Spectroscopy **48 (6)** 891 (2017) *Impact factor: 2,353*

16. Identification of extended defect and interface related luminescence lines in polycrystalline ZnO thin films grown by sol-gel process

S. Guillemin, V. Consonni, L. Rapenne, E. Sarigiannidou, F. Donatini G. Bremond,

RSC ADVANCES **6**, 44987 (2016) *Impact factor: 3,289*

17. Al4SiC4 wurtzite crystal: Structural, optoelectronic, elastic, and piezoelectric properties
L. Pedesseau, J. Even, M. Modreanu, D. Chaussende, E. Sarigiannidou, O. Chaix-Pluchery and O. Durand,
APL Materials **3**, 121101 (2015) *Impact factor : 4,323*

18. Spontaneous shape transition of thin films into ZnO nanowires with high structural and optical quality
S. Guillemin, E. Sarigiannidou, E. Appert, F. Donatini, G. Renou, G. Bremond, V. Consonni
NANOSCALE, **7** 16994 (2015) *Impact factor: 7,76*

19. Synthesis of single crystals of V2AlC phase by high-temperature solution growth and slow cooling technique
L. Shi, T. Ouisse, E. Sarigiannidou, O. Chaix-Pluchery, H. Roussel, D. Chaussende, B. Hackens
Acta Materialia, **83**, 304 (2015) *Impact Factor: 5,058*

20. Macroscopic approach to the nucleation and propagation of foreign polytype inclusions during seeded sublimation growth of silicon carbide
N. Tsavdaris, K. Ariyawong, J.-M. Dedulle, E. Sarigiannidou, D. Chaussende
Crystal Growth and Design, **15,** 156 (2015) *Impact Factor: 4,425*

21. Selective Area Growth of Well-Ordered ZnO Nanowire Arrays with Controllable Polarity
V. Consonni, E. Sarigiannidou, E. Appert, A. Bocheux, S. Guillemin, F. Donatini, I-C.Robin, J. Kioseoglou and F. Robaut, ACS Nano, **8(5),** 4761 (2014) *Impact Factor : 13,334*

22. High temperature solution growth and characterization of Cr_2AlC single crystals
T. Ouisse, E. Sarigiannidou, O. Chaix-Pluchery, H. Roussel, B. Doisneau and D. Chaussende
Journal of Crystal Growth **384,** 88 (2013) *Impact Factor: 1,462*

23. Waveguide saturable absorbers at 1.55 μm based on intraband transitions in GaN/AlN QDs
L. Monteagudo-Lerma, S. Valdueza-Felip, F. B. Naranjo, P. Corredera, L. Rapenne, E. Sarigiannidou, G. Strasser, E. Monroy, and M. González-Herráez *OPTICS EXPRESS* **21** 27578 (2013), *Impact Factor: 3,148*

24. Formation Mechanisms of ZnO Nanowires: The Crucial Role of Crystal Orientation and Polarity
S. Guillemin, L. H. Roussel, E. Sarigiannidou, G. Bremond, and V. Consonni
JOURNAL OF PHYSICAL CHEMISTRY C **117** 20738 (2013), *Impact Factor: 4,509*

25. Thermal stability of the deep ultraviolet emission from AlGaN/AlN Stranski-Krastanov quantum dots
C. Himwas, R. Songmuang, Le Si Dang, J. Bleuse, L. Rapenne, E. Sarigiannidou, and E. Monroy
Appl. Phys. Lett. **101**, 241914 (2012), *Impact Factor: 3,495*

26. Textured YBCO films grown on wires: application to superconducting cables
N. Dechoux, C. Jiménez, P. Chaudouët, L. Rapenne, E. Sarigiannidou, F. Robaut, S. Petit, S. Garaudée, L. Porcar, J. L. Soubeyroux, P. Odier, C.- E. Bruzek and M. Decroux,
Superconductor Science and Technology **25** 125008 (2012) *Impact Factor: 2,34*

27. Microstructural changes induced by the pyrolysis step on epitaxial La2Zr2O7 thin films grown by metalorganic decomposition
V. Roche, C. Jiménez, P. Chaudouët, R. Benaboud, F. Weiss, E. Sarigiannidou,
Thin Solid Films, **520,**2566 (2012), *Impact Factor: 1,939*

28. Strain relaxation in GaN/AlxGa1-xN superlattices grown by plasma-assisted molecular-beam epitaxy
Y. Kostar, B. Doisneau, E. Bellet-Amalric, A. Das, E. Sarigiannidou, E. Monroy,
J. Appl. Phys. **110**, 033501 (2011) *Impact Factor: 2,176*

29. From Si nanowire to SiC nanotube
L. Latu-Romain, M. Ollivier, A. Mantoux, G. Auvert, O. Chaix-Pluchery, E. Sarigiannidou, E. Bano, B. Pelissier, C. Roukoss, H. Roussel, F. Dhalluin, B. Salem, N. Jegenyes, G. Ferro, D. Chaussende, T. Baron, *J Nanopart. Res* **13,** (2011) *Impact Factor: 2,33*

30. Terahertz intersubband absorption in GaN/AlGaN step quantum wells
H. Machhadani, Y. Kotsar, S. Sakr, M. Tchernycheva, R. Colombelli, J. Mangeney, E. Bellet-Amalric, E. Sarigiannidou, E. Monroy, F. H. Julien, *Appl. Phys. Lett.* **97**, 191101 (2010) *Impact Factor: 3,495*

31. GaN-based quantum cascade photodetector with 1.5 μm peak detection wavelength
S. Sakr, Y. Kotsar, S. Haddadi, M. Tchernycheva, L. Vivien, E. Sarigiannidou, N. Isac, E. Monroy, F.H. Julien, *Electron. Lett*. **46**, 1685 (2010) *Impact Factor: 1,232*

32. Effect of doping on the mid-infrared intersubband absorption in GaN/AlGaN superlattices grown on Si(111) templates P. K. Kandaswamy, H. Machhadani, Y. Kotsar, S. Sakr, A. Das, M. Tchernycheva, L. Rapenne, E. Sarigiannidou, F. H. Julien, E. Monroy Appl. Phys. Lett. **96**, 141903 (2010) *Impact Factor: 3,495*

33. Intraband emission at lambda approximate to 1.48 µm from GaN/AlN quantum dots at room temperature

L. Nevou, F. H. Julien, M. Tchernycheva, F. Guillot, E. Monroy, E. Sarigiannidou, Appl. Phys. Lett. **92**, 161105 (2008) *Impact Factor: 3,495*

34. Excitonic giant Zeeman effect in GaN:Mn^{3+}

W. Pacuski, D. Ferrand, J. Cibert, J.A. Gaj, A. Golnik, P. Kossacki, S. Marcet, E. Sarigiannidou, and H. Mariette Phys. Rev. B **76** 165304 (2007) *Impact factor: 3,536*

35. Depth dependence of the Mn valence and Mn-Mn coupling in (Ga,Mn)N

A. A. Freeman, K. W. Edmonds, N. R. Farley, S. V. Novikov, R. P. Campion, C. T. Foxon, B. L. Gallagher, E. Sarigiannidou and G. van der Laan, Phys. Rev. B **76** 081201 (2007) *Impact factor: 3,536*

36. Charge distribution and vertical electron transport through GaN/AlN/GaN single-barrier structuresd

S. Leconte, F. Guillot, E. Sarigiannidou and E. Monroy, *Semiconductor Science and Tech.* **22** 107 (2007) *IF: 2,34*

37. Intrinsic ferromagnetism in wurtzite (Ga,Mn)N semiconductor

E.Sarigiannidou, F. Wilhelm, E. Monroy, R. M. Galera, E. Bellet-Amalric, A. Rogalev, J. Cibert, J.Goulon and H. Mariette, Phys. Rev. B **74** 041306(R) (2006) *Impact factor: 3,536*

38. Comparison of the structural quality in Ga-face and N-face polarity GaN/AlN multiple-quantum-well structures

E.Sarigiannidou, E. Monroy, N. Gogneau, G. Radtke, P. Bayle-Guillemaud, E. Bellet-Amalric, B. Daudin, and J.L. Rouvière, *Semiconductor Science and Technology* **21** 612 (2006) *Impact Factor: 2,34*

39. Resonant Raman scattering in self-assembled GaN/AlN quantum dots

N. Garro, A Cros, JM. Llorens, A. Garcia-Cristobal, A. Cantarero, N. Gogneau, E. Sarigiannidou, E. Monroy, B. Daudin, Phys. Rev. B **74** 075305 (2006) *Impact factor: 3,536*

40. Strain distribution in GaN/AlN quantum dots superlattices

E. Sarigiannidou, A.D. Andreev, B. Daudin, and J.L. Rouvière, *Appl. Phys. Lett.* **87** 203112 *(2005) Impact Factor: 3,495*

41. Theoretical discussions on the geometrical phase method

JL Rouviere , E Sarigiannidou *Ultramicroscopy* **106** 1 *(2005) Impact factor: 3,033*

42. Strain distribution in nitride quantum dots multilayers

V. Chamard, T. Schülli, M. Sztucki, T. H. Metzger, E. Sarigiannidou, J. L. Rouvière, M. Tolan, C. Adelmann and B. Daudin *Phys. Rev. B,* **69**, 125327 *(2004) Impact factor: 3,536*

43. Plastic relaxation of nitride heterostructures

E. Bellet-Amalric, C. Adelmann, E. Sarigiannidou, J. L. Rouviere, G. Feuillet, E. Monroy, B. Daudin *J. Appl. Phys.* **95**, 1127 *(2004) Impact factor: 2,163*

44. *Surfactant effect of gallium during the growth of GaN on AlN(000-1) by plasma-assisted molecular beam epitaxy*

N. Gogneau, E.Sarigiannidou, E. Monroy, S. Monnoye, H. Mank and B. Daudin *Appl. Phys. Lett.* ***85*** *1421 (2004) Impact Factor: 3,495*

45. Growth kinetics of N-face polarity GaN by plasma-assisted molecular beam epitaxy

E. Monroy, E.Sarigiannidou, F.Fossard, N. Gogneau, E. Bellet-Amalric, J.-L. Rouvière, S. Monnoye, H. Mank, B. Daudin *Appl. Phys. Lett.* **84** 3684 *(2004) Impact Factor: 3,495*

46. Influence of AlN overgrowth on Structural Properties of GaN Quantum Wells and Quantum Dots Grown by Plasma-Assisted Molecular Beam Epitaxy

N. Gogneau, D. Jalabert, E. Monroy, E. Sarigiannidou, J.L.Rouvière, T.Shibata, M.Tanaka, J.M. Gerard, B. Daudin *J. Appl. Phys* ***96*** *1104 (2004) Impact factor: 2,163*

47. Polytype transition on N-face GaN:Mg from wurtzite to zinc-blende

E. Monroy, M. Hermann, E. Sarigiannidou,T. Andreev, P. Holliger, S. Monnoye, H. Mank, B. Daudin, and M. Eickhoff *J. Appl. Phys.* ***96*** *3709 (2004) Impact factor: 2,163*

48. Linear alignment of GaN quantum dots on AlN grown on vicinal SiC substrate

J. Brault,S. Tanaka, E. Sarigiannidou, J.-L. Rouvière, B. Daudin, G. Feuillet, H. Nakagawa *J. Appl. Physics* ***93****, 3108 (2003) Impact factor: 2,163*

49. Growth and optical properties of GaN/AlN quantum wells

C. Adelmann, E. Sarigiannidou, D. Jalabert, Y. Hori, J.-L. Rouvière, B. Daudin, S. Fanget, C. Bru-Chevallier, T. Shibata, and M. Tanaka *Appl. Phys. Lett.* ***82****, 4154 (2003) Impact Factor: 3,495*

50. ***GaN islanding by spontaneous rearrangement of a strained two-dimensional layer on (0001) AlN***
C. Adelmann, N. Gogneau, E. Sarigiannidou, J.-L. Rouvière, and B. Daudin
Appl. Phys. Lett. ***81****, 3064 (2002) Impact Factor: 3,495*

51. Structural Transitions of Inversion Domain Boundaries through Interaction with Stacking Faults in Epitaxial GaN.
G.P. Dimitrakopulos, Ph. Komninou, J. Kioseoglou, Th. Kehagias, E. Sarigiannidou, A. Georgakilas, G. Nouet and Th. Karakostas *Phys. Rev. B.,* ***64****, 245325 (2001) Impact factor: 3,536*

52. Structural evolution of super alpha-two Ti_3Al powder ball milled in air.
Th. Kehagias, Ph. Komninou, P. Kavouras, E. Sarigiannidou, S. Kokkou, J.G. Antonopoulos and Th.Karakostas. *J. Mech. Beh. Mater.* ***9****, 257-266 (1998) Impact factor:0,55*

Publications dans des actes de conférences à comité de lecture (ACL)

1. Synthesis and characterization of Al_4SiC_4: a "new" wide band gap semiconductor material
D. Zevgitis, O. Chaix-Pluchery, B. Doisneau, M. Modreanu, J. La Manna, E. Sarigiannidou and D. Chaussende *Materials Science Forum*, **821-823**, 974 (2015) DOI: 10.4028/www.scientific.net/MSF.821-823.974

2. Nitrogen Incorporation during Seeded Sublimation Growth of 4H-SiC and 6H-SiC
N. Tsavdaris, P. Kwasnicki, K, Ariyawong, N. Valle, H. Peyre, E. Sarigiannidou, S. Juillaguet, D. Chaussende *Materials Science Forum*, **821-823**, 60 (2015) DOI:10.4028/www.scientific.net/MSF.821-823.60

3. Photoelectrical Parameters of a PVT Grown Bulk 15R-SiC Crystal at Different Stages of Growth
G. Liaugaudas, D. Dargis, K. Jarašiūnas, N. Tsavdaris, E. Sarigiannidou, Didier Chaussende
Materials Science Forum, **821-823**, 253 (2015) DOI:10.4028/www.scientific.net/MSF.821-823

4. Interface Shape: A Possible Cause of Polytypes Destabilization during Seeded Sublimation Growth of 15R-SiC
N. Tsavdaris, K. Ariyawong, E. Sarigiannidou, JM. Dedulle, O. Chaix-Pluchery, D. Chaussende,
Materials Science Forum, **806**, 61 (2015) DOI: 10.4028/www.scientific.net/MSF.806.61

5. Nondestructive Evaluation of Photoelectrical Properties of a PVT Grown Bulk 15R-SiC Crystal
G. Liaugaudas, K. Jarašiūnas, N. Tsavdaris, E. Sarigiannidou, Didier Chaussende
Materials Science Forum, **806**, 65 (2015) DOI: 10.4028/www.scientific.net/MSF.806.65

6. Open issues in SiC bulk growth
D. Chaussende, K. Ariyawong, N. Tsavdaris, M. Seiss, YJ. Shin, JM. Dedulle, R. Madar, E. Sarigiannidou, J. La Manna, O. Chaix-Pluchery, T. Ouisse, Materials Science Forum **778-780**, 03-08 (2014)

7. Interaction between Vapor Species and Graphite Crucible during the Growth of SiC by PVT
K. Ariyawong, N. Tsavdaris, JM. Dedulle, E. Sarigiannidou, T. Ouisse, D. Chaussende, Materials Science Forum **778-780**, 31-34 (2014)

8. Effect of facet occurrence on polytype destabilization during bulk crystal growth of SiC by seeded sublimation
N. Tsavdaris, K. Ariyawong, O. Chaix-Pluchery, JM Dedulle, E. Sarigiannidou, D. Chaussende, Materials Science Forum **778-780**, 13-16 (2014)

9. On photoelectrical properties of 6H-SiC bulk crystals PVT-grown on 6H-and 4H-SiC substrates
G. Liaugaudas, K. Jarasiunas, N. Tsavdaris, E. Sarigiannidou, D. Chaussende, Materials Science Forum **778-780**, 305-308 (2014)

10. AlGaN/AlN quantum dots for UV light emitters
C. Himwas, M. den Hertog, F. Donatini, LS. Dang, L. Rapenne, E. Sarigiannidou, R. Songmuang, and E. Monroy, Phys. Status Solidi (c) , **10(3)**, pp.285-288 (2013) DOI: 10.1002/pssc.201200679

11. New HTS 2G Round Wires
A. Allais, S. Morice, C.-F., Theune, S. Petit, M. Mikolajczyk, N. Dechoux, C. Jimenez, E. Sarigiannidou, L. Porcar, J. Soubeyroux, P. Odier, T. Waeckerle *IEEE Transactions on Applied Superconductivity*, **22** 5800204 (2012)

12. Stability of High Temperature Chemical Vapor Deposited Silicon Based Structures on Metals for Solar Conversion
I. Gelard, G. Chichignoud, E. Blanquet, H. N. Xuan, R. Cruz, C. Jimenez, E. Sarigiannidou, K. Zaidat Journal of Nanoscience and Nanotechnology, **11** 8318 (2011)

13. Strain relaxation in GaN/Al(0.1)Ga(0.9)N superlattices for mid-infrared intersubband absorption
Y. Kotsar, P.K. Kandaswamya, A. Dasa, E. Sarigiannidou, E. Bellet-Amalric, E. Monroy, J. of Crystal Growth, **323** 64 (2011)

14. Room temperature intraband Raman emission and ultrafast carrier relaxation in GaN/AlN quantum dots
L. Nevou, J. Mangeney, M. Tchernycheva, F. H. Julien, F. Guillot, E. Monroy, and E. Sarigiannidou *Phys. Stat. Sol. (c) 6, pp. S650-S653 (2009)*

15. Near Room temperature intraband Raman emission and ultrafast carrier relaxation in GaN/AlN QDs
L. Levou, J. Mangeney, M. Tchernycheva, F.H. Julien, F. Guillot, E. Monroy, E. Sarigiannidou Phys. Stat. Solidi C **6** 650-653 (2009)

16. Near-infrared intersubband emission from GaN/AlN quantum dots and quantum wells
L. Levou, F.H. Julien, M. Tchernycheva, F. Guillot, E. Sarigiannidou, E. Monroy Phys. Stat. Sol. c **5** 2120 (2008)

17. Elastic Strain Distribution in GaN/AlN Quantum Dot Structures: Theory and Experiment
A. Andreev, E. Sarigiannidou, E. Monroy, B. Daudin, J-L. Book Series: Springer Proceedings in Physics **120** 13 (2008)

18. Intrinsic ferromagnetism in wurtzite (Ga,Mn)N grown by plasma-assisted molecular-beam epitaxy
E.Sarigiannidou, F. Wilhelm, E. Monroy, R. M. Galera, E. Bellet-Amalric, A. Rogalev, J. Cibert, J.Goulon and H. Mariette Physics of Semiconductors, Pts A & B AIP CONFERENCE PROC. **893** 1173 (2007)

19. Hard X-ray linear dichroism using a quarter wave plate for structural characterization of diluted magnetic semiconductors
F. Wilhelm, E. Sarigiannidou, E. Monroy, A. Rogalev, N. Jaouen, H. Mariette, J. Goulon Synchrotron Radiation Instrumentation, AIP CONFERENCE PROCEEDINGS **879** 1675 (2007)

20. Electronic structure and vertical transport in single-barrier AlN/GaN heterostructures
S. Leconte, E. Sarigiannidou, E. Monroy Physics of Semicond., Pts A B, AIP CONFERENCE PROCEEDINGS **893** 309 (2007)

21. Quantitative study of the Giant Zeeman Effect in (Zn,Co)O and (Ga,Mn)N
W. Pacuski, D. Ferrand, P. Kossacki, J. Cibert, J. A. Gaj, A. Golnik, S. Marcet, C. Deparis, C. Morhain, E. Sarigiannidou, H. Mariette Physics of Semiconductors, Pts A and B AIP CONFERENCE PROCEEDINGS **893** 1171 (2007)

22. Intrinsic magnetism in wurtzite (Ga,Mn)N
S. Marcet, W. Pacuski, E. Sarigiannidou, F. Wilhelm, D. Ferrand, S. Kuroda, R. M. Galera, E. Gheeraert, J. Cibert, A. Rogalev, H. Mariette, P. Kossacki *Phys. Stat. Sol. (c)* **3** 4062 (2007)

23. Plasma-assisted molecular beam epitaxy of wurtzite GaMnN displaying ferromagnetism assessed by means of X-ray magnetic circular dichroism
E. Sarigiannidou, E. Monroy, E. Bellet-Amalric, H. Mariette, RM. Galera, J. Cibert, F. Wilhelm, A. Rogalev S*uperlattices and Microstructures* **40** 239 (2006)

24. Growth of GaN quantum dots on nonpolar A -plane SiC by molecular-beam epitaxy
S. Founta, F. Rol, E. Bellet-Amalric, E. Sarigiannidou, B. Gayral, C. Moisson, H. Mariette, B. Daudin *Phys. Stat. Sol. (b)* **243** 3968 (2006)

25. Quantitative strain analysis of GaN/AlN quantum dot multilayers
E. Sarigiannidou, A.D. Andreev, B. Daudin, and J.L. Rouvière, *Phys. Stat. Sol. (c)* **3** 1667 (2006)

26. Phase transition by Mg doping of N-face polarity GaN
E. Sarigiannidou, E. Monroy, M. Hermann, T. Andreev, P. Holliger, S. Monnoye, H. Mank, B. Daudin, and M. Eickhoff *Phys. Stat. Sol. (c) **1-4** 2216 (2005)*

27. GaN quantum dots by molecular beam epitaxy
B. Daudin, C. Adelmann, N. Gogneau, E. Sarigiannidou, E. Monroy, F. Fossard, J. L. Rouviere *Physica E* **21** 540 *(2004)*

28. Influence of AlN overgrowth on GaN nanostructures grown by molecular beam epitaxy.
N. Gogneau., E. Monroy., D.Jalabert, E. Sarigiannidou, J.L. Rouvière and B. Daudin *Mat. Res. Soc. Symp. Proc., **798, Y4.4,**1 (2004)*

29. Growth of III-nitride heterostructures with N-face polarity on C-face 4H-SiC by plasma-assisted MBE
E. Monroy, E. Sarigiannidou, F. Fossard, F. Enjalbert, N. Gogneau, E. Bellet-Amalric, J. Brault, J.-L. Rouvière, Le Si Dang, S. Monnoye, H. Mank, B. Daudin *Mat. Sci. Forum **457-460**, 1573 (2004)*

30. Comprehensive overview on elastic strain relaxation mechanisms in nitride heterostructures: Stranski-Krastanow versus Frank-Van der Merwe growth mode

B. Daudin, N. Gogneau,C. Adelmann, E. Sarigiannidou, E. Monroy, E. Bellet-Amalric, J.L. Rouviere *Physica Status Solidi (c)* ***0****, 2525-2528 (2003)*

31. Quantitative analysis of AlN/GaN HRTEM images

E Sarigiannidou, J L Rouvière, G Radtke, P Bayle-Guillemaud, E Monroy and B Daudin

Microscopy of Semiconducting Materials, Inst. Phys. Conf. Ser. ***180*** *301 (2003)*

32. Characteristics of AlN growth on vicinal SiC(0001) substrates by molecular beam epitaxy

J. Brault, E. Bellet-Amalric, S. Tanaka, F. Enjalbert, D. Le Si Dang, E. Sarigiannidou, J.-L. Rouviere, G. Feuillet, B. Daudin *Physica status solidi (b)* **240** 314 *(2003)*

33. Lateral Arrangement of Self-Assembled GaN Islands on Periodically Stepped AlN Surfaces

J. Brault, S. Tanaka, E.Sarigiannidou, H. Nakagawa, J.L.Rouvière, G.Feuillet, B.Daudin *Phys. Stat. sol.(b)* ***234****, 939 (2002)*

34. Controlling the morphology of GaN layers grown on AlN in Ga self-surfactant conditions: from quantum wells to quantum dots

C. Adelmann, B. Daudin, E. Monroy, E. Sarigiannidou, J. L. Rouviere, Y. Hori, J. Brault, N. Gogneau, S. Fanget, C. Bru-Chevallier *Physica Status Solidi (b)* ***234****, 931 (2002)*

35. Interaction between basal stacking faults and prismatic inversion domain boundaries in GaN.

Ph. Komninou, J. Kioseoglou, E. Sarigiannidou, G.P. Dimitrakopulos, Th. Kehagias, K. Animer, A. Georgakilas, G. Nouet, P. Ruterana and Th. Karakostas *Mat. Res. Soc. Symp.,* ***639****, G3.44 (2001).*

36. Microstructure of GaN films grown by RF-plasma assisted molecular beam epitaxy.

Ph. Komninou, Th. Kehagias, J. Kioseoglou, E. Sarigiannidou, K. Animer, A. Georgakilas, G. Nouet, P. Ruterana and Th. Karakostas *Mat. Res. Soc. Symp.,* ***639****, G3.47 (2001).*

37. Morphological and structural aspects of GaN films grown on sapphire by MBE.

Th. Kehagias, Ph. Komninou, J. Kioseoglou, E. Sarigiannidou, G.P. Dimitrakopulos, S. Mikroulis, K. Tsagaraki, A. Georgakilas, Th. Karakostas, *Bolg. fiz. z.,* ***27****, 90. (2000)*

Brevets acceptés

STRUCTURE ADAPTEE A LA FORMATION DE CELLULES SOLAIRES

Guy CHICHIGNOUD, Elisabeth BLANQUET, Isabelle GELARD, Carmen JIMENEZ, Eirini SARIGIANNIDOU, Kader ZAIDAT, François WEISS and Michel PONS

Référence du dossier du déposant ou du mandataire : B10511 PCT

Numéro de demande internationale (s'il est déjà disponible) : PCT/FR2012/050195

Communications orales et par affiche à des conférences

Le tableau 3 regroupe l'ensemble des conférences internationales et nationales dans lesquelles mes travaux ont été présentés par moi-même ou par un de mes thésards/collaborateurs. La liste des communications qui suit correspond à celles que j'ai présentées moi-même.

Table 3 : *Summary of Oral and Poster participation in conferences .*

Année	Communications Orales		Communications par affiche	
	Conférences internationales	Conférences nationales/Workshop	Conférences internationales	Conférences nationales/workshop
2009	2	1	2	
2010	3			
2011	5	2	2	
2012	5 : 3+ 2 invitées		2	1
2013	4 : 3+ 1 invitée		5	
2014	2	2	4	
2015	1		2	1

2016	5 : 2 + 3 invitées		1	
2017	1			1
2018	3 : 2+ 1 invitée		1	2
2019	1	1	2	
2020[1]	(4)		(2)	
2021	2 :1 + 1 invitée			
2022	3 : 1 +2 invitées	1 : 1 invitée	1	1

1. **Orale/ Internationale– EUCAS 2009**
   Effect of the annealing process on the microstructure of La2Zr2O7 films obtained by MOD
   C. Jiménez, L. Rapenne, T. Caroff, N. Marcellin, S. Morlens, V. Roche, E. Sarigiannidou, F. Weiss, P. Odier
   European Conference on Applied Superconductivity, Dresden, Germany Sept. 2009

2. **Orale / Internationale – Electroceramics XI 2010**
   Influence of the pyrolisis process on the microstructue of pyrochlore La2Zr2O7 films obtained by MOD
   V. Roche, E. Sarigiannidou, C. Jiménez, L. Rapenne, P. Chaudouët, R. Benaboud, S. Petit, P. Odier
   Electroceramics XI, Trondheim, Norway June 2010

3. **Orale / Nationale– Matériaux 2010**
   Etude de la qualité cristalline et la microstructure des couches de LZO par MOD
   E. Sarigiannidou, V. Roche, P. Chaudouët, R. Benadou, S. Petit, L. Rapenne, P. Odier, F. Weiss, C. Jiménez
   Materiaux 2010, Nantes, France 2010

4. **Conférence invitée / Internationale – EDS 2012**
   Strain relaxation in GaN/AlGaN superlattices grown by PAMBE for intersubband applications
   E. Sarigiannidou, B. Doisneau, Y. Kotsar, E. Bellet-Amalric, A. Das, and E. Monroy
   Extended Defects in Semiconductors EDS2012. Thessaloniki, Greece. June 2012

5. **Affiche / Internationale – EMRS 2013**
   Plasma Enhanced Oxidation of Nickel Silicide at Low Temperature
   E.Sarigiannidou, A. Lacoste, J. Elsabahy, A. Bes and R. Madar
   EMRS, Spring meeting, Strasbourg, France, Mai 2013

6. **Orale / Nationale– Matériaux 2014**
   Selective Area Growth of Well-Ordered Epitaxial ZnO Nanowire Arrays with Controllable Polarity
   E. Sarigiannidou, E.Appert, S.Guillemin, A. Bocheux, F. Donatini, F. Robaut, I.C. Robin, J. Kioseoglou, V.Consonni
   Matériaux, Montpellier, France, Novembre 2014

7. **Affiche / Internationale – ECSCRM 2014**
   Synthesis and characterization of Al4SiC4 : a “new” wide band gap semiconductor material
   E. Sarigiannidou, D. Zevgitis, O. Chaix-Pluchery, B. Doisneau, M. Modreanu, J. La Manna, D. Chaussende
   European Conference on Silicon Carbide and Related Materials, Grenoble, France September 2014

8. **Affiche / Nationale– Sfμ 2015**
   Polarity control of well-ordered epitaxial ZnO nanowire arrays by selective area growth
   E. Sarigiannidou, E.Appert, S.Guillemin, A. Bocheux, F. Donatini, F. Robaut, I.C. Robin, J. Kioseoglou, V.Consonni
   Société Française de microscopie Sfμ, Nice, France, July 2015

9. **Conférence invitée / Internationale – HTCMC-9 2016**
   Al-Si-C ternary alloys: a “new” family of semiconductors
   Eirini Sarigiannidou, Hoang Long Le Tran, Odette Chaix and Didier Chaussende
   International Conference on High Temperature Ceramic Matrix Composites (HTCMC-9) & Global Forum on Advanced Materials & Technologies for Sustainable Development (GFMAT 2016), Toronto, Canada, June 2016

10. **Orale / Internationale – HTCMC-9 2016**

Selective Area Growth of Well-Ordered Epitaxial ZnO Nanowire Arrays with Controllable Polarity
E. Sarigiannidou, E.Appert, S.Guillemin, A. Bocheux, F. Donatini, F. Robaut, I.C. Robin, J. Kioseoglou, V.Consonni
International Conference on High Temperature Ceramic Matrix Composites (HTCMC-9) & Global Forum on Advanced Materials &Technologies for Sustainable Development (GFMAT 2016), Toronto, Canada, June 2016

11. Conférence invitée / Internationale – Workshop 2018

The model FAME
Eirini Sarigiannidou

New trends in nanoengineering research and education Wroclaw, Poland, June 2018

12. Conférence invitée / Internationale – NN22 2022

Defect engineering in highly conductive ZnO nanowires grown by chemical bath deposition
Eirini Sarigiannidou, José Villafuerte, Joseph Kioseoglou, Fabrice Donatini, Julien Pernot, Vincent Consonni
International Conference on Nanoscience and Nanotechnologies, 5-8 July, Thessaloniki, Greece 2022

13. Conférence invitée / Nationale– J2N 2022

Doping of ZnO nanowires grown by chemical bath deposition: the specific case of Ga investigated by XLD and ab-initio calculations
Eirini Sarigiannidou, Pierre Gaffuri, Fabrice Wilhelm, Josept Kioseoglou, Estelle Appert, Vincent Consonni
Journees Nationales de Nanofils, 28-30 septembre, Nice, France 2022

PhD and Post-doctorate supervision

Table 4 : *Summary of co-supervised PhD and Post Doc.*

		% of super vision	Période	Articles	Devenir
Thèse	**Alexandre DIEULESAINT (avec V. Consonni)** *Etude des propriétés liées à la piézoélectricité des nanofils de ZnO : la question des défauts liés à l'hydrogène*	80%	Oct. 2018-		
	José Guillermo VILLAFUERTE DÍAZ (avec V. Consonni 40% & J. Pernot 30%) *Nanofils de ZnO résistifs synthétisés par dépôt en bain chimique pour capteurs piézoélectriques flexibles*	30%	Oct. 2018- Juil. 2022	RICL : 1,2,5,7, 12	New Market developer in Guatemala Bank
	Hoang Long LE TRAN (avec D. Chaussende) *Synthesis and characterization of new wide band gap semiconductor materials starting from the Al-Si-C ternary system*	60%	Oct. 2014 Juin. 2018	RICL : 9,13	Ingénieur recherche/développement à *Univ. De Lille/UMET*
	Nikolaos TSAVDARIS (avec D. Chaussende) *Cristallogenèse de carbure de silicium à partir de la phase gazeuse*	20%	Oct. 2009- Oct. 2014	RICL : 20, ACL : 2-9	SiC Epitaxy development engineer à *Infineon Technologies*
Post-doctorat	**Rym Benaboud (avec C.Jimenez)** *FUI / FEDER : SUPERFACTS*	50%	Nov. 2009- Nov. 2010	RICL : 26,27 ACL : 11,12	Chief Corporate marketing & Strategic communication à *Wise-integration*
	Virginie Roche (avec C.Jimenez) *FUI / FEDER : SUPERFACTS* Préparation de couches minces épita xiées de Zirconate de Lanthane par MOD sur des rubans métalliques texturés	50%	Dec. 2010- Aout 2011		MCF à *Polytech Grenoble / LEMPI*

Participation in PhD juries

Jurys de thèses

1. (President) **Mr. Rémy BERTHIER** "*Development of characterization methods for in situ annealing and biasing of semiconductor devices in the TEM*" soutenu le 11/06/2018, Université Grenoble Alpes, Ecole doctoral de physique.

2. (Examinatrice) **Mr. Fabio AGNESE** « Advanced TEM Studies on Colloidal Semiconductor Nanocrystals » soutenu le 16/10/2018, Université Grenoble Alpes, Ecole doctoral de physique.

Comité de suivi Individuel (CSI) de thèses

1. Mr. Édouard VILLEPREUX. Titre de la thèse « Observation in-situ par microscopie électronique en transmission du fonctionnement de mémoires résistives à base d'oxyde » sous la direction de Mireille Mouis et de David Cooper. Université Grenoble Alpes, école doctorale EEATS.
2. Mr. Athanasios GKOUNTARAS. Thèse sur l'exfoliation des monocristaux de composés de phases MAX et leur caractérisation sous la direction de Thierry Ouisse. Université Grenoble Alpes, école doctorale I-MEP2.
3. Mrs. Ioanna DIMKOU. Thèse sur microscopie corrélative des nanostructures de nitrures d'éléments III : application à la photonique sous la direction de Eva Monroy, Lorenzo RIGUTTI et Adeline GRENIER. Université Grenoble Alpes, école doctorale Physique.
4. Mr. Omar Hassan. Thèse sur le développement d'une nouvelle génération de graphène ponté pour le stockage de l'énergie: vers l'utilisation de piliers impliqués dans les mécanismes électrochimiques sous la direction de Lionel DUBOIS et Florence DUCLAIROIR. Université Grenoble Alpes, école doctorale CSV.
5. Mr. TEMPELAERE Matthieu. Thèse sur l'étude et l'optimisation de composites nanotubes de carbone verticalement orientés et catalyseurs pour applications pile à combustible sous la direction de Marian CHATENET et Marc ZIMMERMANN. Université Grenoble Alpes, école doctorale école doctorale I-MEP2

Supervision of Internships

Table 5 : *Summary of co-supervision of internships (M1, M2 et IUT).*

		Taux d'encadrement	Période
Stage Master 2	**Wondimu GEBREYES** *Synthesis and caracterization of LaAlO3 oxides*	100%	Mai 2010 – Aout 2010
	Julien EL SABAHY *Nanostructuring of a silicon surface for the local, selforganized and catalytic growth of group IV nanowires (Si, Ge)*	100%	Fev. 2012 – Sept. 2012
	Leonidas KAZIANIS (with V. Consonni) *Shape transition of ZnO thin films into nanowires: a growth and characterization study*	60%	Sept. 2017-Feb 2018
Stage Master 1	**Enrique Alonso ENRIQUEZ GONZALEZ** *Nanostructuring of a silicon surface for the local, self-organized and catalytic growth of group IV nanowires (Si, Ge).*	100%	Mai 2012 – Aout 2012
	Eléa Matheret (avec V. Consonni) *Advanced Structural Characterization of ZnO Nanowires For Solar Cells and LEDs*	80%	Mai 2019 – Aout 2019

	Ana Bujak (avec V. Consonni) *Advanced structural characterization of Ga2O3 microrods for solar cells and LEDs*	80%	Mai 2021 – Aout 2021
Stage DUT/BUT	**Didier Foue** *Montage, automatisation et instrumentation d'un appareillage de type Dip-Coating pour dépôt de couches minces*	100%	Avr. 2009 - Jul. 2009
	Jeremy Desormneau *Préparation d'échantillons pour la microscopie électronique à transmission*	100%	Avr. 2010 - Juin 2010
	Nicolas Garnier *Étude de la formation de Carbure ternaire-Al4SiC4 à l'interface entre l'Aluminium et le Carbure de Silicium.*	100%	Nov. 2016 - Fevr. 2017

Teaching activities

Appointed as a teacher (maitresse de conférences) since September 2006 at Grenoble INP-UGA, I carry out most of my teaching activity within **the Phelma school** (PHysics, ELectronics, Materials) since its creation in 2008. For the period 2006 to 2008 I was teaching at the ENSPG school (Ecole National Supérieur de Physique de Grenoble). Two periods of **maternity leave** are to be noted: January-May 2008 and January-May 2011. For the rest of the time, I have always worked at 100% (statutory teaching of 192h) without any interruption such as CRCT leave or delegation. Since September 2021, I have been appointed **Vice-President of International Relations at Grenoble INP-UGA**, an assignment that impacts my teaching service as the statute requires a service of 64H eq.TD per year.

For the last ten years I have benefited from the **research bonus**: PES (Campaign 2013) from 10/2013 to 09/2017, PEDR (Campaign 2017) from 10/2017 to 09/2021 and PEDR (Campaign 2021) from 10/2021 and until 09/2025.

My teaching activities are mainly divided between the disciplines of **physics and materials science** as shown in Figure 1, in good correlation with my research activities. Table 1 is a summary of my teaching since my recruitment until today. The subjects in bold refer to the courses I have set up and for which I am responsible for teaching. The table shows that my teaching has been very varied over the years and that I have never hesitated to teach a subject only for a few years or even for a single year to help a colleague in difficulty. Some subjects, such as practical work in transmission electron microscopy (TEM), remain constant because they are very specific and linked to my research expertise. My teaching is given in its entirety to a post-baccalaureate public, mainly **in initial training**: engineering cycle (3 years), master (2 years), but also in **professional training**. From the point of view of format, I teach lectures, tutorials, practical work, study and project offices (see Figure 2). From the point of view of the number of students: a Master's class has about 30 students, a course at Phelma has about 45 engineering students, while in the first year we teach a series of 36 students. About 30% of my teaching and 80% of my discussions with students are in English.

Between 2011 and 2021, I was the coordinator of the **Erasmus Mundus Joint Master Degrees programme FAME (Functional Advanced Materials & Engineering**, http://www.fame-master.eu/). This is an international Master's degree that has been awarded the valuable Erasmus Mundus label by the European Commission's EACEA agency (Erasmus+, Key Action 1 project) since its creation in 2007. The FAME Master's consortium includes 7 European universities: University of Augsburg (D), University of Aveiro (P), University of Bordeaux (FR), Université Catholique de Louvain (B), University of Darmstadt (D), University of Liège (B) and Grenoble-INP (FR) as coordinator.

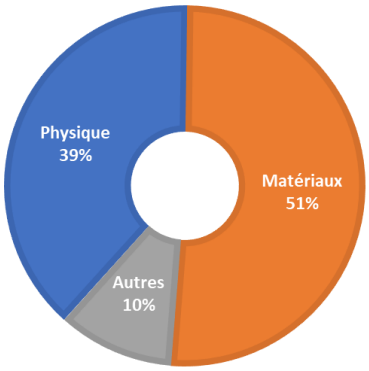

Figure 1 : *Summary of my teaching disciplines*

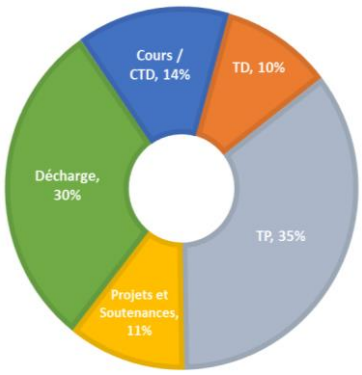

Figure 2 : *Division of my teaching according to its nature.*

My first interaction with the **FAME Master** was in 2009-2010 when I was in charge of the internships for the M1 students. The following year, 2010-2011, I was asked to contribute to the writing of the application for the renewal of the FAME Master's degree to Europe and at the same time to be the director of the Master's degree. We succeeded in obtaining again the **Erasmus Mundus label** for our Master for a period of 5 years (2012-2018) with a budget of 3.2 M€ for this reference period. I would like to mention that my participation in the Erasmus Mundus EMMC call for proposals in April 2011, which led to the renewal of the FAME Master, was very active (writing, monthly and weekly conference calls, meetings,...) despite my maternity leave during this period. For this second edition of the FAME Master (2012-2018), 6 associated partners joined the FAME consortium: Bosch, CEA, EMMI, Imec, Rhodia, and SusChem. In 2017, we reapplied for a third labelling and despite the low chances of success, we convinced the European Commission agency that we can be innovative and provide quality training. The third edition of FAME+ (2017-2022) with a budget of €3.37M and 27 associated partners, started with a year of preparation to set up the new teaching modules and recruited the first students in 2018.

Between 2016 and 2021, I coordinated the **AMIS (Advanced Materials for Innovation and Sustainability,** https://amis-master.eitrawmaterials.eu/) master's programme funded by the EIT (European Institute of Innovation & Technology) via the KIC Raw Materials (budget ~ 900 K€/year). For the first two years, I was in charge of setting up this master's degree for Grenoble INP with the other members of the consortium and also of ensuring its accreditation by the EIT. The AMIS master's degree is a master's level course that deals with the problems of substitution of critical and/or toxic materials and the durability of functional materials based on strong links between academic and industrial partners. It opened the doors to its first class in 2017. The AMIS consortium includes 5 European universities: Grenoble INP, Aalto University (F), University of Bordeaux (FR), University of Liège (B), Technical University of Darmstadt (D) and 3 industrial partners: Arcelor Mittal (FR), Fraunhofer-Gesellschaft (D), CEA (FR) and IMEC (B).

Within Phelma, these two masters are included as such in the international Advanced Materials (AM) programme for engineering students.

.

Tableau 1 : *Summary of my teaching since my employment in terms of: nature, level, subject and time volume. The subjects for which I am or was the teacher in charge appear in bold.*

Nature / Matière		Niveau	Volume horaire / Année scolaire																
			06-07	07-08	08-09	09-10	10-11	11-12	12-13	13-14	18-19	15-16	16-17	17-18	18-19	19-20	20-21	21-22	22-23
Cours & Cours TD intégrés	***Caractérisation des matériaux***	3A			18	12	12	12	12	12	12	12	12	12	12	12	22	18	18
	Matériaux pour les composants	2A	16		10	20		18	18	18									
	Cristallographie																24	24	24
	Structures & propriétés des matériaux	1A							12	12	12	32	35	35	35				
	Physique Quantique	1A							24										
	Cellules Photovoltaïque	M1					4	4	4										
	Matériaux															8	8	6	
Travaux dirigés	*Propriétés Electroniques de la matière*	2A			24	24		24	24										
	Structures et propriétés des matériaux	1A			12	12	12	12	12	14	12								
	Matériaux	1A														18	18		
	Thermodynamique	1A			12	10		8	8	8									
		CPP	44																
	Physique des semiconducteurs													4	10	10	8		
	TD physique du solide	1A	16	16	22														
Travaux Pratique	***Physique-Matériaux***	M1			16	28		28	16	24	24	28	24	32	20	16	8		
	Physique	1A	84		68	33													
	TP TEM	*FC, 3A M1*	36	28	32	12		16	16	16	8	4	12	20	27	33	30		
	TP Salle Blanche	M1			32	48		*49*	*24*		32	16							
	TP Matériaux	*1A*	88	60									12						
	TP Préorientation	*1A*			32	24		*16*	*16*										
	TP caractérisation	*FC*			12	15	*30*	*32*	*48*		24	31							
Projet	***Remote ou e-project***	M1							4	4	8	8	8	*2*	*11*	*8*			
	Mini-Project	M1				4		*8*	4										
	P3/MAP	1A				8	*4*	*8*	8	8	11	20	10	*10*	*10*	*10*	*20*		
	REX	1A					*6*	*9*	9	3	3	8	4	*4*	4	4	8	3	*6*
Soutenance	*2A ou 3A*	2-3A	3	2	3	8	*21*	*13*	12	9	18	26	15	*2*	5	11	17	6	
Décharge						12	*12*	*18*	72	72	78	72	120	*144*	144	144	*188*	*128*	*128*
TOTAL			**280**	**104**	**235**	**285**	***106***	***290***	**368**	**213**	**249**	**256**	**252**	***263***	***273***	**278**	**366**	**68**	**64**

Teaching responsibilities

Responsible for training and specific pedagogical actions

As mentioned in the previous paragraph "Teaching activities", I have been for 10 years the coordinator of the EMJMD FAME Master (http://www.fame-master.eu/) and since 2016 and until September 2021 of the EIT Raw Materials AMIS Master (https://amis-master.eitrawmaterials.eu/). These two international Masters courses train students in materials science with links to industry and the latest scientific advances in an international and multicultural environment. Each course is over two years and delivers a double degree and a diploma supplement depending on the pathway within the Master's programme of each student. Students spend their first year either at Grenoble INP in France, TUD in Germany or Aalto in Finland and their second year in one of the partners of each consortium. Since its creation in 2007, more than 350 students have graduated from FAME with an average of 14 nationalities per class. Each AMIS class has about 30 students with an average of 8 nationalities per class.

My purely **pedagogical tasks** concerning the management of these two courses covered several aspects. Some of the following responsibilities were shared with my colleagues and others were entirely my responsibility. It should be noted that for this part of my responsibilities, the work, willingness and determination of Mrs. Zammit Eliane (Phelma's international relations administrative staff) were more than valuable.

1) Updating of the pedagogical curriculum of the M1 and M2 years offered by Phelma in close correlation with the other academic years offered by each consortium.

2) Recruitment of visiting professors and temporary staff and rotation of teachers assigned to the various subjects.

3) Communication: participation in forums and presentations of the various courses of study, half-yearly reviews with students and teachers, organisation of industrial conferences, links with alumni, updating of the dedicated website, response to various surveys.

4) Participation in the juries and in the course meetings as well as in the half-yearly meetings of the Pedagogical Commission and of the student life.

The above responsibilities were shared with my colleagues Annie Antoine for the M1 and Fabien Volpi for the M2.

5) Recruitment of international students for each Master (~60 applications/year per university partner). Phase 1: Analysis of applications for admission. Phase 2: if the analysis score of the file is higher than 80/100, organisation and realisation of interviews with each candidate. Phase 3: Analysis of applications for scholarships. Pooling of our recruitment results in order to finalise the list of each class with the other partners of each consortium (2 meetings/year/consortium).

6) In charge of relations with companies for each Master's degree. Validation of internship agreements (2A/M1), appointment of school tutors, appointment of examining boards and organisation of the schedule. Maintaining the link with the industrialists who host our students and graduates.

7) Pedagogical follow-up of each student with regard to their integration into the Master's programme, their academic performance, any difficulties they may have and preparation of the school's jury.

8) Accompaniment and distribution of each student on their mobility in 3A/M2 at a partner of the consortium (compulsory mobility if validation of the M1).

9) Organisation of innovative projects specific to each Master's degree in connection with the consortium.

10) Responsible for international relations in the field with the reception of foreign students on academic exchange (~5 students/year) during the 2A/M1 year. Verification and acceptance of their learning agreement, follow-up of their education during their mobility.

11) Negotiation with the partners of each consortium in the event of a change in the regulations of a partner institution and/or changes in legislation in order to measure and anticipate the impact on our teaching models.

Responsible of community Innovative pedagogical activities of Unite!

Grenoble INP -UGA is a member of the European alliance unite! (University Network for Innovation, Technology and Engineering) since 2019. I am the Grenoble coordinator of the community dealing with innovative teaching and learning topics of the alliance. The aim of our community is to provide the whole alliance with: a toolkit for the development of unite! joint programmes, joint programmes and collaborative educational offers, a unite! training kit for capacity building to achieve the best pedagogical quality and a unite! training programme which includes joint programmes and collaborative offers and the implementation of the European Diploma.

Administrative Responsibilities in research and teaching

Vice-President Internationale Relations of Grenoble INP -UGA

I have been appointed Vice President (VP) in charge of International Relations ("RI") at Grenoble INP-UGA for the period from 01/09/2021 to 29/02/2024. Amplifying the international and intercultural posture is one of the four strategic axes of the institution. My mandate is structured around four priorities set out in Grenoble INP's strategic plan: - Mobilise our networks of international partners (academics and companies) to transform ourselves and become a major international centre. - Rely on our flagship themes and the quality of our platforms to increase our attractiveness and strengthen our collaborations. - Develop an offer abroad, in the image of our institute, by relying on our group networks (INP, IAE, Polytech). - Develop balanced collaborative approaches with developing countries.

In addition to the usual missions linked to this responsibility, there are those specific to Grenoble INP-UGA and to the mandate of the General Administrator, such as: an investment in the construction of an attractive and recognised engineering and management institute within our EPE UGA and beyond, the reinforcement of the international dimension of all our activities, the representation of the institution within the UGA, our networks and the various bodies of the Grenoble site.

Management of major international programmes

Coordination of Erasmus Mundus Joint Master Degree FAME+

My first interaction from an administrative point of view with the FAME Master was at the end of 2010 when I was offered to contribute to the drafting of the application for the renewal of the Master's degree to the European Commission's agency EACEA. We succeeded in obtaining again (the Master exists since 2007) the Erasmus Mundus label for our Master for a period of 5 student promotions (2012-2018). In 2017, I took charge of the new submission of the label to Europe which led to the third renewal of the FAME Master under the precious label of the EMJMD for a period of 3 classes of students (2017-2022, one year of preparation and 3 classes of 2 years).

The FAME Master Course consortium includes 7 European universities (University of Augsburg (D), University of Aveiro (P), University of Bordeaux (FR), Université Catholique de Louvain (B), University of Darmstadt (D), Grenoble-INP (FR), and University of Liège (B)) and 27 associated partners (http://www.fame-master.eu/)

My **purely administrative** tasks concerning the management of the FAME+ Master EMJMD are

a) Coordination of the FAME Consortium and its quality management. Creation at the beginning of each project renewal and subsequent updating of documents such as the consortium agreement, the double degree agreement, the financial agreements, the diploma supplements…These documents reflect our organisation of the internal management of the consortium. Setting up an annual external evaluation committee (EQAB: external quality assessment board, 3 members: 2 meetings/year, one report/year which we submit with our report to the agency).

b) Coordination with the European Commission's agency EACEA. This involves, for example, the drafting and validation by the agency of two reports per class of students: one at the end of the first year (progress report) and one at the end of the second year (final report of the class and financial report), drafting of a report for each edition of the Master. Updating of various European circulars and their application within our Master (i.e. New Erasmus Charter every 5 years). Audit and visits of the agency for the follow-up of the project.

c) The financial follow-up of each edition of the Master Course. With a budget per edition of about 3.3M€ various financial procedures have been set up and regularly reviewed (e.g. payment of scholarships to students, redistribution of funds between partners, funds for the organisation of various events, insurance contract that meets European standards, recruitment of staff...)

d) Organisation of winter school (every February in Grenoble, 3 days) and FAME consortium meetings either physical or virtual (at least 2 per year). Participation in the organisation of the summer school (every July at a partner's place, 4 days).

e) Accreditation of the Master's degree by the HCERES. The FAME Master is a course of the local SGM Master (Science and Engineering of Materials). Each course leader contributes to the drafting of the master's accreditation file.

It should be noted that I had under my responsibility an administrative staff to ensure with me the good follow-up of the Project/Master. For the period 2011-2021, seven people succeeded one another in this position with a period of staffing shortage between each recruitment.

Coordination of Master AMIS – Label EIT, KIC Raw Materials

Between 2015 and Sept 2021, I coordinated the AMIS (Advanced Materials for Innovation and Sustainability) programme funded by the EIT (European Institute of Technology) via the KIC Raw Materials. The aim of the project is to set up a master's level training course that deals with the problems of substitution of critical and/or toxic materials and the durability of functional materials based on strong links between academic and industrial partners and to ensure its operating costs and its accreditation by the EIT. The AMIS consortium includes 5 European universities (Grenoble INP (FR), Aalto University (F), University of Bordeaux (FR), University of Liège (B), Technical University of Darmstadt (D)) and 3 industrial partners (Arcelor Mittal (FR), Fraunhofer-Gesellschaft (D) and CEA (FR)).

The first three years (2015 and 2018) my main role was to set up the master's level training: search for partners within the KIC Raw Materials community, set up courses and innovative projects in connection

with research projects, validations of the agreements by the boards of directors and CEVU of my institution, and above all the application (via a project submission) and obtaining of the EIT Raw Materials label and funding for the AMIS project. The AMIS master's programme recruited its first class in September 2017 (https://amis-master.eitrawmaterials.eu/).

My purely administrative tasks concerning the management of Master AMIS are:

a) Coordination of the AMIS Consortium and its quality management. Creation at the beginning of the project and subsequent updating of documents such as the project business plan, the consortium agreement, the double degree agreement, the visual identity of the master, the diploma supplements....

b) Coordination in relation to EIT Raw Materials. This implies for example the drafting of an annual report, a project review every 4 months, submission of a "change request" each time we have a request to the EIT, 1-2 meetings per year between labelled Masters organised by the EIT....

c) Annual financial monitoring in close collaboration with the DAFA of Grenoble INP, the EIT and the financial department of Phelma (total budget excluding grants of around €0.8M).

d) Organisation of winter schools (every March, 3 days) and AMIS consortium meetings, either physical or virtual (at least 3 per year)

e) Submission of projects to the EIT to ensure the financing of the Master's programme (submission of KAVA project in 2015, 2017 and 2020, submission of Fast Track project in 2017 and 2020) and its labelling (submission of project in 2016 and 2021).

Since 2017, I have trained and had under my responsibility an administrative staff (CATA) to ensure the good follow-up of the Project/Master.

Member of local bodies

Elected member of the Phelma School Council from 2021 to 2024. The council meets two to three times a year to discuss various issues related to the life and management of the school, such as pedagogical developments, the budget, major projects and future directions. The restricted council (only for elected members) meets at regular intervals to deal with mobility requests, promotions, recruitments, ATER recruitments....
Appointed member of Phelma's Pedagogical and Student Life Commission (CPVE) between 2012 and 2021 as Head of the Master's programme/field.
Appointed member of the Board of Directors, the Scientific Council, the Board of Studies and University Life and the Bureau (management committee) of Grenoble INP -UGA in connection with my mandate as VP IR.

References

[1] F. Capasso and A. Y. Cho, Bandgap engineering of semiconductor heterostructures by molecular beam epitaxy: physics and applications, Surface Science **299-300**, 878-891 (1994).

[2] C. F. Zhe, Silicon Carbide: Materials, Processing & Devices. (CRC Press, 2003)

[3] D. Kim et al, Thin Solid Films **557** (2014) 216–221.

[4] L. Pedesseau, J. Even, M. Modreanu, D. Chaussende, E. Sarigiannidou, O. Chaix-Pluchery and O. Durand, APL Materials 3, 121101 (2015).

[5] S. D. Peteves, P. Tambuyser, P. Helbach, M. Audier, V. Laurent and D. Chatain, Microstructure and microchemistry of the Al/SiC interface, Journal of Materials Science **25** (8), 3765-3772 (1990).

[6] J. Viala, P. Fortier and J. Bouix, Stable and metastable phase equilibria in the chemical interaction between aluminium and silicon carbide, Journal of Materials Science **25** (3), 1842-1850 (1990).

[7] G. Charlot, Qualitative inorganic analysis: a new physio-chemical approach. (Methuen, 1954).

[8] J.-C. Viala, P. Fortier, B. Bonnetot, J. Bouix, Mater. Res. Bull. **1986**, 21, 387.

[9] J. Kioseoglou, H.-L. Le-Tran, S. Giaremis, I. Gelard, T. Ouisse, D. Chaussende, E. Sarigiannidou Phys. Stat. Sol. B 256: 1900037 (2019).

[10] Y. Sun, H. Cui, L. Gong, J. Chen, J. She, Y. Ma, P. Shen, C. Wang, ACS Nano **2011**, 5, 932.

[11] Y. Le Page, P. Saxe, Phys. Rev. B **2002**, 65, 104104

[12] L. Sun, Y. Gao, K. Yoshida, T. Yano, W. Wang, Mod. Phys. Lett. B 2017 31 1750080.

[13] J. Viala, F. Bosselet, V. Laurent and Y. Lepetitcorps, Journal of materials science 28 (19), 5301-5312 (1993)

[14] H.-L. Le-Tran, Sublimation growth of Al4SiC4 and study of heterostructures of Al-Si-C system on SiC. (Université Grenoble Alpes, 2018). https://tel.archives-ouvertes.fr/tel-01859586v1

[15] M. J. Hÿtch, E. Snoeck and R. Kilaas, Quantitative measurement of displacement and strain fields from HREM micrographs, Ultramicroscopy 74 (3), 131-146 (1998).

[16] J. L. Rouvière and E. Sarigiannidou, Theoretical discussions on the geometrical phase analysis, Ultramicroscopy 106 (1), 1-17 (2005).

[17] D. Brandon and W. D. Kaplan, Microstructural characterization of materials. (John Wiley & Sons, 2013).

[18] T. Liao, J. Wang and Y. Zhou, Atomistic deformation modes and intrinsic brittleness of Al4SiC4: A first-principles investigation, Physical Review B 74 (17) (2006).

[19] R. People and J. Bean, Calculation of critical layer thickness versus lattice mismatch for Ge x Si1− x/Si strained-layer heterostructures, Applied Physics Letters 47 (3), 322-324 (1985).

[20] H.L. Le-Tran, E. Sarigiannidou, I. Gelard and D. Chaussende JOURNAL OF THE EUROPEAN CERAMIC SOCIETY, **37** (15), 4475 (2017)

[21] J. E. Ayers, T. Kujofsa, P. Rago and J. Raphael, Heteroepitaxy of semiconductors: theory, growth, and characterization. (CRC press, 2016).

[22] N. Tsavdaris, D. Harza, S. Coindeau, G. Renou, F. Robaut, E. Sarigiannidou, M. Jacquemin, R. Reboud, M. Hofheinz, E. Blanquet and F. Mercier, Chemitry of Materials, 29 (14) 5825 (2017)

[23] Manoël Jacquemin, Structure et propriétés supraconductrices de films de nitrure de niobium épitaxiés par CVD à haute température, Université Grenoble Alpes, 2019. Français. ⟨NNT : 2019GREAI054⟩. ⟨tel-02441642⟩

[24] T. Dietl et al., Science 6287, 1019 (2000).

[25] K. Sato et al., Phys. Rev. B 70, 201202R (2004)

[26] G. Bouzerar, T. Ziman, and J. Kudrnovsky, Europhys. Lett. 69, 812 (2005).

[27] S. Dhar et al., Phys. Rev. B 67, 165205 (2003).

[28] S. Sonoda et al., J. Cryst. Growth 237-239, 1358 (2002)

[29] E.Sarigiannidou, F. Wilhelm, E. Monroy, R. M. Galera, E. Bellet-Amalric, A. Rogalev, J. Cibert, J.Goulon and H. Mariette, Phys. Rev. B 74 041306(R) (2006)
[30] Y. Joly, Phys. Rev. B 63, 125120 (2001).
[31] A. Arrott, Phys. Rev 108, 1394 (1957).
[32] T. G. Chirayil, M. Paranthaman, D.B. Beach, D.F. Lee, A. Goyal, R.K. Williams, X. Cui, D.M. Kroeger, R. Feenstra, D.T. Verebelyi, D.K. Christen, Physica C: Superconductivity 336 (2000) 63.
[33] V. Cloet, J. Feys, R. Hühne, S. Hoste, I. Van Driessche, Journal of Solid State Chemistry 182 (2009) 37
[34] C. Jiménez, T. Caroff, L. Rapenne, S. Morlens, E. Santos, P. Odier, F. Weiss, Journal of Crystal Growth 311 (2009) 3204
[35] L. Rapenne, C. Jiménez, T. Caroff, C. Millon, S. Morlens, P. Bayle-Guillemaud, F. Weiss, Journal of Materials Research 24 (2009) 1480
[36] V. Roche, C. Jiménez, P. Chaudouët, R. Benaboud, F. Weiss, E. Sarigiannidou, Thin Solid Films, 520,2566 (2012).
[37] N. Dechoux, C. Jiménez, P. Chaudouët, L. Rapenne, E. Sarigiannidou, F. Robaut, S. Petit, S. Garaudée, L. Porcar, J. L. Soubeyroux, P. Odier, C.- E. Bruzek and M. Decroux, Superconductor Science and Technology 25 125008 (2012)
[38] Stadelmann, P.A. EMS-a Software Package for Electron Diffraction Analysis and HREM Image Simulation in Materials Science. *Ultramicroscopy* **1987**, *21*, 131.
[39] V. Consonni, E. Sarigiannidou, E. Appert, A. Bocheux, S. Guillemin, F. Donatini, I-C.Robin, J. Kioseoglou and F. Robaut, ACS Nano, **8(5),** 4761 (2014)
[40] Baxter, J.B.; Wu, F.; Aydil, E.S. Growth Mechanism and Characterization of Zinc Oxide Hexagonal Columns. Appl. Phys. Lett. 2003, 83, 3797-3799.
[41] Cherns, D.; Sun, Y. Defect Reduction by Epitaxial Lateral Overgrowth of Nanorods in ZnO/(0001) Sapphire Films. Appl. Phys. Lett. 2008, 92, 051909.
[42] Sun, Y.; Cherns, D.; Doherty, R.P.; Warren, J.L.; Heard, P.J. Reduction of Threading Dislocations in ZnO/(0001) Sapphire Film Heterostructure by Epitaxial Lateral Overgrowth of Nanorods. J. Appl. Phys. 2008, 104, 023533.
[43] Wang, Z.L.; Song, J.H. Piezoelectric Nanogenerators Based on Zinc Oxide Nanowire Arrays. Science 2006, 312, 242-246.
[44] Puyoo, E.; Rey, G.; Appert, E.; Consonni, V.; Bellet, D. Efficient Dye-Sensitized Solar Cells Made from ZnO Nanostructure Composites. J. Phys. Chem. C 2012, 116, 18117-18123.
[45] Levy-Clement, C.; Tena-Zaera, R.; Ryan, M.A.; Katty, A.; Hodes, G. CdSe-Sensitized p-CuSCN / Nanowire n-ZnO Heterojunctions. Adv. Mater. 2005, 17, 1512-1515.
[46] Wu, Z.; Zhang, Y.; Zheng, J.; Lin, X.; Chen, X.; Wang, B.; Wang, H.; Huang, K.; Li, S.; et al. J. Mater. Chem. 2011, 21, 6020-6026.
[47] V. Cantelli, S. Guillemin, E. Sarigiannidou, F. Carla, B. Berini, JM Chauveau, DD Fong, H. Renevier, V. Consonni Nanoscale, 14, 680, (2022)
[48] E.F. Rauch, M. Veron, Materials Characterization, 98 1–9 (2014)
[49] S. Guillemin, E. Sarigiannidou, E. Appert, F. Donatini, G. Renou, G. Bremond, V. Consonni NANOSCALE, 7 16994 (2015)
[50] C. Stampf and C. G. Van de Walle, Phys. Rev. B: Condens. Matter, 1998, 57, 15052(R).
[51] S. Guillemin, L. Rapenne, H. Roussel, E. Sarigiannidou, G. Brémond and V. Consonni, J. Phys. Chem. C, 2013, 117, 20738–20745.
[52] Q.C Bui, G. Ardila, E. Sarigiannidou, H. Roussel, C. Jimenez, O. Chaix-Pluchery, Y. Guerfi, F. Bassani, F. Donatini, X. Mescot, B. Salem, V. Consonni ACS APPLIED MATERIALS & INTERFACES, 12 (26) 29583 (2020)
[53] Guillemin, S.; Appert, E.; Roussel, H.; Doisneau, B.; Parize, R.; Boudou, T.; Bremond, G.; Consonni, V. Controlling the Structural Properties of Single Step, Dip Coated Zno Seed Layers for Growing Perfectly Aligned Nanowire Arrays. J. Phys. Chem. C 2015, 119, 21694−21703.

[54] Park, J. Y.; Lee, D. J.; Yun, Y. S.; Moon, J. H.; Lee, B. T.; Kim, S. S. Temperature-Induced Morphological Changes of ZnO Grown by Metalorganic Chemical Vapor Deposition. J. Cryst. Growth 2005, 276, 158−164.
[55] Munuera, C.; Zuniga-Perez, J.; Rommeluere, J. F.; Sallet, V.; Triboulet, R.; Soria, F.; Munoz-Sanjose, V.; Ocal, C. Morphology of ZnO Grown by Mocvd on Sapphire Substrates. J. Cryst. Growth 2004, 264, 70−78.
[56] Sieber, B.; Addad, A.; Szunerits, S.; Boukherroub, R. Stacking Faults-Induced Quenching of the Uv Luminescence in ZnO. J. Phys. Chem. Lett. 2010, 1, 3033−3038.
[57] Yang, S.; Kuo, C. C.; Liu, W. R.; Lin, B. H.; Hsu, H. C.; Hsu, C. H.; Hsieh, W. F. Photoluminescence Associated with Basal Stacking Faults in C-Plane ZnO Epitaxial Film Grown by Atomic Layer Deposition. Appl. Phys. Lett. 2012, 100, No. 101907.
[58] Khranovskyy, V.; Eriksson, M. O.; Radnoczi, G. Z.; Khalid, A.; Zhang, H.; Holtz, P. O.; Hultman, L.; Yakimova, R. Photoluminescence Study of Basal Plane Stacking Faults in ZnO Nanowires. Physica B 2014, 439, 50−53.
[59] Janotti, A.; Van de Walle, C. G., Fundamentals of Zinc Oxide as a Semiconductor. Rep. Prog. Phys. 2009, 72, 29.
[60] McCluskey, M. D.; Jokela, S. J., Defects in Zno. J. Appl. Phys. 2009, 106, 13.
[61] Janotti, A.; Van de Walle, C. G., Oxygen Vacancies in ZnO. Appl. Phys. Lett. 2005, 87, 3.
[62] Paudel, T. R.; Lambrecht, W. R. L., First-Principles Calculation of the O Vacancy in Zno: A Self-Consistent Gap-Corrected Approach. Phys. Rev. B 2008, 77, 9.
[63] Janotti, A.; Van de Walle, C. G., Native Point Defects in Zno. Phys. Rev. B 2007, 76, 22.
[64] Lyons, J. L.; Varley, J. B.; Steiauf, D.; Janotti, A.; Van de Walle, C. G., First-Principles Characterization of Native-Defect-Related Optical Transitions in Zno. J. Appl. Phys. 2017, 122, 12.
[65] J. Villafuerte, F. Donatini, J. Kioseoglou, E. Sarigiannidou, O. Chaix-Pluchery, J. Pernot, V. Consonni, Journal of Physical Chemistry CVolume 124, (30) 16652 (2020)
[66] Villafuerte, O. Chaix-Pluchery, J. Kioseoglou, F. Donatini, E. Sarigiannidou, J. Pernot, V. Consonni, Physical Review Materials 5, 056001 (2021)
[67] J. Villafuerte, E. Sarigiannidou, F. Donatini, J. Kioseoglou, O. Chaix-Pluchery, J. Pernot, V. Consonni Nanoscale Advances, 4, 1793 (2022)
[68] Pearton, S. J.; Yang, J.; Cary, P. H.; Ren, F.; Kim, J.; Tadjer, M. J.; Mastro, M. A. A Review of Ga2O3 Materials, Processing, and Devices. Appl. Phys. Rev. 2018, 5 (1), 011301.
[69] Chen, X.; Ren, F.; Gu, S.; Ye, J. Review of Gallium-Oxide-Based Solar-Blind Ultraviolet Photodetectors. Photonics Res. 2019, 7 (4), 381.
[70] Chang, P.-C.; Fan, Z.; Tseng, W.-Y.; Rajagopal, A.; Lu, J. G. β- Ga2O3 Nanowires: Synthesis, Characterization, and p-Channel Field- Effect Transistor. Appl. Phys. Lett. 2005, 87 (22), 222102.
[71] G. Hector, E. Appert, E. Sarigiannidou, E. Matheret, H. Roussel, O. Chaix-Pluchery, V. Consonni Inorg. Chem. 59 (21) 15696–15706 (2020)
[72] Ciatto, G.; Di Trolio, A.; Fonda, E.; Alippi, P.; Testa, A. M.; Bonapasta, A. A., Evidence of Cobalt-Vacancy Complexes in Zn1-xCoxO Dilute Magnetic Semiconductors. Phys. Rev. Lett. 2011, 107, 127206.
[73] Ma, Q.; Prater, J. T.; Sudakar, C.; Rosenberg, R. A.; Narayan, J., Defects in Room-Temperature Ferromagnetic Cu-Doped Zno Films Probed by X-Ray Absorption Spectroscopy. Journal of Physics: Condensed Matter 2012, 24, 306002.
[74] Sarigiannidou, E.; Wilhelm, F.; Monroy, E.; Galera, R. M.; Bellet-Amalric, E.; Rogalev, A.; Goulon, J.; Cibert, J.; Mariette, H., Intrinsic Ferromagnetism in Wurtzite (Ga,Mn)N Semiconductor. Phys. Rev. B 2006, 74, 041306.
[75] Ney, A.; Ollefs, K.; Ye, S.; Kammermeier, T.; Ney, V.; Kaspar, T. C.; Chambers, S. A.; Wilhelm, F.; Rogalev, A., Absence of Intrinsic Ferromagnetic Interactions of Isolated and Paired Co Dopant Atoms in Zn1-xCoxO with High Structural Perfection. Phys. Rev. Lett. 2008, 100, 157201.
[76] E. Sarigiannidou, P. Gaffuri, F. Wilhelm, J. Kioseoglou, A. Rogalev, E. Nikidis, E. Appert, and V. Consonni, Physical Review Materials (under revision).